THE FEASIBILITY OF DIAMOND-ALUMINA AS A WEAR RESISTANT MATERIAL

by **Sarel Duvenage**

Submitted in partial fulfilment of the requirements for the degree

Master of Engineering

in the Faculty of Engineering, University of Pretoria

October 1999

Supervisor: F. K. Bader

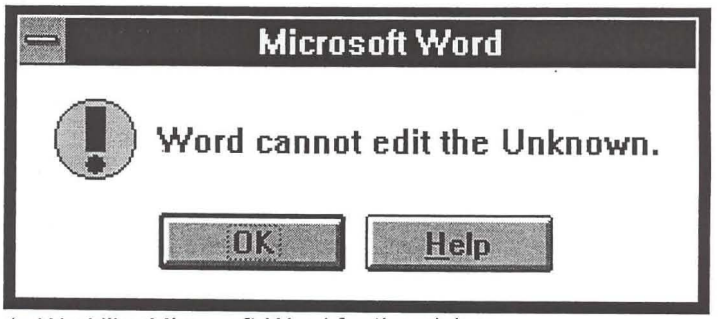

'n Werklike Microsoft-Word foutboodskap.

"Wir irren des Nachts im Kreis umher
und werden vom Feuer verzehrt"
(Einstürzende Neubauten, 1992)

"Die anargie is bestel maar het te laat oor die pos gearriveer."
(Letoit, 1994)

"There is a theory which states that if ever anyone discovers exactly what the Universe is for and why it is here, it will instantly disappear and be replaced by something even more bizarre and inexplicable.

There is another theory which states that this has already happened."
(Adams, 1980)

"It has not escaped our notice that the specific pairing we have postulated immediately suggests a possible copying mechanism for the genetic material."
(Watson en Crick, 1953)

Dankbetuigings

Aan my ouers, vir alles.

Aan Kiëv vir sy uiterste lojaliteit. Mag ons mekaar weer sien.

Aan Fritz Bader vir raad, aanmoediging en geduld.

Aan Martin Krämer (waar hy ookal nou is) en Robert Fries van DRL vir hulle raad en geduld.

Aan Cebile Ntshali, Karen Massyn, Roberto Mulone en veral Peter Ravenhill van DRL vir hulle hulp en raad.

Aan Tuks se Laboratorium vir Mikroskopie en Mikro-Analise veral prof. Jan Coetzee vir al hulle moeite en raad. Ook vir interessante gesprekke oor skoenlapperspermselle en so meer.

Aan prof. Labuschagne, dr Alna van der Merwe en mev. Coetzer van Tuks se Departement Wiskunde en Toegepaste Wiskunde wat gehelp het dat ek my verstand behou in die donker dae van empiriese hel.

The feasibility of diamond-alumina as a wear resistant material

Sarel Duvenage, supervised by F. K. Bader

Department of Materials Science and Metallurgical Engineering

M. Eng. (Met.)

Abstract

There is some reason to believe that an alumina matrix with imbedded diamond particles would have superior wear properties when compared with the unreinforced matrix material. There are mixing laws which predict wear resistance intermediate to that of diamond and alumina. Diamond can be expected to reinforce an alumina matrix in some way. Diamond is an excellent conductor of heat and can improve the rather poor heat conduction properties of alumina.

The objective of this work was to test the anticipation that the incorporation of diamond particles in an alumina matrix would improve wear properties. This was done by fabricating samples of diamond-alumina composites and evaluating the properties deemed most strongly related to wear performance. It was possible that graphite, or other non-diamond carbon allotropes, could form in the diamond-alumina interface during manufacturing of samples. Since the presence of graphite was expected to detrimentally affect bonding between diamond and alumina, methods like the use of nano-sized powders, filter casting and HIPping were used in efforts to minimise the temperature necessary for full densification. The use of the above methods makes this work unique in the rather limited field of diamond-alumina composites.

All samples in this study made with α-alumina and by HIPping were dense (> 96 % relative density). Graphite still formed under all conditions, even at HIPping temperatures as low as 1 250 °C. Artificial fracture surfaces showed good dispersion of diamond in general, and close contact between diamond and alumina. Vickers hardness was around 25 GPa. Toughness, measured by the hardness indentation crack length method, varied between 2.7 and 4.2 $MPa.m^{½}$.

Actual wear performance was measured by cutting a rod of so-called 'Siffer'. Diamond-alumina compared unfavourably to the commercially available zirconia-alumina cutting material Toshiba LX11. Diamond-alumina is not resistant to wear experienced in a relatively aggressive cutting test environment.

A correlation exists between toughness and wear, but against all expectations brittle samples exhibited greater wear resistance (hardness did not vary significantly between samples and can be ruled out as the source of wear rate variation).

In this work graphitisation was restrained. In contrast, other researchers actually extensively graphitised the diamond in their composites by additional heat treatment. This resulted in increased toughness, which shows that diamond-alumina bonding need not be a major consideration. In other work, diamond-alumina was shown to outperform zirconia-alumina in wear tests on magnetic discs. This creates the impression that the application of diamond-alumina as a cutting material visualised in this research was inappropriate.

Keywords

diamond, alumina, composites, submicron, HIPping, graphitisation, microstructure, hardness, toughness, wear.

Die lewensvatbaarheid van diamant-alumina as 'n slytasiewerende materiaal

Sarel Duvenage, studieleier F. K. Bader

Departement van Materiaalkunde and Metallurgiese Ingenieurswese

M. Ing. (Met.)

Samevatting

Dit is moontlik dat 'n alumina-matriks waarin diamant-partikels ingebed is beter slytasie-eienskappe sal hê as die matriks-materiaal op sy eie. Daar is vermengingswette wat slytasieweerstand tussen dié van diamant en alumina voorspel. Diamant kan die alumina-matriks verstewig. Diamant is 'n uitstekende hitte-geleier en kan die relatief swak hitte-geleiding van alumina verbeter.

Die doel van hierdie werk was om die vermoede dat die inkorporasie van diamant-partikels in 'n alumina-matriks slytasie-eiensakappe sal verbeter te toets. Dit is gedoen deur diamant-alumina-monsters te vervaardig en hulle eienskappe wat geag is om die sterkste invloed op slytasie te hê te meet. Dit is moontlik dat grafiet, of ander nie-diamant-allotrope van koolstof, in die diamant-alumina-raakvlak kon vorm tydens die vervaardigingsproses. Omdat dit verwag is dat grafiet die hegting tussen diamant en alumina kan benadeel, is metodes soos die gebruik van nano-grootte poeier, drukgiet en warm isostatiese druk ('HIP') toegepas om die temperatuur vir verdigting laag te hou. Die gebruik van bogenoemde tegnieke maak hierdie werk uniek in die ietwat beperkte veld van diamant-alumina-komposiete.

Alle monsters in hierdie studie wat met α-alumina en deur warm isostatiese druk gemaak is, was dig (> 96 % relatiewe digtheid). Grafiet het nog steeds gevorm, selfs by monsters wat teen so laag as 1 250 °C gevuur is. Kunsmatige breekvlakke het oor die algemeen goeie uitspreiding van diamant getoon, en goeie kontak tussen diamant en alumina. Hardhede en taaihede gemeet deur Vickers-indentasie was onderskeidelik rondom 25 GPa en tussen 2.7 en 4.2 $MPa.m^{½}$.

Werklike slytasie-werkverrigting is deur 'n snytoets op sogenaamde 'Siffer' gemeet. Diamant-alumina het sleg met die kommersiëel beskikbare zirkonia-alumina-snymateriaal, Toshiba LX11, vergelyk. Diamant-alumina is nie bestand teen slytasie in 'n snytoets-omgewing nie.

Daar is 'n verband tussen taaiheid en slytasie, maar, teen alle verwagting in, was bros monsters meer bestand teen slytasie (hardheid het nie betekenisvol tussen monsters gewissel nie en kan uitgeskakel word as 'n moontlike bron van variasie in slytasie-tempo's).

In hierdie werk is grafitisering beperk. In teenstelling hiermee, is daar ander navorsers wat doelbewus die diamant in hulle komposiete grafitiseer het deur addisionele hitte-behandeling. Dit het groter taaihede tot gevolg gehad, wat aantoon dat alumina-diamant-hegting nie 'n groot oorweging hoef te wees nie. In nog ander navorsers se werk het alumina-diamant beter as zirkonia-alumina in 'n slytasie-toets op 'n magnetiese skyf gevaar. Dit alles skep die indruk dat 'n ongeskikte toepassing vir diamant-alumina in hierdie werk in die vooruitsig gestel is.

Sleutelwoorde

diamant, alumina, komposiete, submikron, warm isostatiese druk, grafitisering, mikrostrukture, hardheid, taaiheid, slytasie.

Table of contents

Definitions

Cutting speed	:	Surface speed of workpiece.
Diamond-alumina	:	A composite material consisting of diamond and alumina.
Filter casting	:	Also known as filter pressing. Formation of a green body from a suspension by applied pressure.
Firing	:	Any densification by sintering, hot pressing or HIPping.
Graphitisation	:	This term is used fairly loosely. In some instances it means both the transition to graphite and amorphous carbon.
Green	:	The state of a compact before firing, e.g. green density.
HIP	:	Hot isostatic pressing.
Nanocomposites	:	Composites with a matrix of nanosize grains and a hard phase of indeterminate size.
Nanosize	:	In the order of magnitude of 10 nm.
Sintering	:	Specifically pressureless sintering
Superficial speed	:	The length-wise speed of a liquid in a vessel divided by the empty, cross-sectional vessel area.

Symbols

This work encompasses work from a variety of fields, and to avoid confusion, the conventional symbols were not always used. In the case of the more commonly used symbols, it was attempted to retain the conventional symbols.

In this document the symbol k is used commonly to refer to constants or coefficients. The following convention is followed for the differentiation of k: The first letters of the surnames of the equation's authors is subscripted to k. In the case of multiple constants or coefficients additional numbers are given. As an example take equation 5-11

$$N = k_{SV1}V + k_{SV2} \qquad (5\text{-}8)$$

which gives the normal force (N) on the tip of an insert as a simple linear function of the span (V) of a wear feature. Singh and Vajpayee (1980) originally authored this equation, and, accordingly, the coefficients k_{SV1} and k_{SV2} are used.

The definitions of abbreviations used as subscripts are given in table S-2.

The definitions of mathematical operators are given in table S-3.

***Table S-1**: Definition of variables, coefficient and constants*

Symbol	Definition
c	Distance from centre of indentation to end of crack.
d	Diameter
d	Indentation diagonal length
E	Young's modulus
$\mathcal{E}$	Activation energy
f	Component volume fraction
F	F(d) indicates *the mass fraction smaller than d*
g	Component area fraction
$\mathcal{G}$	Gibbs free energy
$\mathcal{H}$	Enthalpy

***Table S-1** continued*

H	Hardness
k	Coefficient or constant (see note above)
k	Thermal conductivity
K	Maximum crater depth
K	Toughness
$\mathcal{K}$	Equilibrium constant
$\mathfrak{k}$	Permeability
L	Depth
M	Indentor load
m	Wetted perimeter
N	Normal force
P	Pressure, chemical activity
Q	Volume lost due to wear
Q	Volume of material
R	An amount directly proportional to rate of graphitisation
R	Ideal gas constant
S	Entropy
ς	Specific surface area (volume basis, e. g. m^2/m^3)
S	Sliding distance
T	Temperature
t	Time
u	Cutting speed (distance/time)
V	Span of flank wear
v	Superficial speed
V	Activation volume
z	Ratio of the volume of filtrate to the volume of consolidated layer formed
*	Saturation
Ω	Wear resistance
ε	Volume fraction not occupied by solids. Note that this is used for volume fraction not occupied by solids in general and not only the volume fraction of voids in a solid compact, as the conventional usage is.
μ	Viscosity

***Table S-1** continued .*

τ	Tortuousity
υ	Poisson's ratio
ϵ	Strain
$\Diamond$	Diamond

***Table S-2**: Abbreviations used in subscripts*

Abbreviation	Meaning
0	Initial
cl	Consolidated layer
fin	Final
part	Particle
sl	Suspending liquid
susp	Suspension
V	Vickers

***Table S-3**: Mathematical operators.*

Operator	Meaning
~	Of the order of magnitude of
$\overline{\quad}$	Average, i.e. $\bar{x}$ signifies the average value of x.
δ	Derivative operator
Δ	Difference in
( )	p(x) indicates *p as a function of x*

Indexing of samples

Samples are uniquely identified by a reference number that indicates diamond content, primary alumina powder constituent, suspension preparation route, firing route, and firing temperature:

$$\underbrace{AA}_{}\underbrace{\Diamond}_{}\text{-}\underbrace{B}_{}\text{-}\underbrace{CC}_{}\text{-}\underbrace{D}_{}\underbrace{EEEE}_{}$$

Letters signify the following:

- 'AA' gives the diamond content of a sample in % v/v.
- 'B' gives the primary alumina powder constituent (either α or γ).
- 'CC' gives the suspension preparation route as indexed in table 6-1, page 45 (HP, pHα, pH$\alpha\Diamond$, Pα, Pγ, or CP).
- 'D' gives the firing method (only HIPping, denoted by H, was used for samples described in this thesis).
- 'EEEE' gives the dwell temperature in °C.

A consistent dwell time was used with each firing method for all samples and accordingly no indication of dwell time is given.

Chapter 1: Introduction

1.1 Background

This thesis is part of research on nano-composites conducted by the Diamond Research Laboratory of De Beers[‡] from 1996 to 1997.

1.2 Rationale for diamond-alumina composites

The incorporation of diamond particles in an alumina matrix may result in a composite with superior wear properties to pure alumina due the following reasons:

1) Intuitively, one might expect that hardness might be additive in some way. Although this may seem simplistic at first hand, this is in fact the case. In fig 1-1, the range of wear resistance of a composite as a function of composition as predicted by Axén and Jacobson (1994) is shown. 'Wear resistance' as defined by Axén and Jacobson is roughly proportional to hardness.

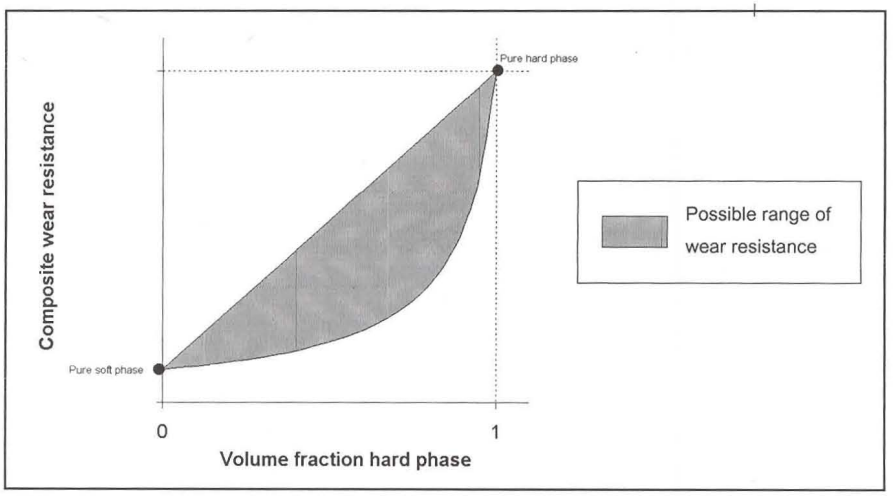

***Fig. 1-1**: The range of wear resistance for composites as predicted by Axén and Jacobson (1994).*

2) The presence of the strong diamond particles may reinforce alumina in some way.

[‡] Synthesis Division, Diamond Research Laboratory, Industrial Diamond Division, De Beers, Johannesburg, South Africa.

3) Diamond has superior heat conduction properties. Thermal conductivity is additive, ideally,

$$k_{Composite} = f_{Diamond} k_{Diamond} + f_{Alumina} k_{Alumina} \qquad (1\text{-}1)$$

where k is thermal conductivity and f volume fraction. Materials with high thermal conductivity conduct heat away from the friction zone more efficiently, which results in less thermal stressing and less chemical reactions at the friction zone.

4) Empirical evidence from published work of Chu *et al* (1992) and Noma and Sawaoka (1984 and 1985). Chu *et al* showed that diamond-alumina have superior wear qualities to zirconia toughened alumina (see fig. 5-12 on page 43). Noma and Sawaoka showed that diamond-alumina can be tougher than alumina alone, although hardness is sacrificed in their work (see fig. 5-10 to 5-12 on pages 43 to 44).

1.3 Rationale for nano-sized particle powders and filter casting

Although diamond is very inert under normal conditions, it is in fact only metastable. Diamond rapidly converts to graphite at high temperature. If diamond particles are to be incorporated into an alumina matrix, they will experience high temperature when the composite body is fired.

To minimise the temperature and firing time needed for the densification of the composite green body, easily sinterable alumina should be used. An obvious way to achieve this is to use alumina powders consisting of nano-sized particles.

As discussed in chapter 2, a further way to reduce both the firing time and temperature is to start off with green compacts that are as dense as possible. 'Wet' processing e.g. slip casting or filter casting, gives superior green density. As formation rate of filter cake (the wet green body) increases with decreasing particle size, filter casting is the only feasible option of the two 'wet' processing routes.

1.4 The interrelationship between factors

The interrelationship between the processing variables and the properties of a fired alumina compact is complex. For this survey, some of the stronger dependencies between the final properties and the variables for this work may be approximated as in fig. 1-2.

The factors at the extreme left of the diagram in fig. 1-2 can be controlled during processing. These processing variables determine the quality of the final product.

Green body density is shown as a separate branch in fig. 1-2, as it depends on the green microstructure. The green body has other properties that could have been shown on the diagram. Green density, however, is given special significance in the diagram as it is an easily measurable and frequently measured quantity, which gives a good impression of the general quality of the green body.

Like green density, fired density and strength are shown as separate, dead ending branches. Again, as is the case with green density and green body quality, the fired density is a function of the general quality of the fired compact. Like green density, fired density is an easily measurable property of the fired compact, and it gives a good indication of the general quality of the fired compact. Strength, although important in most other applications, is of lesser importance in the wear performance of a material (personal communication, Hickman). For these reasons, the diagram does not indicate any relationship between wear resistance and fired density or strength (which is not strictly true).

Wear resistance depends strongly on hardness and toughness. Hardness and toughness are indicated in fig. 1-2 as the only two properties that would determine wear resistance (which, again, is not strictly true).

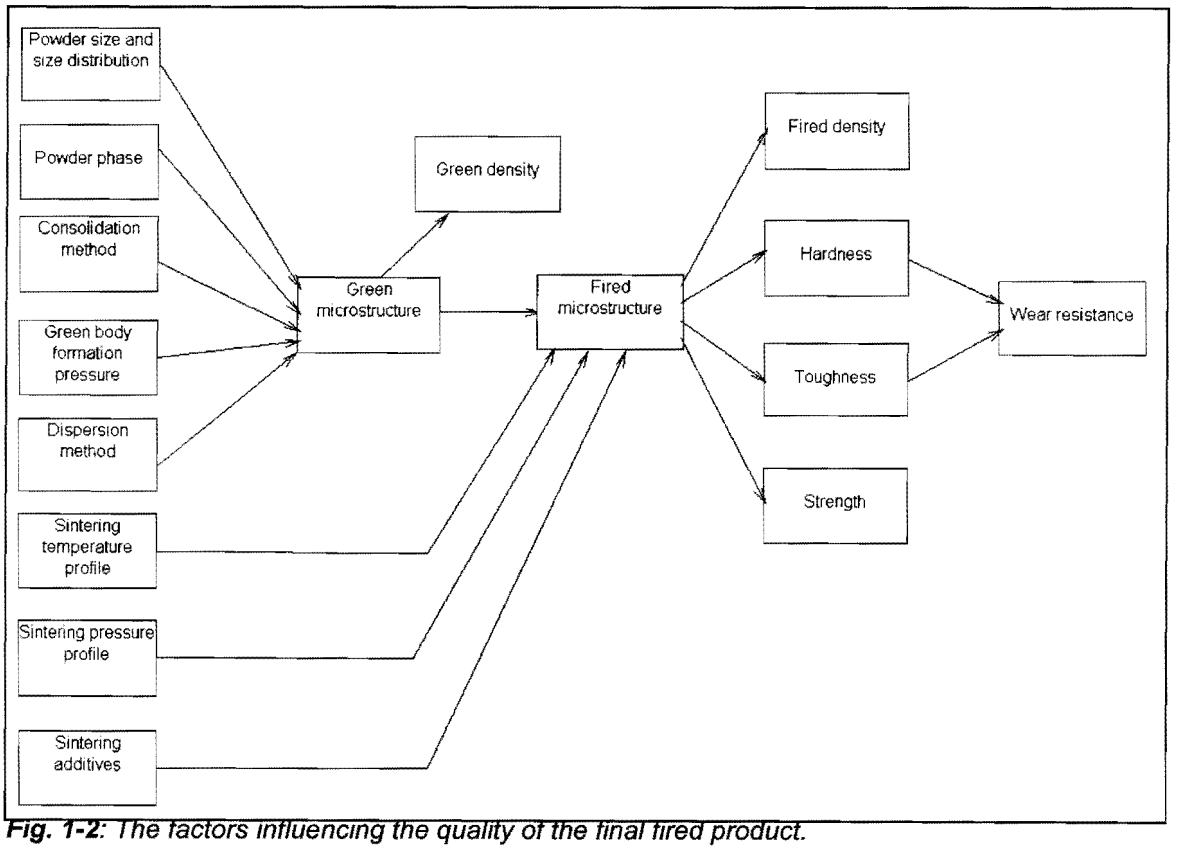

***Fig. 1-2**: The factors influencing the quality of the final fired product.*

1.5 Organisation of thesis

This thesis follows the following structure:

Introduction	Chapter 1
Literature review. Experimental principles.	Chapter 2: Green processing Chapter 3: Firing Chapter 4: Graphitisation Chapter 5: Wear
Preparation of samples	Chapter 6
Characterisation of samples	Chapter 7: Routine characterisation Chapter 8: Microstructure Chapter 9: Hardness and toughness Chapter 10: Wear testing
Discussion	Chapter 11:

1.6 Related document

As part of the requirements of the degree, for which this thesis is a partial fulfilment, a review of literature ('Aspects of the processing of diamond-alumina composites'[§]) relevant to the processing of nano-composites, was also completed. It essentially includes the same material covered in chapters 2 to 5 of this thesis, but it also includes some material that is not covered in this thesis. Excluded material was judged not be relevant enough to the experimental work reported here, but may nonetheless be useful in future evaluation of nano-composites.

[§] Copies with R. Fries of the Diamond Research Laboratory of De Beers and F. K. Bader of the Department of Materials Science of the University of Pretoria.

Chapter 2: Green processing

2.1 Introduction

This chapter primarily gives an overview of literature deemed relevant to the green processing of diamond-alumina.

Fabrication of ceramics from powders comprises two steps. The first step is green processing where the raw powder is formed into the so-called green body. A green body should roughly have the required shape of the desired final product and it has to stand up to some handling. In the second step, the green body is fired to bond the constituent particles and give the product its final strength.

Filter casting was chosen from several options as the green wet processing route to be used in this study, as discussed in the following section (section 2-2).

Literature references in this chapter were chosen for their relevance to the processing of suspesions of submicron suspensions. The experimental conditions of references are summarised in table 2-1 at the end of the chapter.

2.2 Motivation for filter casting

Green processing can be performed in various ways. For the purpose of discussion, the possible methods of green body formation are divided into 'dry' and 'wet' processing routes. In fig. 2-1 some green body formation methods are illustrated. Dry pressing is a common 'dry' processing route. In dry pressing, a dry powder is pressed into shape in a die. 'Wet' processing includes methods like slip casting, filter casting, and centrifugal casting. In slip casting, a suspension ('slip') of particles is poured into a porous mould. The suspending liquid is withdrawn into the mould by capillary force, eventually leaving the consolidated particles in the mould. After total consolidation the wet green body is removed from the mould and dried. The mechanism of filter casting is similar to slip casting. In filter casting the suspending liquid is filtered from the suspension by the application of pressure, followed by the drying of the wet green body. In centrifugal casting, the particles in a suspension are forced to settle from the suspension by centrifugation.

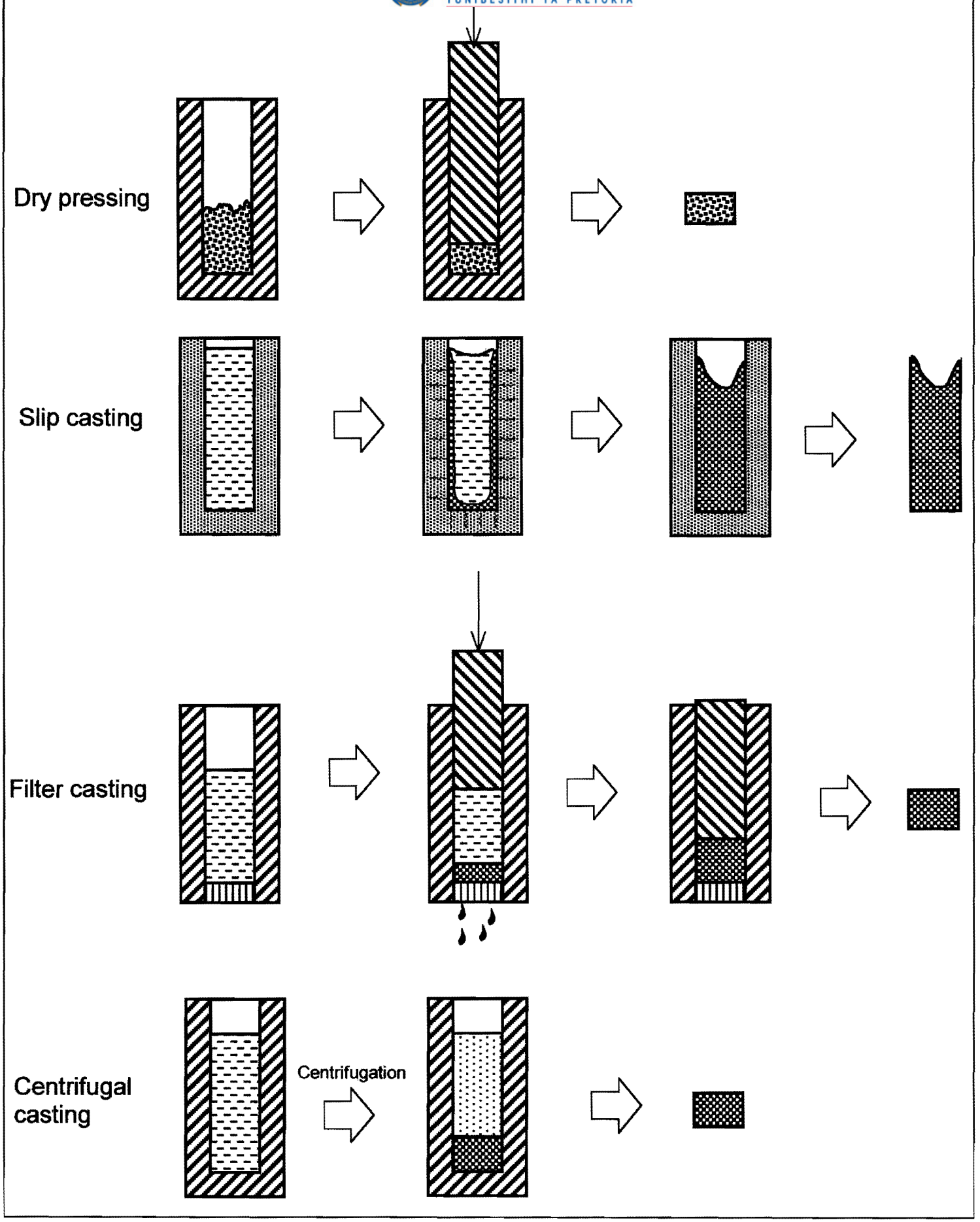

***Fig. 2-1**: Diagrammatic comparison of green body formation methods.*

A green body should have a compact particle arrangement, but particles should be evenly distributed. Uneven distribution is usually due to so-called hard agglomerates that were originally present in the raw powder and were not broken during green processing. If the green body is not compact, a longer firing time or higher firing temperature might be required to fully densify the compact in the firing step. In the case of diamond-alumina composites, these more aggressive firing conditions might lead to damage to the diamond particles, as is discussed in chapter 3. If particles are unevenly distributed, the fired body might also have an uneven microstructure of inferior quality.

The compactness of particle arrangement is easily evaluated by measuring the green body's density. Even distribution is not defined and measured as easily. A possible way of quantifying the evenness of distribution is by mercury porosimetry, as was done by Roosen and Bowen (1988). The presence of areas where particles are more closely associated, which corresponds with an uneven microstructure, would show up as larger volumes of coarse pores. The principles of mercury porosimetry are discussed in section 2.3.1.

Roosen and Bowen showed that 'wet' processing is generally superior to dry processing, both in terms of achieving maximum green density and in terms of achieving a finer green structure, provided that particles are properly dispersed. A detailed discussion of the conditions necessary for proper dispersion is beyond the scope of this work, but alumina disperses well in suspensions of low pH of around 4. In fig. 2-2 it is shown that wet processed suspensions of low pH (less than 4.5, i.e. well dispersed) gave green bodies with relative densities of greater than 60 %, whereas no dry pressed green bodies did.

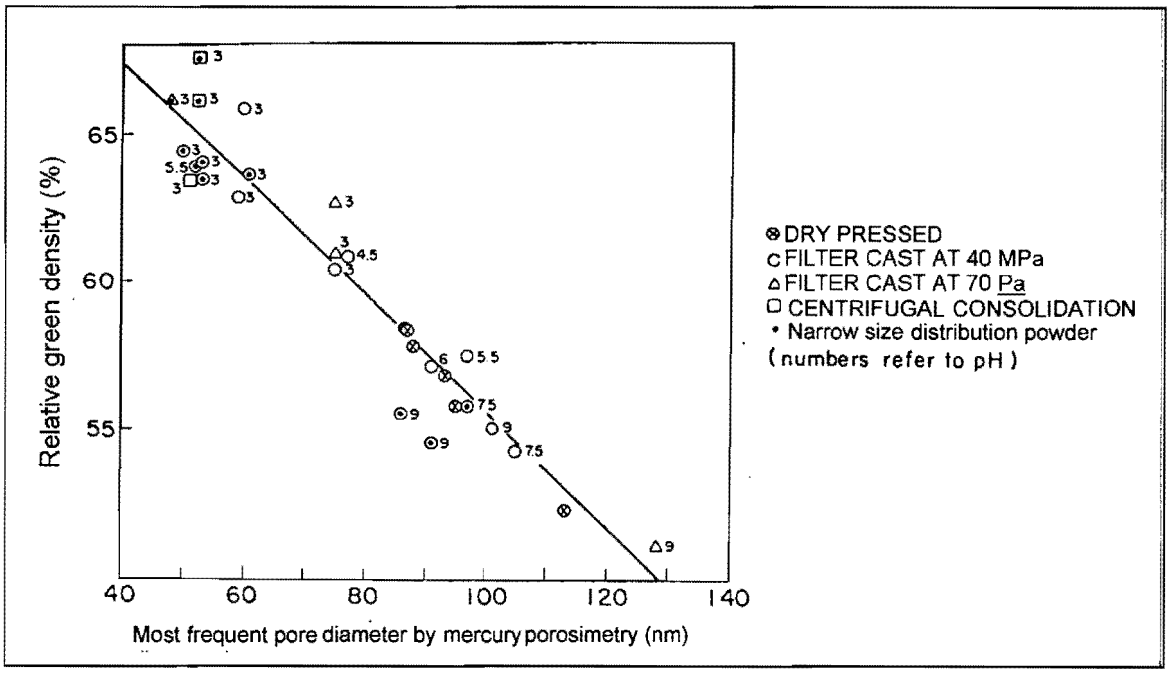

***Fig.2-2**: Green density as a function of green microstructure. The data points were determined with different consolidation methods (both 'wet' and 'dry') and under varying conditions. Suspensions were prepared from two powders: A narrow and a wide particle size distribution. (From Roosen and Bowen, 1988). Suspensions with pH values ~4 can be considered to be well dispersed.*

Having shown that 'wet' processing is preferable to dry processing, one is left with the choice of the specific 'wet' route, i.e. slip casting, filter casting or centrifugal casting. Since equipment for slip casting and filter casting are easy to manufacture and operate, centrifugal casting is not a good choice. This leaves slip casting and filter casting. The rate of consolidation in both slip casting and filter casting is determined by the size of the suspended particles (see section 2-4). Suspensions of finer particles take longer to consolidate, with the time required for the consolidation of the same volume of suspension being inversely proportional to the square of particle size:

$$t_{fin} \propto \frac{1}{d_{part}^{-2}} \quad ‡ \qquad (2\text{-}1 \,/\, A1\text{-}40^{§})$$

Slip casting is commonly used to process powder with coarse (roughly larger than 1 μm) particles. However, with the particles used in this study being an order of magnitude smaller than the usual micron-sized particles, time required for slip casting would have been in the order of 100 times longer than that required for micron-sized powders. This left filter casting as the chosen green processing route for this study.

2.3 The measurement of green properties

2.3.1 Density

The density of non-porous samples is easily measured by immersion in water (the 'Archimedes method'), with the density given by

$$[\text{Density}] = \frac{[\text{Weight in air}] \times [\text{Density of water}]}{[\text{Weight in air}] - [\text{Weight in water}]} \qquad (2\text{-}2)$$

The density of porous samples (like green bodies) cannot be measured in this way, as intrusion in the pores would give a false value for the immersed weight. Instead, the fact that pores in a wet green body are completely filled with water was used to approximately determine green density. Density of a green body relates to its dry and wet weight as follows[#]:

$$[\text{Green density}] = \frac{[\text{Dry weight}]}{\frac{[\text{Wet weight}]-[\text{Dry weight}]}{[\text{Density of water}]} + \frac{[\text{Dry weight}]}{[\text{Particle density}]}} \qquad (2\text{-}3)$$

Conceptually it is useful to express density relative to the true density, i.e.

---

‡ Derived in appendix A1.

§ The second number "A1-40" refers to the number used in appendix.

$[\text{Green density}] = \frac{[\text{Dry weight}]}{[\text{Total volume}]} = \frac{[\text{Dry weight}]}{[\text{Volume of pores}] + [\text{Volume of solids}]} = \frac{[\text{Dry weight}]}{\frac{[\text{Wet weight}]-[\text{Dry weight}]}{[\text{Density of water}]} + \frac{[\text{Dry weight}]}{[\text{Particle density}]}}$

$$[\text{Relative density}] = \frac{[\text{Measured density}]}{[\text{True density}]} \qquad (2\text{-}4)$$

2.3.2 **Mercury porosimetry** (Smith, 1981)

Mercury does not wet most surfaces. This implies that pressure is needed to force mercury into pores. By immersing a sample in mercury and increasing pressure, mercury is forced into smaller and smaller pores. The pressure P required to force mercury into pores of size d_{pore} is

$$P = -\frac{4\sigma\cos\theta}{d_{pore}} \qquad (2\text{-}5)$$

with θ the contact angle, as illustrated in fig. 2-3, and σ the surface tension of the mercury. In mercury porosimetry, 140° is normally used for θ on any surface. Surface tension of mercury is 0.47 N/m (Atkins, 1990). Substituting these values in equation 2-5 gives

$$d_{pore} = \frac{1440}{P} \qquad (2\text{-}6)$$

with d in µm if P is in kPa. By measuring the volume of mercury penetrating at a given pressure, pore size distribution can be determined.

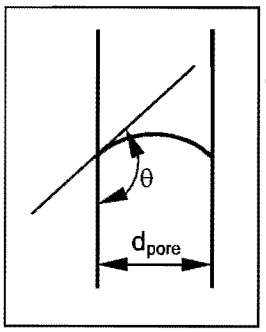

***Fig. 2-3**: Mercury penetration in a circular pore.*

2.4 Consolidated layer growth

At the onset of filtration, particles in suspension are free to follow streamlines that form, and they move towards openings in the filtration medium. There some particles bridge and clog entrances to channels in the medium. This is a beneficial process since it blocks the migration of any further particles through the medium (Heertjes, 1964). Pores in the filtration medium therefore need not be smaller than suspended particles.

The initial clogging action is followed by the growth of the consolidated layer. The thickness of the consolidated layer L_{cl} at a time t is given by‡

$$L_{cl} = \sqrt{\frac{2\mathbb{k}\Delta P t}{z\mu_{sl}}} \qquad (2\text{-}7 \,/\, A1\text{-}6)$$

where ΔP is the applied pressure difference across the filtration apparatus as illustrated in fig. 2-4. μ_{sl} is the viscosity of the suspending liquid. z is given by

$$z \equiv \frac{Q_{filt}}{Q_{cl}} = \frac{\varepsilon_{susp} - \varepsilon_{cl}}{1 - \varepsilon_{susp}} \qquad (2\text{-}8 \,/\, A1\text{-}20)$$

with Q_{filt} and Q_{cl} respectively the volume of filtrate and consolidated layer. ε_{susp} is the volume fraction of liquid in the unconsolidated suspension and ε_{cl} is porosity of the consolidated layer. $\mathbb{k}$ is the permeability of the consolidated layer. Permeability can be experimentally determined but it can also be predicted from other properties of the consolidated layer.

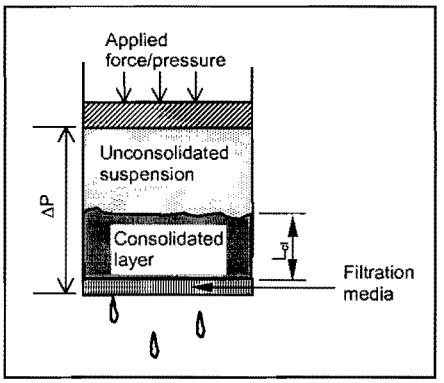

***Fig. 2-4**: Consolidated layer growth.*

Equation 2-7 van be rewritten to predict the time needed to consolidate a given load of suspension. The alternative formulation was used in this study to determine the required 'dwell time' for filter casting. If a filtration device is initially loaded to a depth $L_{susp,0}$ then the time needed to fully consolidate a suspension is‡

$$t_{fin} = \frac{z\mu_{sl}L_{susp,0}^2}{2(1+z)^2\mathbb{k}\Delta P} \qquad (2\text{-}9 \,/\, A1\text{-}10)$$

It is is possible to determine t_{fin} because z is known from equation 2-8, μ_{sl} can be approximated as the viscosity of water (c. 1 mPa.s), $\mathbb{k}$ can be approximated as shown in the following paragraph, and ΔP is known from the filtration device set-up.

There are a variety of models which predict permeability but the Carmen-Kozeny equation is most commonly used. The Carmen-Kozeny model gives permeability as‡

‡Derived in appendix A1.

$$\mathfrak{K} = \frac{\varepsilon_{cl}^3}{\theta\tau^2(1-\varepsilon_{cl})^2 S^2} \qquad (2\text{-}10 \,/\, A1\text{-}33)$$

with ε_{cl} the porosity of the consolidated layer, τ its tortuosity, S its specific surface area, and θ the Poiseuille factor. For the conditions of this work the following is true[‡]

$$\mathfrak{K} \approx 1\times 10^{-3} d_{part}^2 \qquad (2\text{-}11 \,/\, A1\text{-}38)$$

Fig 2-5 gives the progress of consolidated layer growth, as predicted by equation 2-10 and 2-7, for a case typical of this study.

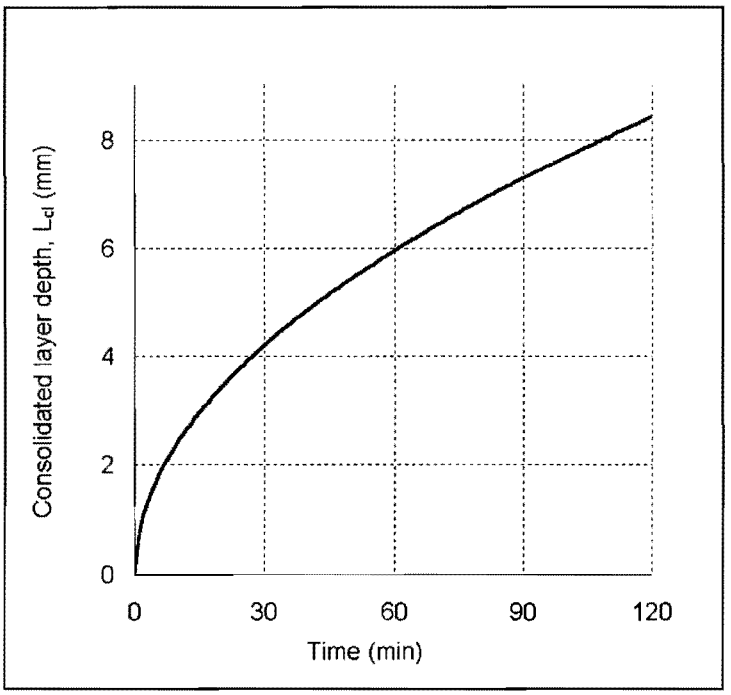

***Fig. 2-5**: Consolidated layer growth for the typical values of ε_{cl} = 40 %, ε_{susp} = 70 %, μ_{sl} = 1 cP, d_{part} = 100 nm and ΔP = 0.5 MPa.*

2.5. Factors affecting green structure

2.5.1 Relationship between green texture and green density

In exhaustive work on green body formation, Roosen and Bowen (1988) investigated the effect various factors in cake formation. They quantified the texture of the green microstructure by mercury porosimetry (fine pores corresponding with a finer microstructure) and found the relationship already shown in fig. 2-2 where a finer structure is shown to correlate with a denser green body.

[‡] Derived in appendix A1.

2.5.2 Solids volume fraction in suspension

In filter casting, there are no clear trends on the effect of solids fraction in the suspension on the density of the green body formed from it. The results of Hampton *et al* (1988) and Velamakanni and Lange (1991) as given in fig. 2-6 and 2-7 are in conflict, giving both positive and negative trends. As Hampton *et al* (1988) and Velamakanni and Lange (1991) used different dispersion methods (deflocculent and pH, see table 2-1), these trends cannot really be compared. As seen in fig. 2-6 and 2-7, variations are smaller than 3 percentage points for both references. To a good approximation, one can therefore state that solids fraction does not have a significant effect on green density.

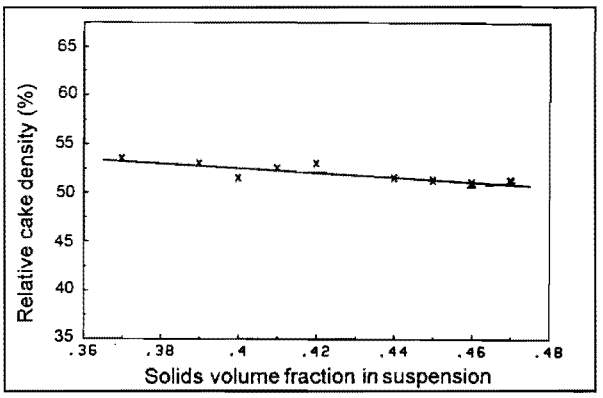

***Fig. 2-6**: The effect of solids volume fraction in suspension on green density as given by Hampton* et al *(1988).*

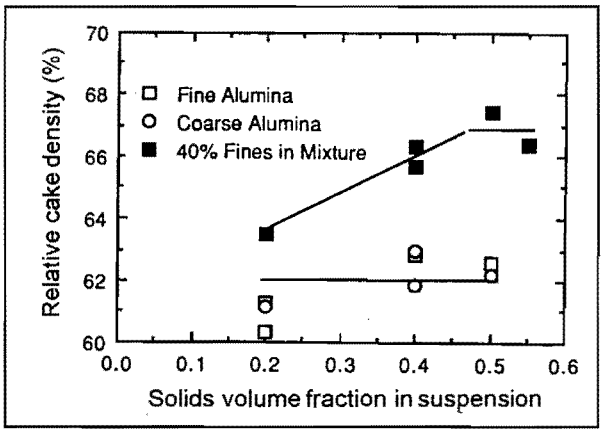

***Fig. 2-7**: The effect of solids volume fraction in suspension on green density as given by Velamakanni and Lange (1991).*

2.5.3 Particle size distribution

A narrow distribution of particle sizes is desirable from a firing point of view, since it leads to fired microstructures having a narrow grain size distribution. Fired compacts with narrow grain size distributions generally have preferable qualities. However, higher green density occurs with wide distributions of particle sizes, as fine particles can fill the voids between coarser particles, as illustrated in fig. 2-8.

In work done specifically on filter casting Smith and Haerle (1995) and Smith and Haber (1995) used the particle distribution function

$$F(d_{part}) = \frac{d_{part}^{k_{SH}} - d_{smallest\ part}^{k_{SH}}}{d_{largest\ part}^{k_{SH}} - d_{smallest\ part}^{k_{SH}}} \qquad (2\text{-}12)$$

where F is the cumulative fraction of particles smaller than a d_{part}. They showed experimentally that the closer the modulus k_{SH} is to 0.37 the greater the green density. This implies that particle size distribution can be adjusted to give a maximum green density (on the condtion that suspensions are well dispersed).

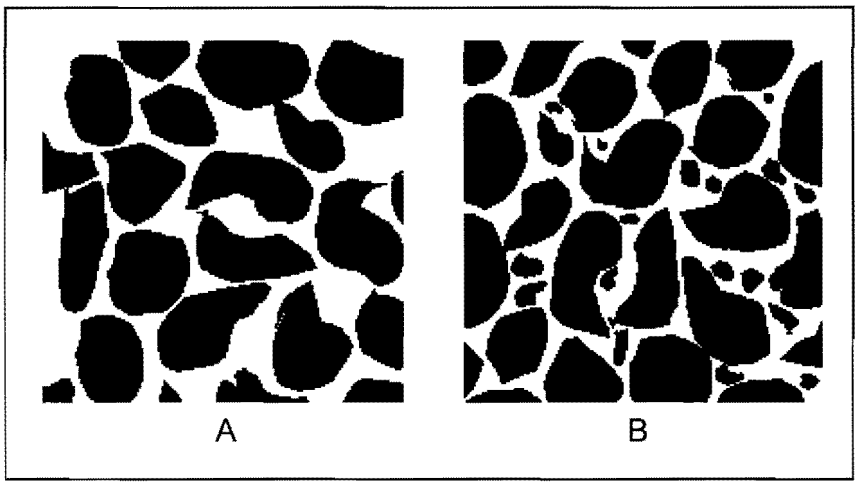

***Fig. 2-8**: Particle packing with narrow (A) versus wide (B) size distributions. The wide size distribution is seen to fill space more efficiently.*

2.5.4 Pressure

Lange and Miller (1987) found no significant dependance on pressure for dispersed suspensions. With flocculated suspensions, however, they found that cake density increased considerable with increasing pressure as seen in fig. 2-9.

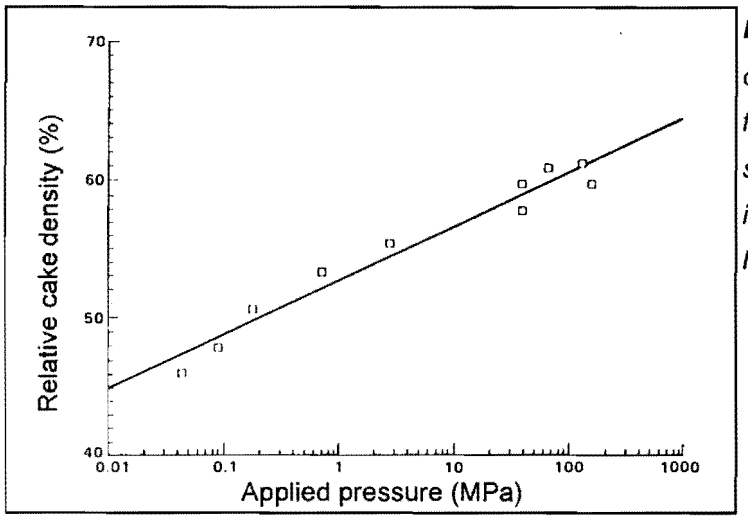

***Fig. 2-9**: The pressure dependence of solids loading on green density for flocculated suspensions subjected to filter casting at the indicated pressure (Lange and Miller, 1987).*

Straight filtration of flocculated suspensions at low pressure does therefore not yield green densities comparable to those from the filtration of dispersed suspensions at equally low pressure. This is unfortunate, since green bodies formed from flocculated suspensions have the advantage of experiencing less seperation with regard to particle size and components. In flocculated composite suspensions, particles of different components and sizes are fixed into flocs which do not break down during consolidation into the cake. The cake would therefore retain the state of mixture that existed in the unconsolidated flocculated suspension. In filtration of dispersed suspensions this advantage is lost, and particles of different components are free to separate under influence of other forces such differences in their density.

Prevention of component separation by using flocculated suspensions was not employed in this study.

2.5.5 Suspension viscosity

A detailed discussion of this effect is beyond the scope of this survey.

Although suspension viscosity itself is a function of other factors it can give one an idea of the quality of dispersion. Low viscosity is generally characteristic of well-dispersed suspensions which leads to denser compacts (Smith *et al*, 1994; Chou and Senna, 1987).

2.6. Recovery strain

Lange and Miller (1987) also conducted research to determine the amount of deformation of green bodies after filtration, i.e. upon removal of pressure. In fig. 2-10 recovery strain between green bodies formed from flocculated and dispersed suspensions is compared. It can be seen that green bodies formed from flocculated suspensions show gradual 'recovery' of up to 2.8 %, while green bodies formed from dispersed suspensions 'recover' rapidly and 'recover' to the slightly smaller extent of 2.2 %. It cannot be imagined that all sections of a wet green compact would always recover at the same rate in all its sections. The recovery strain effect could therefore lead to cracking of the wet green compact.

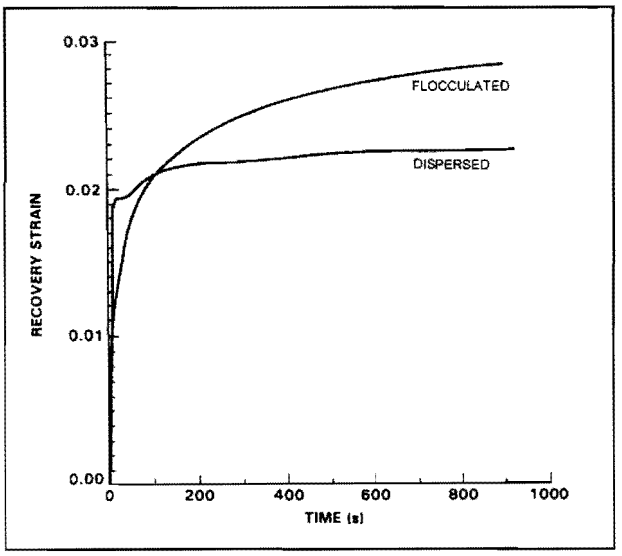

***Fig. 2-10**: Strain 'recovery' of green bodies formed from flocculated and dispersed suspensions after unloading from a filtering pressure of 80 MPa (Lange and Miller, 1987).*

2.7 Non-homogeneity in green bodies

2.7.1 Seperation of particle sizes

The consolidated layer growth kinetics in section 2.4 assumes a homogeneous consolidated layer by accepting a pressure gradient and constant porosity. In practice neither of these assumptions may hold.

Hampton *et al* (1988, 1992), for instance, conducted work on fine particle migration during filtration. They filtered suspensions of mixtures of fine and coarse particles and found that substantial migration of fine particles towards the filtrate withdrawal side of the cake occurred. Fig. 2-11 shows a substantial concentration of fine particles at the bottom of the cake after filtration.

2.7.2 Seperation of composite suspension components

Lange and Miller (1987) and Aksay *et al* conducted filtration with suspensions made of alumina zirconia composite powders. No mention was made of segregation of alumina and zirconia. Chang *et al* (1991) specifically investigated the mass segregation of alumina-zirconia composites, unfortunately with centrifugal consolidation. They found that mass segregation does not occur with flocculated and coagulated suspensions but that it does occur with disperse suspensions with a distinct higher concentration of zirconia towards the bottom of the cake.

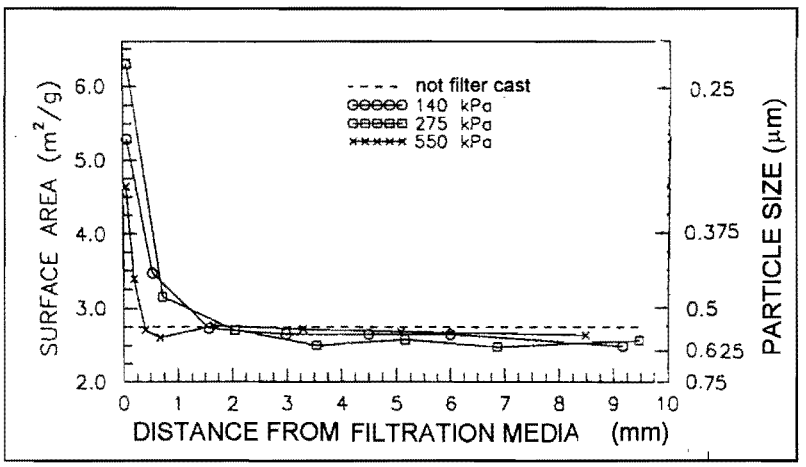

***Fig. 2-11**: Surface area and particle size versus distance above cake bottom for alumina. Pressures are the filter casting pressures. Surface area was determined by BET. The indicated particle size is the size based on the surface area (d_{part}= 6/ś). (Modified from Hampton* et al, *1992).*

***Table 2-1**: Some of the experimental conditions of authors referred to in chapter 2. The differentiation between 'fine', 'intermediate' and 'coarse' is arbitrary and does not have any special significance.*

Authors		Hampton *et al* (1988)	Hampton *et al* (1992)	Velamakanni and Lange (1991)	Lange and Miller (1987)		Roosen and Bowen (1988)				Smith and Haerle (1995)	Smith and Haber (1995)
Description of work referred to		Effect of solids fraction in suspension	Fine particle migration	Effect of solids fraction in suspension	Effect of pressure on green bodies formed from dispersed suspensions	Effect of pressure on green bodies formed from flocculated suspensions	Effect of green microstructure on green density				Effect of particle size distribution on green density	
Suspension dispersion method		Commercial Deflocculent 'Darvan 7'		pH 4 by HNO_3/NH_4OH	pH by HCl/ NH_4OH	pH 2 by HCl	pH 3- 9 by HNO_3/NH_3				Tetrasodium pyrophosphate	
Suspension flocculation method		Not applicable		Not applicable	pH by HCl/ NH_4OH	pH 8.5 by NH_4OH					Not applicable	
Fine powder	d_{50}	0.4 µm	0.4 µm	0.3 µm	0.4 µm	0.4 µm	0.61 µm*#	0.19 µ m*#	0.38 µm‡†	0.132 µm‡†	0.6 µm	
	d_{90}	2 µm	2 µm	0.9 µm	1 µm	1 µm					3 µm	
Intermediate powder	d_{50}										5 µm	
	d_{90}										20 µm	
Coarse powder	d_{50}	Not applicable	4 µm	1 µm	Not applicable						3 µm	
	d_{90}	Not applicable	8 µm	2 µm	Not applicable						40 µm	
Mixture of fine and coarse powders	d_{50}	Not applicable	?	0.9 µm	Not applicable							
	d_{90}	Not applicable	?	1 µm	Not applicable							
	Percentage fines in mix	Not applicable	20 %	40 %	Not applicable							
Particle size determination method		X-ray sedimentation	X-ray sedimentation	X-ray sedimentation	Sedimentation?	Manufacturer claim	Stokes settling	N_2 adsorption	Stokes settling	N_2 adsorption	X-ray sedimentation	
Forming technique		Slip casting	Filter casting	Filter casting	Filter casting		Filter casting, centrifugal casting and dry pressing.				Filter casting	Slip casting

* The same powder characterised in two ways.

‡ The same powder characterised in two ways.

Broad size distribution powder.

† Narrow size distribution powder.

Chapter 3: Firing

3.1. Introduction

Green processing is followed by firing of the compact. During firing particles are bonded and voids between particles shrink. Bonded particles join together to form grains. Whereas bonding and elimination of voids are beneficial processes, as they bring about better mechanical properties, grain growth is detrimental, but unavoidable.

Heat treatment is conventionally divided into 'initial', 'intermediate' and 'final' stages, as illustrated in fig. 3-1. The initial stage is also referred to as 'neck growth'. It ends when particles are intersected by true pores and not mere voids as during the initial stage. No grain growth occurs during the initial stage. The intermediate stage ends when pores are pinched of into isolated pockets. Limited grain growth occurs during the intermediate stage. In the final stage the isolated pockets are eliminated and larger grains grow by incorporating smaller pores. Grains continue to grow after the elimination of pockets. (Coble, 1961).

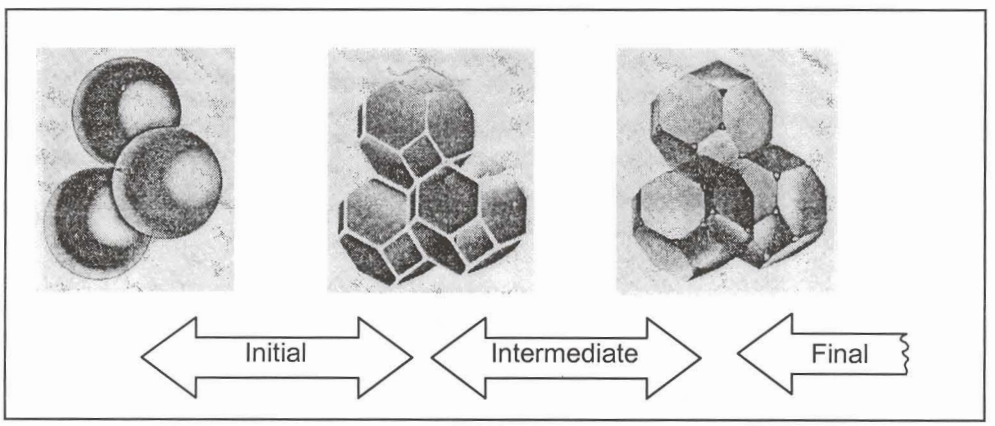

***Fig. 3-1**: The stages of heat treatment. After Coble (1961).*

Heat treatment may be enhanced by the application of either unidirectional pressure ('hot pressing') or isostatic pressure ('hot isostatic pressing' or 'HIPping').

In this work 'firing' is used as a broad term to refer to any form of heat treatment, be it pressureless sintering, hot pressing, or HIPping. The term 'sintering' is used here to specifically refer to pressureless sintering.

No details of the pre-firing processing are given in this chapter. To limit the amount of details only the initial particle size and green density are quoted. These two variables should give a sufficient representation of the pre-firing condition of the compact.

As in the chapter on green processing, literature reviewed here were chosen for its relevance to processing of similar alumina powder to that used in the experimental part of this work. Literature of work on submicron powders was therefore chosen for review.

3.2 Reduction of firing temperature by reducing particle size

Table 3-1 compares some results of pressureless sintering of compacts of submicron particle powders. It illustrates the possibility of reducing sintering temperature by reducing particle size, while still achieving high density. Of special interest is the result of Yeh and Sacks (1988), who claimed to have achieved 100 % relative density in under 2 hours at only 1 150 °C in air.

***Table 3-1**: Particle sizes and sintering temperatures compared. Note that all fired densities are ≥ 95 %.*

Powder		Run-up to sintering	Relative density at start of sintering (%)	Sintering		Relative fired density (%)	Reference
Average particle size (nm)	Characterisation			Temperature (°C)	Time (h)		
60	BET	None	70	1 150	2	100	Yeh and Sacks (1988a)
300	Not stated	Heating at 4 °C/min.	Not stated. Green body formed with dry pressing.	1 450	2	95	Kwon *et al* (1987)
				1 500		97	
				1 550		98	
~ 400	Median Stokes	None	73	1 260	12	96	Yeh and Sacks (1988b)
			65				
			73?	1 340		99	
			65?				
720	Manufacturer	• Ambient to 275 °C in 0.3 h • 0.5 h at 275 °C • 275 to 900 °C in 1 h • 900 to 1600 °C in 0.25 h	80	1600	1.5	98	Cameron and Raj (1990)
			76				

3.3 Less aggressive firing by controlling green structure

Roosen and Bowen (1988) found experimentally that green bodies formed through a 'wet' processing route densify more easily than those formed by dry pressing. In fig. 3-2 the temperature of the maximum shrinkage rate of green bodies formed through dry pressing and 'wet' routes are compared. It can be seen that the temperature of maximum shrinkage is more than 50 °C higher for dry pressed green bodies than for 'wet' processed green bodies of a similar green structure. In addition to this, a dramatic drop in temperature of maximum shrinkage occurs below an average pore size of 51 nm for green bodies formed through wet routes. As 'dry' and "wet' data follow the same trend in the relationship between green texture and green density (fig. 2-2), this effect cannot be explained in terms of green density alone. Roosen and Bowen suggest two possible explanations for this effect:

1) Cappilary forces during drying improve the green microstructure as compared to 'dry' processed samples, or

2) Particles are 'cemented' to each other due to hydrolysis during 'wet processing', which enhances densification.

Further evidence for the beneficial effect of using fine textured green bodies are shown in fig. 3-3, where finer textured green bodies are seen to result in higher fired densities under the same firing conditions.

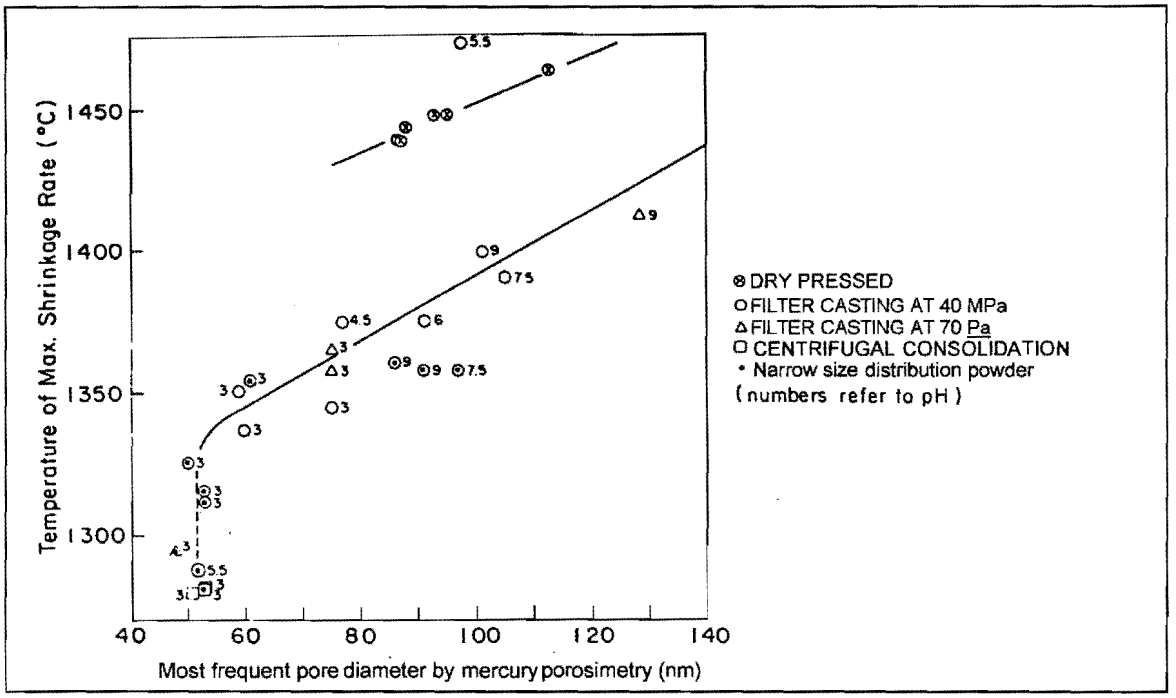

***Fig. 3-2**: Temperature of maximum shrinkage rate compared to green microstructure. Heating rate 10 °C/min. See table2-1 for green processing details not mentioned on graph. (Roosen and Bowen, 1988).*

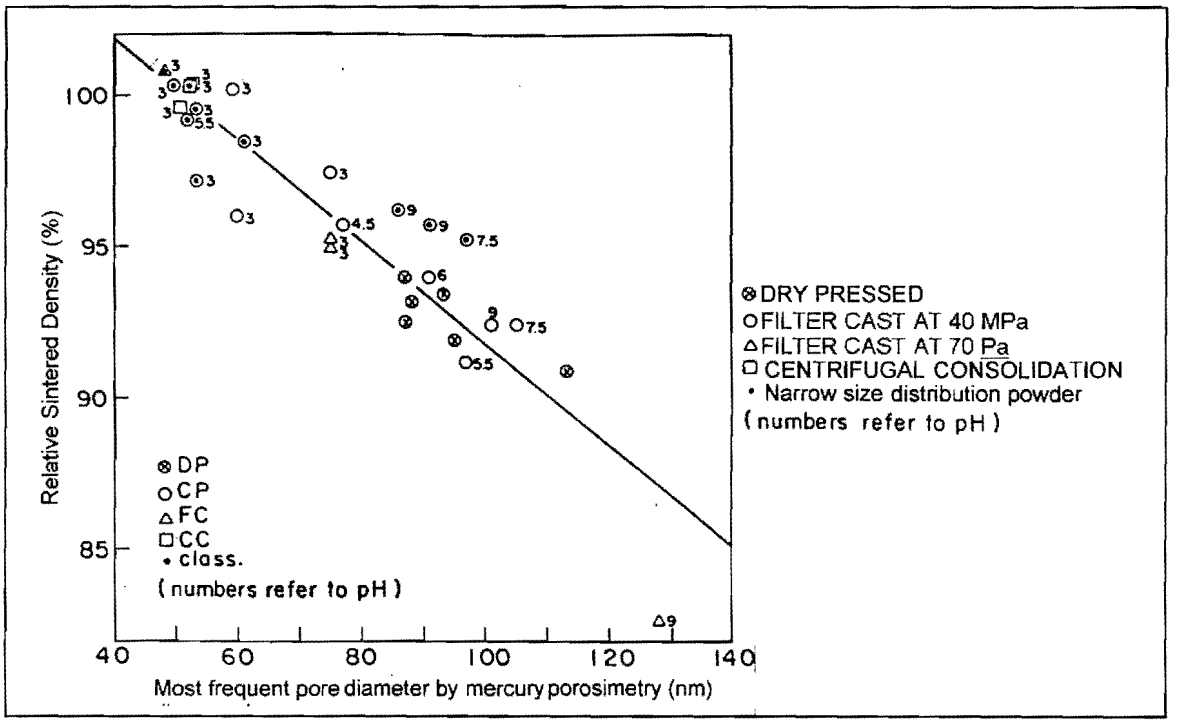

***Fig. 3-3**: Sintered density related to green microstructure. Heating rate 10 °C/min and dwell at 1 500 °C for 30 min. See table2-1 for processing details not mentioned on graph. (Roosen and Bowen, 1988).*

3.4 The influence of powder size distribution on grain size and fired density

As long as finer particles are free to move to fill the voids between larger particles (as in well-dispersed suspensions), broad size distributions lead to more efficient packing of particles in the green body. It is difficult for finer particles to penetrate unfilled voids between larger particles during dry pressing, while more rearrangement of particles is possible during 'wet' processing. In wet processing, smaller particles would therefore be able to penetrate voids between larger particles. This would lead to a greater green density, which should lead to faster densification during firing. However, it is generally accepted that powders with narrow size distribution produce compacts that are superior in terms of having narrow grain size distribution and the ability to densify at lower temperatures. Yeh and Sacks (1988b) criticised this view, citing a lack of evidence. In Yeh and Sacks's work (1988b), a broadly and narrowly distributed powder (fig. 3-4) were dispersed by controlling pH at ~ 4. Both powders have an average particle size of 0.4 μm. The suspensions were slip cast, and the resulting green bodies were sintered at a range of temperatures between 1 180 and 1 340 °C. As can be expected the broadly distributed powder densified faster (fig. 3-5). Contrary to the conventional view though, in this instance it was indeed found that narrow size distribution did not have an advantage above a broad distribution in terms of fired microstructure, showing a similar average grain size and grain size distribution (fig. 3-6 and 3-7).

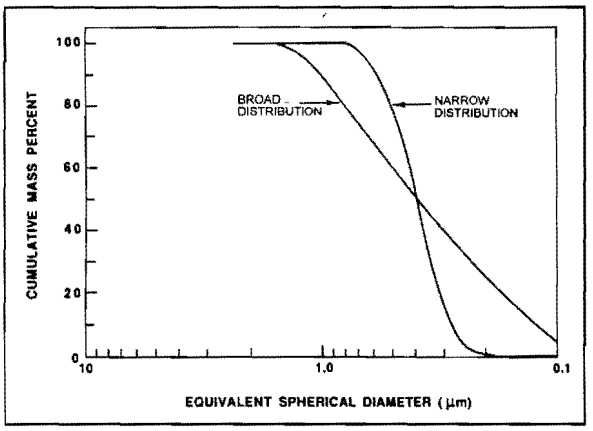

***Fig. 3-4**: X-ray sedimentation data for the powders used by Yeh and Sacks (1988b). Note that <u>different</u> powders was actually used; the difference in distribution is not due to different suspension preparation routes, i.e. the difference was not due to differences in the breakdown of agglomerates.*

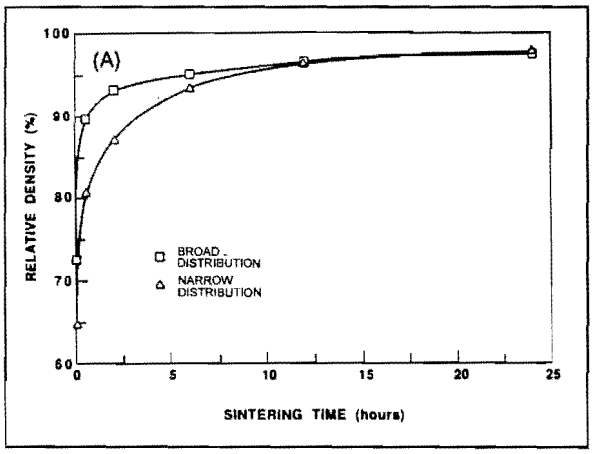

***Fig.3-5**: A comparison between the densification of green compacts prepared from powders with broad and narrow size distribution. The compacts were sintered at 1 260 °C. (Yeh and Sacks, 1988b.) Note the difference between starting, i.e. green density, of the two compacts.*

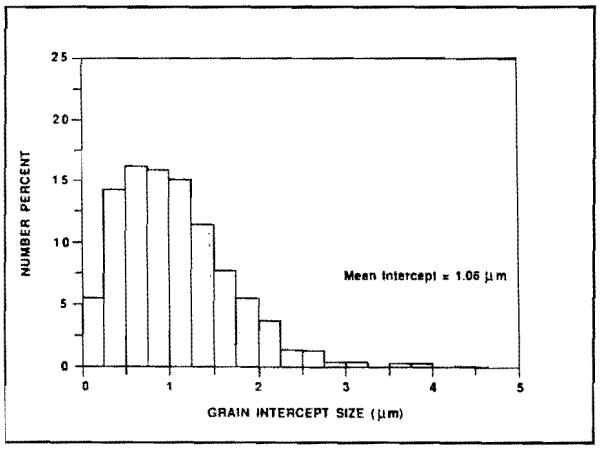

***Fig. 3-6**: Histogram for a sample sintered for 48 h at 1 340 °C prepared with powder with a narrow size distribution (Yeh and Sacks, 1988 b).*

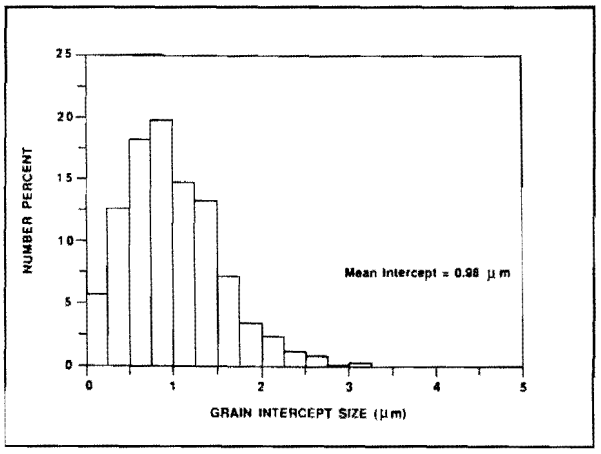

***Fig. 3-7**: Histogram for a sample prepared as in fig. 3-5, but with broad size distribution powder (Yeh and Sacks, 1988 b).*

3.5 The effect of pressure (under HIP) on grain size

Applied pressure during sintering provides an additional means of reducing firing temperature and time. Pressure speeds sintering up by enhancing interparticle contact. Unfortunately, enhanced interparticle contact also aids grain growth.

A specific case of grain growth enhancement by pressure is given by Besson and Abouaf (1991) (fig. 3-8 and 3-9). Their relative green density was 51 % and initial grain size was 0.25 µm. The heating rate up to the constant dwell temperature was 20 °C/min. Grain size showed a linear increase with increasing pressure (fig. 3-8), and an asymptotic increase with time (fig. 3-9).

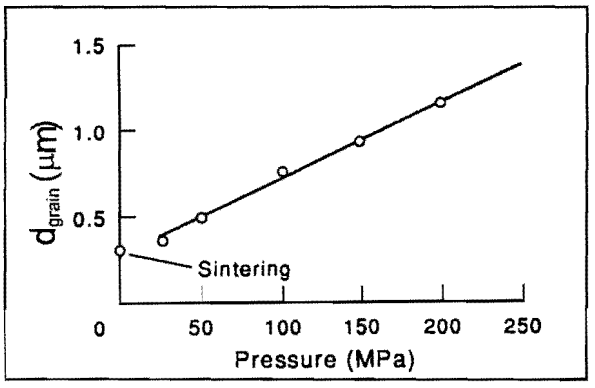

***Fig. 3-8**: Grain size as a function of pressure during HIPping for a dwell of 1 h at 1 300 °C. Final relative density for all data, except at zero pressure, was > 96 %. (Besson and Abouaf, 1991).*

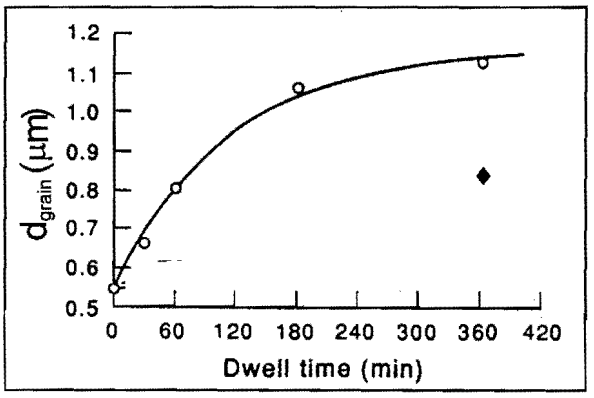

***Fig. 3-9**: Grain size as a function of dwell time during HIPping at 100 MPa and 1 300 °C. ♦ represents the grain size after pressureless sintering. Final relative density for all data was > 96 %. (Besson and Abouaf, 1991)*

3.6 The influence of the temperature and pressure profile (under HIP) on fired density

To provide a quantitative basis of comparison for HIPping results, HIPping data from several sources are collected in fig. 3-10 to 3-13. The progress of density for a variety of conditions is given. A summary of experimental conditions and references for the data presented in fig. 3-10 to 3-13 are given in table 3-2. The data represented for actual HIPping are for relatively large particle sizes, with the result that they are not quite comparable to nano-sized particles. Compacts of nano-sized powders can be expected to densify much faster under the same conditions.

Note that full density sets in rather fast, in less than 20 minutes at 100 MPa (fig. 3-11). It is therefore critical to only HIP for the time necessary for densification, as the only effect on longer HIPping would be grain growth.

***Table 3-2**: The green bodies used in the HIPping results depicted in fig. 3-9 to 3-12.*

Pressure (MPa)	Green body			Reference
	Particle size (nm)	Particle size method	Density at start of densification (% relative)	
50 and 200	500	BET	48?	Uematsu *et al* (1990)
	1 000		56?	
100	< 500	Initial grain size	Not stated	Shin, Orr, and Schubert (1990)
Sintering	60	BET	70	Yeh and Sacks (1988a)
	~ 400	Median Stokes	73	Yeh and Sacks (1988b)

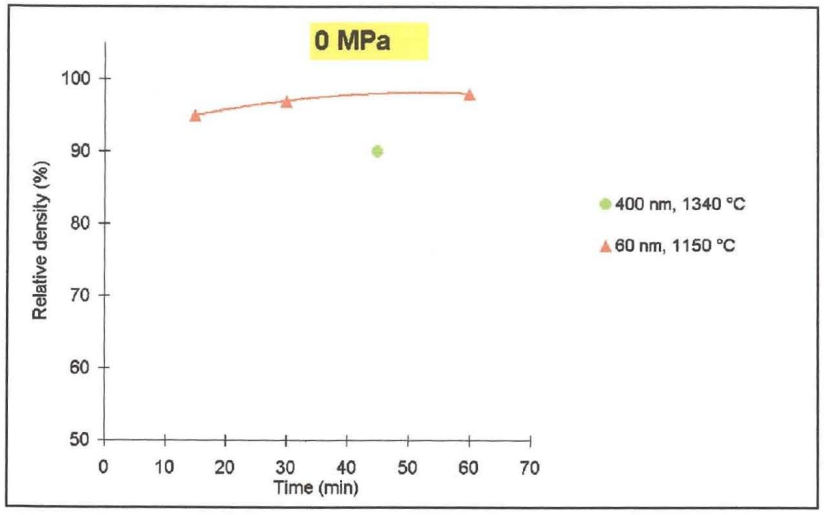

***Fig. 3-10**: Sintering of submicron alumina for comparison with HIPping in fig. 3-10 to 3-12.*

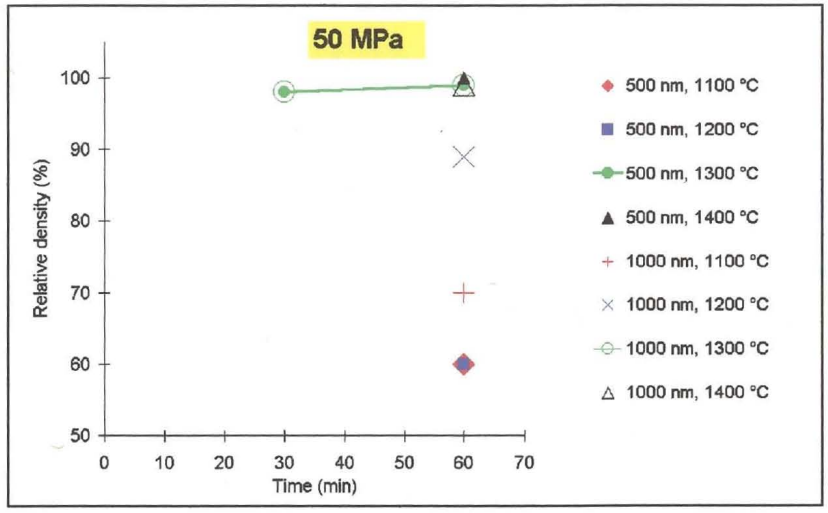

***Fig. 3-11**: HIPping of submicron alumina at 50 MPa.*

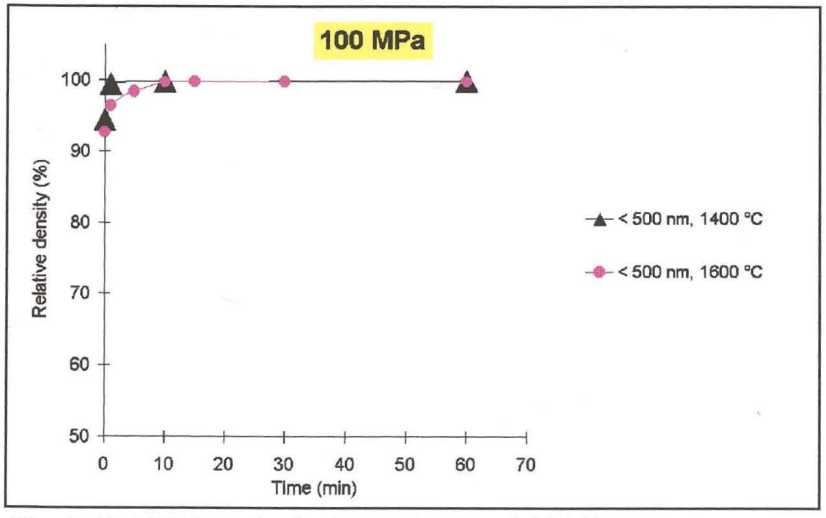

***Fig. 3-12**: HIPping of submicron alumina at 100 MPa.*

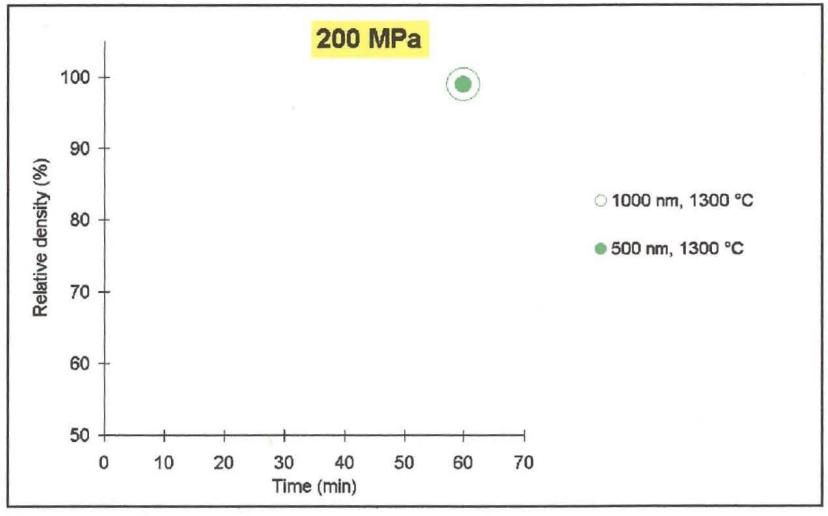

***Fig. 3-13**: HIPping of submicron alumina at 200 MPa.*

3.7 The influence of sintering additives on fired microstructure and density

Magnesia (MgO) and titanium oxide (TiO_2) are commonly used as additives to alumina to improve densification. However, no data were found on the effect of these additives when sintering submicron powders below 1 600 °C.

Dörre and Hübner (1984) also states that MgO inhibits grain growth while TiO_2 promotes it. Whereas this is true of conventional sintering of particles in the micron range at c. 1 600 °C, Dörre and Hübner do not give any specific results for smaller particles at lower temperatures.

Ikegami, Kotani, and Eguchi (1987) conducted work with particles of c. 330 nm (by BET) in diameter. They increased temperature steadily at 10 °C/min to temperatures of up to 1 600 °C followed by quenching (no dwell). For these heating conditions their findings were as follows:

- The rate of densification in the initial and intermediate stages was affected in the order:
  TiO_2 added >> No additives ≈ MgO added.
- Grain sizes at densities greater than 90 % relative were c. 7 μm or larger.
- Grain sizes (not at full density) achieved between 900 and 1 600 °C were in the order:
  No additives ≈ TiO_2 > MgO.

Under the same conditions as above, but with an additional dwell of 1 h at 1 600 °C they found that final density achieved was in the order:

No additives (97 to 98 % relative density),
MgO added (97 to 98 % relative density),
TiO_2 added (99 % relative density).

Chapter 4: Graphitisation

4.1 Introduction

Graphitisation in the diamond-alumina interface was seen as a possible cause of lack of bonding. For this reason, special attention is given to this topic.

Literature on the graphitisation of diamond can be divided into four categories:

- Graphitisation of diamond by itself, i.e. not in contact with any matrix,
- Graphitisation in oxide ceramic matrices,
- Graphitisation in non-oxide ceramic matrices, and
- Graphitisation in metal matrices.

The distinction between oxide and non-oxide matrices is made, since the graphitisation in non-oxide matrices is not applicable to this work. Other oxide matrices might be expected to affect diamond in the same way as alumina due to the presence of an oxygen potential. Non-oxides, of course, do not have an oxygen potential. Non-oxide matrices were therefore not considered in this literature survey. Likewise, metal matrices were ignored.

Graphitisation depends on various factors, including diamond type, pressure, temperature, oxygen partial pressure (Liu and Ownby, 1991), the presence of other forms of chemical attack (Pipkin, personal communication) and even the way of heating (Sozin *et al*, 1992). Of these, the effects of temperature, pressure and oxygen pressure are of relevance in this work and are discussed here.

4.2 Graphitisation of non-integrated diamond

As the pressure-temperature diagram in fig. 4-1 shows, diamond is only metastable at pressures of less than 40 kbar (and below 4000 K), with graphite being the more stable phase. At low temperature the rate of conversion to graphite is, of course, utterly insignificant, as exemplified by very old deposits of natural diamond. At high temperature (> ~ 1 000 °C) the conversion to graphite accelerates significantly.

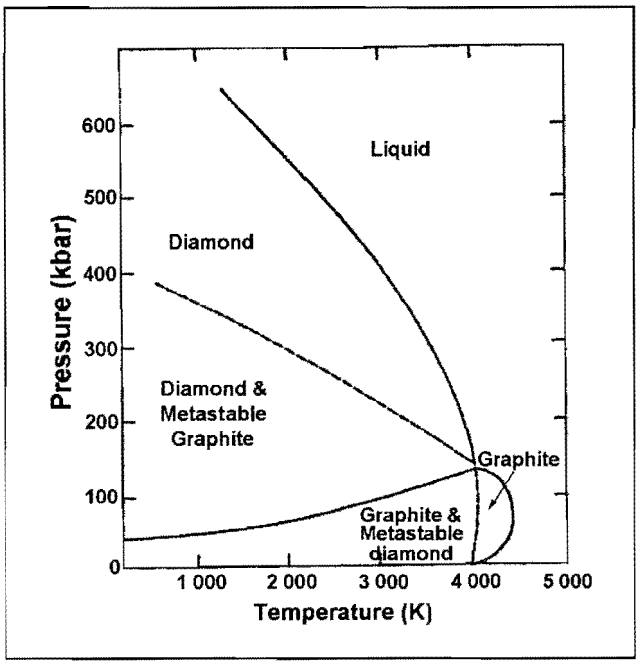

***Fig. 4-1**: Carbon phase diagram (Pierson, 1993). The entire diagram is included for interest; actually the only area of interest falls in the stable graphite area, at the lowest part of the diagram.*

The mechanism of graphitisation seems to be the detachment of singe carbon atoms from the diamond surface, followed by their condensation as graphite. This theory is supported by comparison between the activation energy of graphitisation and the vaporisation energy of diamond. Vaporisation entails detachment of single atoms, as opposed to groups of atoms. Since the activation energy of graphitisation is similar to that of vaporisation, it is likely that graphitisation also entails single atom detachment (Evans, 1979).

Any chemical attack on diamond might induce and accelerate graphitisation (Pipkin, personal communication). Graphitisation accompanies the oxidation of diamond surfaces and oxygen actually seems to catalyse thermal graphitisation (Evans and Phaal, 1962; Evans, 1994a, b). This has the result that the temperature at which graphitisation starts varies with the concentration of surrounding gaseous species. In fig. 4-2, several data of the extent of graphitisation at high temperature in the presence of oxygen or under vacuum are compared. If the general tendency of these data is followed, it seems as though the oxygen potential of alumina would start to cause graphitisation at around 1 700 °C. However the presence of titanium (from the HIPping capsules), as is the case in experimental work done for this thesis, would decrease the oxygen potential, as titanium is an reduction agent. The above deduction may therefore not be valid in the case of HIPping in the experiments of this work, since the possible influence of titanium is not investigated further.

Graphitisation starts at discrete sites on the surface and spreads out. After covering the surface, graphitisation proceeds into the diamond. Graphitisation is essentially a surface phenomenon,

although limited graphitisation can occur internally (Evans, 1979, 1992; Noma and Sawaoka, 1985).

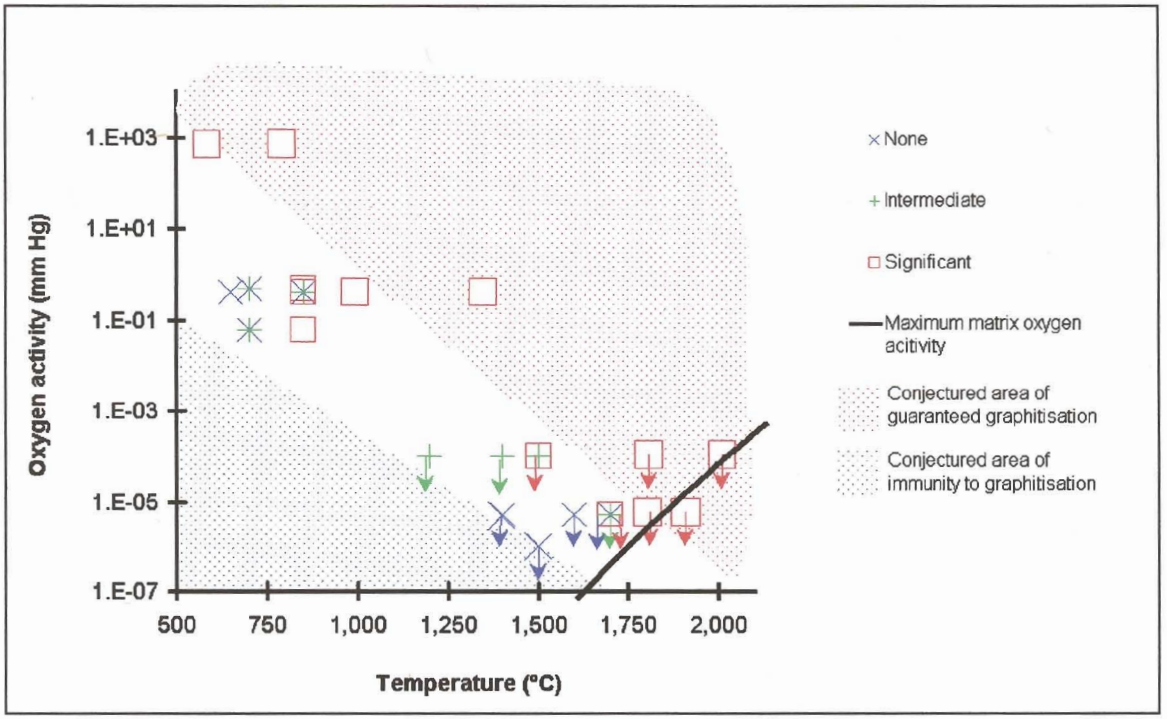

***Fig. 4-2**: Graphitisation as an effect of oxygen potential and temperature (Data from Howes, 1962; Seal, 1958; Evans and Phaal, 1962; and Liu and Ownby, 1991. See appendix A2 for details of the diagram's construction and its limitations.)*

The only work on the kinetics of graphitisation is that of Davies (1972) and Davies and Evans (1972). They proposed a first order equation that accounts for the dual effect of temperature and pressure:

$$\frac{\delta L_{graphitisation}}{\delta t} = k_{DE} e^{\frac{-E+PV}{RT}} \qquad (4\text{-}1)$$

The coefficient k_{DE} incorporates the effect of the number of graphitisation sites. If the diamond surface is not saturated with sufficient sites, or not adequately 'rough', k_{DE} is not constant initially. It is only constant after a graphite layer has spread over the surface and, consequently, the surface is saturated with graphitisation sites. No values for k_{DE} are given even though they can be calculated from the experimental data. Much uncertainty is involved with the coefficient k_{DE} and the primary aim of the work was to determine activation energy (Davies, personal communication). Nonetheless, some indication of the relative magnitude of the graphitisation rates on the three low index faces of diamond is given. The rate of graphitisation is very much dependent on the exposed face of the diamond and follows the trend: {110}>{111}>>{100}. In

table 4-1, the rate of graphitisation on the {110} and {111} faces is compared at specific temperatures. Specific quantitative data are not available for oxygen catalysed graphitisation, but it is known that the {100} face is also more resistant in the presence of oxygen (Evans, 1979).

Arrhenius plots for the {110} and {111} faces (at zero pressure) are given in fig. 4-3 and 4-4, and values for the activation energy, $\mathcal{E}$ and activation volume $\mathcal{V}$ are given in table 4-2.

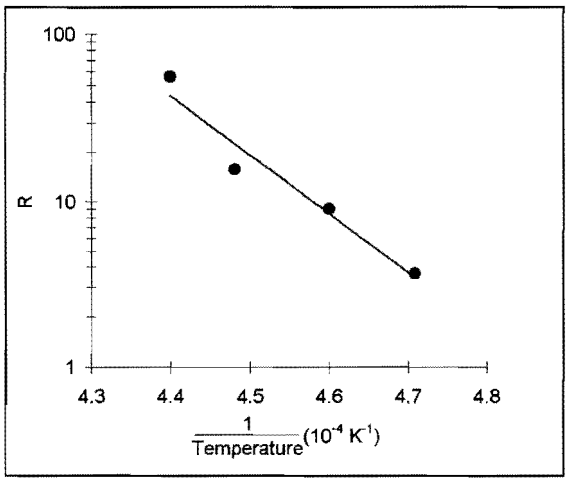

***Fig. 4-3**: Arrhenius plot for the {110} face. R is directly proportional to the graphitisation rate. (Davies, 1972.)*

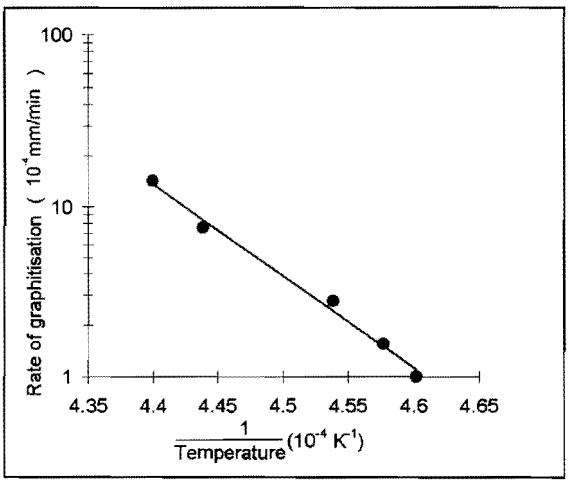

***Fig. 4-4**: Arrhenius plot for the {111} face. (Davies, 1972.)*

***Table 4-1**: Comparison of graphitisation rates on low index faces.*

Temperature (°C)	$\left(\frac{\delta L_{\{110\}}}{\delta t} \Big/ \frac{\delta L_{\{111\}}}{\delta t}\right)_{graphitisation}$
1 900	70
1 700	30

***Table 4-2**: Activation energy and activation volumes for graphitisation*

Face	$\mathcal{E}$ (kJ/mol)	$\mathcal{V}$ (cm^3/mol)
{110}	730 ± 50	10.2 ± 3
{111}	1 060 ± 80	9.7 ± 2

4.3 Graphitisation of diamond in oxide matrices

Available data for graphitisation in alumina matrices are summarised in table 4-3, which compares the extent of graphitisation encountered by different authors.

***Table 4-3**: Graphitisation in alumina matrices*

Densification					Analysis		Reference
Method	Temperature (°C)	Solid pressure (kbar)	Duration (h)	Atmosphere	Method	Amount of graphitisation (%)	
Hot press	1 250	0.32	Not given	Ar	Powder XRD	0	Liu and Ownby (1991)
Degassing followed by 'high pressure sintering'	500 1 300	60	2 1	0.0008 mm Hg vacuum	XRD	15	Noma and Sawaoka (1984)
Degassing followed by 'high pressure sintering'	500 1 300	60	1 1	0.0008 mm Hg vacuum	XRD?	15	Noma and Sawaoka (1985)
HIP	1 200	1.5	3		Not given	0	Kume *et al* *(1992)*
Hot press	1 550	0.35	c. 0.25	1.5×10^{-5} mm Hg vacuum	XRD	0	Chu *et al* (1992)

The emphasis in this work has been the suppression of graphitisation to enhance alumina-diamond bonding. Noma and Sawaoka (1984, 1985) followed the approach of intentionally graphitising the diamond for the toughening effect of the volume expansion on graphitisation (0.28 cm^3/g to 0.44 cm^3/g). This graphitisation was done in addition to the graphitisation already existing after firing. It is interesting to note in fig. 4-5 that extensive graphitisation still occurred in a dense (> 99 % theoretical density) composite, even though one might assume that diamond particles, being restricted in rigid voids, do not graphitise readily. Details of the toughening effect of graphitisation are given in chapter 5. Noma and Sawaoka (1985) also reported a significant change in the aspect ratio of diamond particles accompanied by internal layered graphitisation after extended post-hot pressing heat treatment. This will weaken diamond particles, and limit the reinforcement provided to the matrix. Noma and Sawaoka do not explain the change in aspect ratio, but the difference in graphitisation rates depending on the specific crystallographic face (mentioned in section 4.2) suggests a possible mechanism.

4.4. Raman analysis

Raman analysis is a convenient tool for identifying graphitisation. It is a particularly useful as diamond exhibits a distinct peak as shown in fig 4-6. Diamond particles without graphitised surfaces would show up as distinct peaks, while other forms of carbon also show on a Raman spectrum. Spectra for other forms of carbon are shown in fig.'s 4-7 and 4-8. In fig. 4-9 the

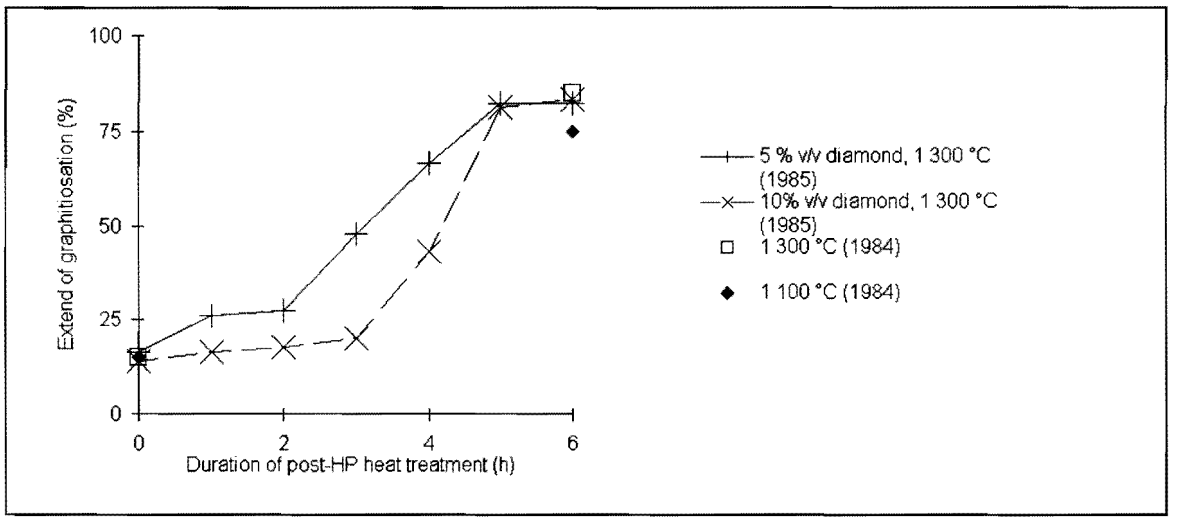

***Fig. 4-5**: Graphitisation of diamond in an alumina matrix after post densification heat (Noma and Sawaoka, 1984 and 1985).*

spectrum for diamond film deposited on alumina is shown. As such, it should not be directly comparable to the case of contact between non-deposited diamond and alumina as in the case of samples manufactured in this work. Nonetheless, one might intuitively expect similar peaking patterns.

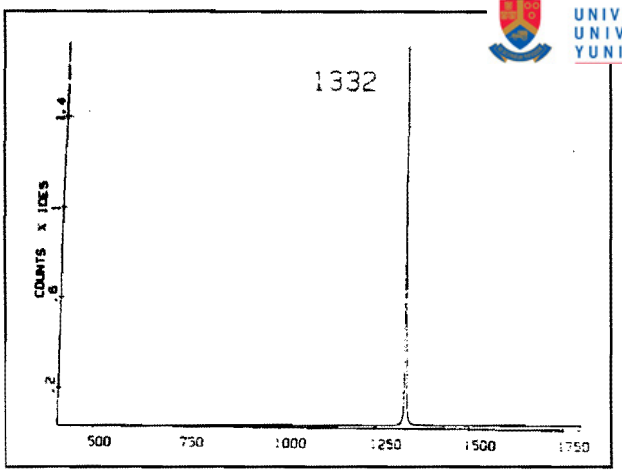

ctrum for natural diamond (Knight and White, 1989).

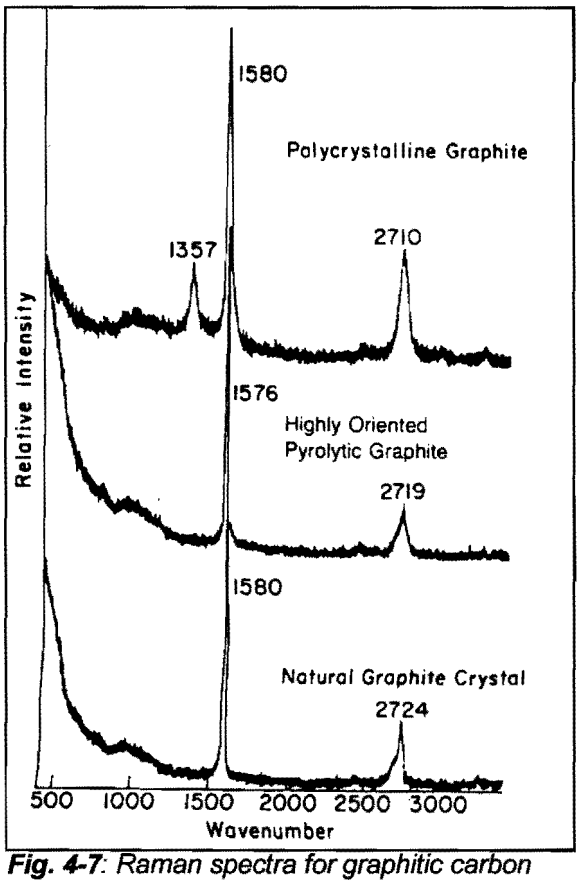

***Fig. 4-7**: Raman spectra for graphitic carbon (Knight and White, 1989).*

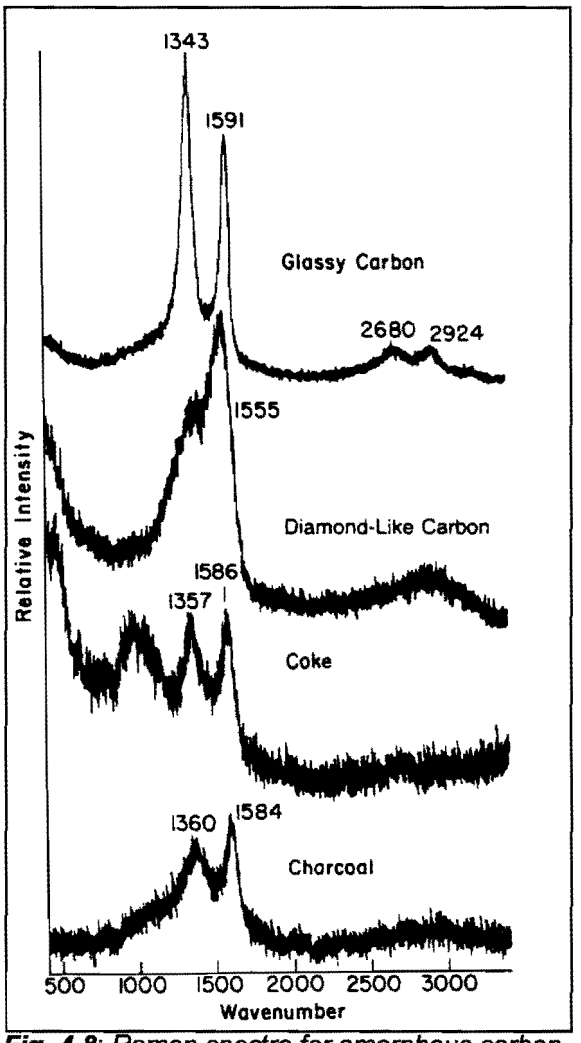

***Fig. 4-8**: Raman spectra for amorphous carbon (Knight and White, 1989).*

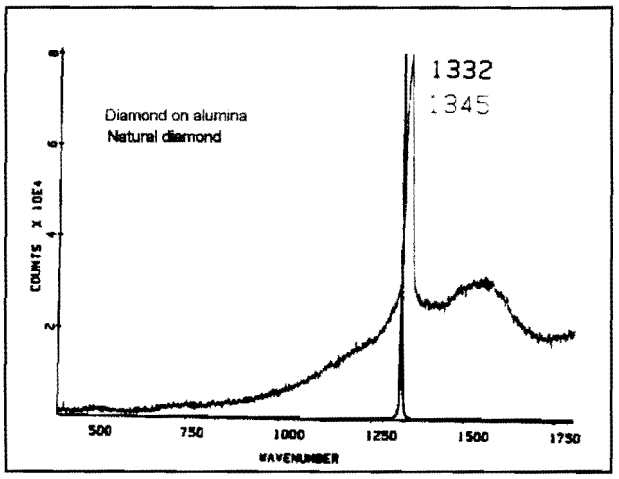

***Fig. 4-9**: Raman spectra for diamond film deposited on alumina (Knight and White, 1989).*

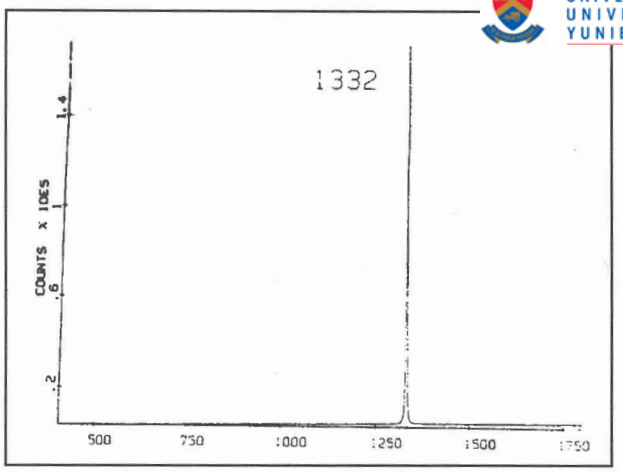

ectrum for natural diamond (Knight and White, 1989).

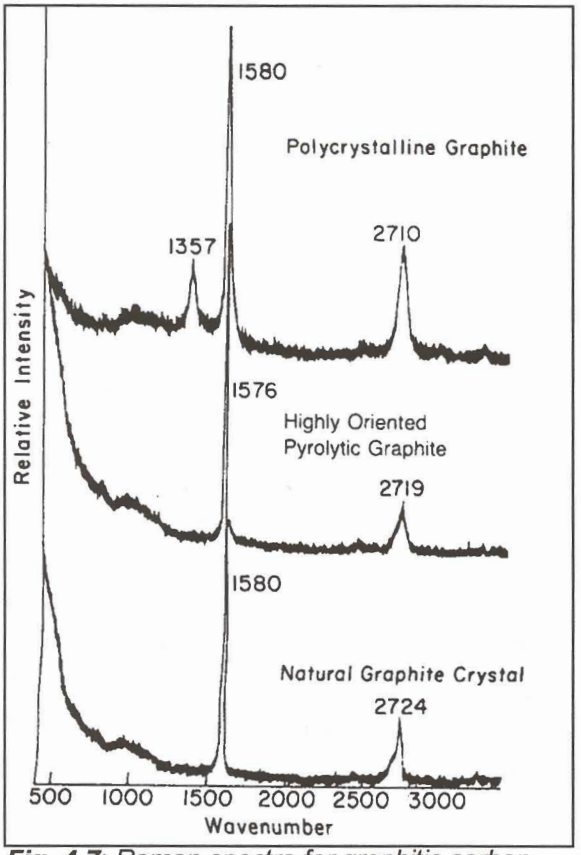

***Fig. 4-7**: Raman spectra for graphitic carbon (Knight and White, 1989).*

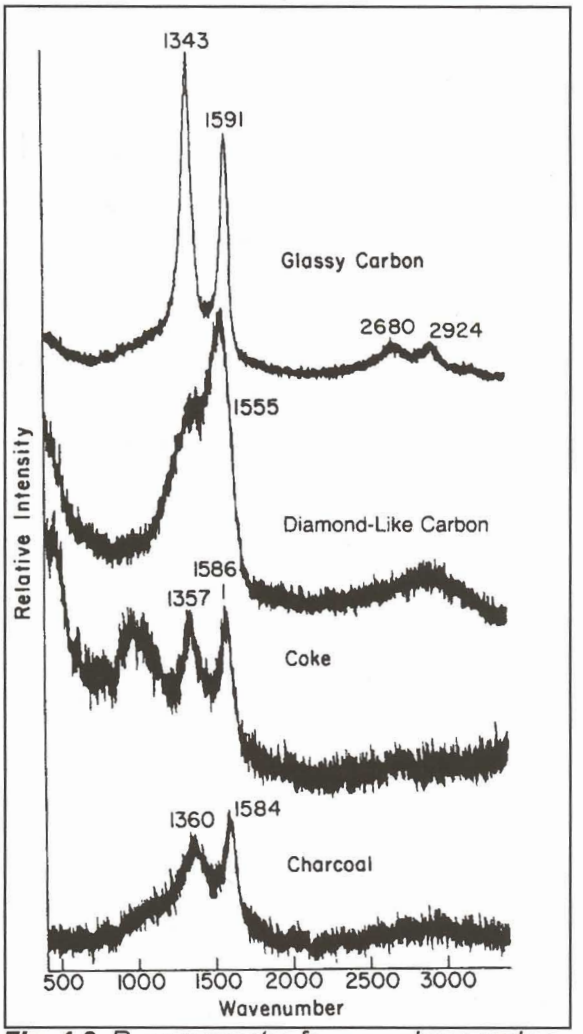

***Fig. 4-8**: Raman spectra for amorphous carbon (Knight and White, 1989).*

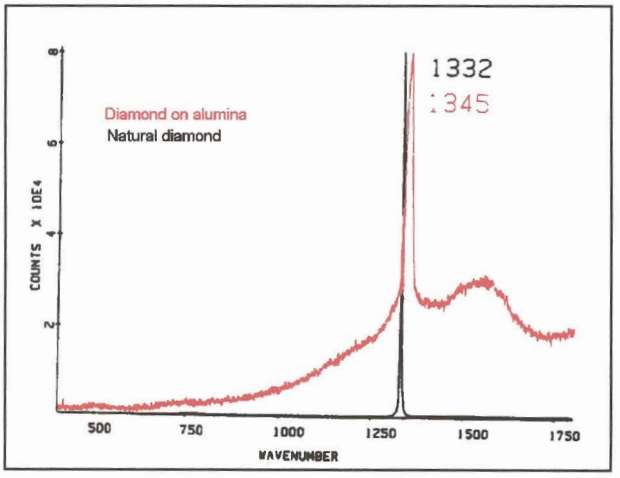

***Fig. 4-9**: Raman spectra for diamond film deposited on alumina (Knight and White, 1989).*

Chapter 5: Wear

5.1 Introduction

This chapter aims to summarise literature on wear as it applies to the work of this thesis. It therefore concentrates on wear as experienced in cutting tests, i. e. the evaluation of the performance of samples when used as a tool tip in a lathe. Other forms of wear testing are largely excluded here.

The terminology used in cutting is illustrated in fig. 5-1.

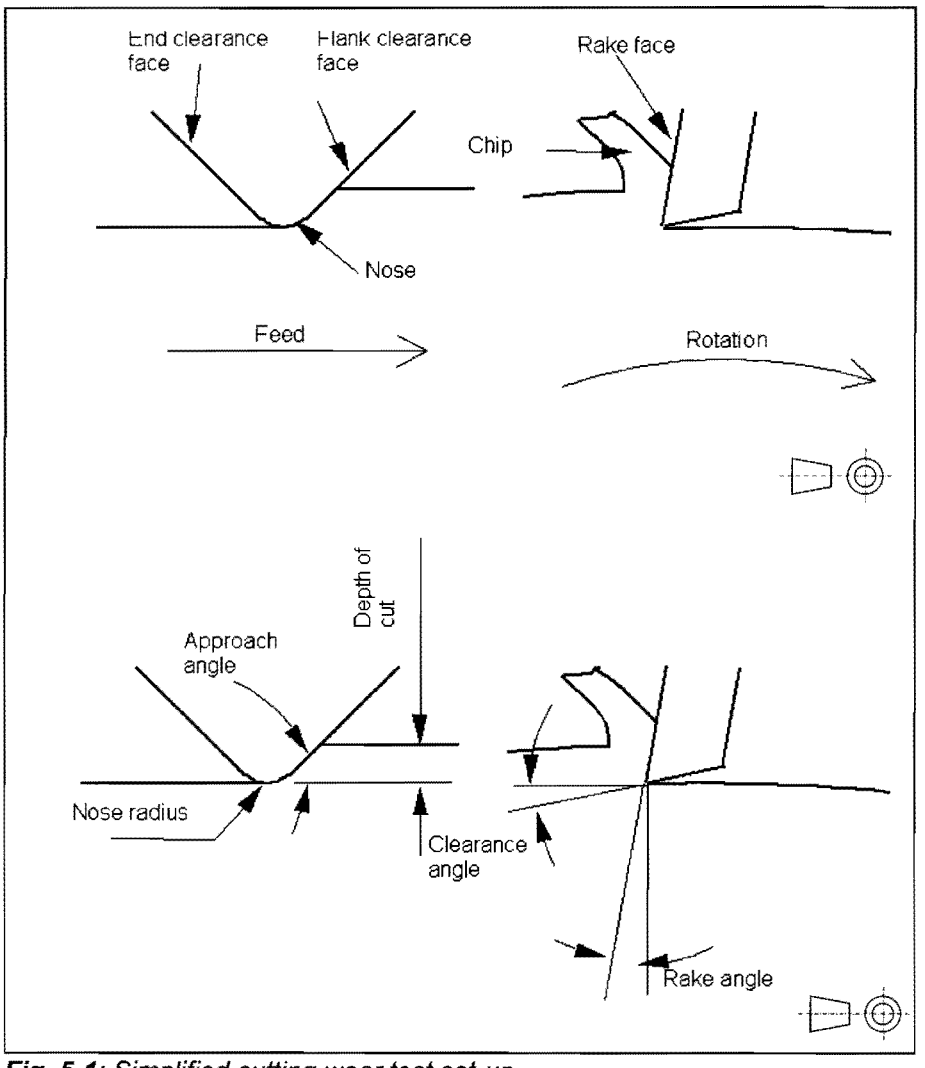

***Fig. 5-1**: Simplified cutting wear test set-up.*

5.2 Wear qualitatively

Wear is a complex phenomenon and several mechanisms contribute to the overall wear of a tool. During turning a cutting tool is subjected to friction, which results in high temperature, and various forces, causing high internal pressures and stresses in the tool. High temperature in turn results in chemical reactions at the interface between the insert and the workpiece. Three types of 'loading' are commonly identified: Mechanical, thermal and chemical (Stachowiak and Stachowiak, 1994).

Considerable confusion exists as to the terminology and classification of wear mechanisms in general (Blau, 1989; Hutchings, 1992; Lancaster, 1990). A satisfactory classification for ceramics is that of Stachowiak and Stachowiak (1994). Their classification, together with descriptions of the different wear mechanisms, is summarised in table 5-1.

***Table 5-1**: Wear mechanisms (Stachowiak and Stachowiak, 1994; Blau 1989).*

Mechanism		Description	Appearance of wear scar	Remarks
Mechanical wear	Abrasion	Wear caused by particles or protuberances forced against a surface	Grooves parallel to movement	Usually the dominating mechanism on the flank.
	Adhesive wear	Grains or groups of grains jerked from tool surface.	Rough.	Aggravated by weak interphase bonding in the tool
	Fracture	Ranges from complete catastrophic failure of the cutting edge to less severe chipping.		Caused by large thermal expansion and/or low thermal conductivity
Chemical wear		Chemical reaction between workpiece material and the tool leading to the formation of detrimental compounds in the tool.	Smooth.	

Wear damage on cutting tool inserts is divided into distinct wear features: Crater wear on the rake face, and flank and notch wear on the flank clearance face (fig. 5-2). Flank wear is caused by abrasive contact between the tool and the freshly cut workpiece. Notch wear is caused by fracture and occurs especially on brittle tools cutting hard materials. Crater wear is caused by contact between the chip and the rake face.

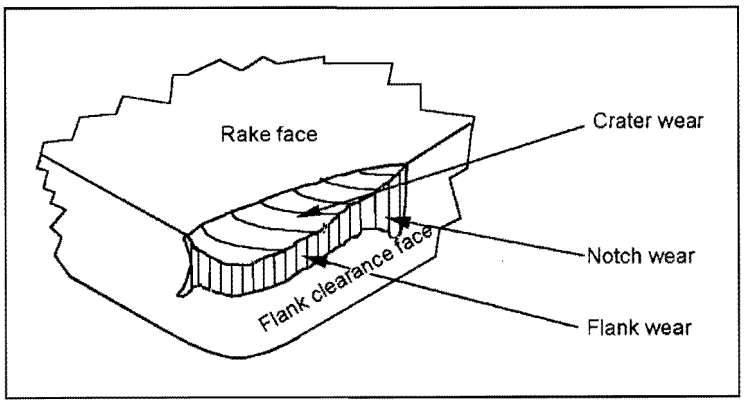

***Fig. 5-2**: Typical wear features on a cutting tool insert (see fig. 5-1 for feed direction and the position of the chip) (Stachowiak and Stachowiak, 1994).*

5.3 Testing

In industry the criterion for tool performance is its satisfactory performance. 'Satisfactory performance' can imply satisfactory surface finish and tolerance. In the extreme 'satisfactory performance' can even mean the lack of excessive vibration in the lathe or the non-occurrence of catastrophic failure of the tool (personal communications, Ravenhill and Jarvis). When testing an insert in the laboratory various measurements can be taken to evaluate an insert: Weight loss of the insert, surface roughness of the work piece and dimensions of the work piece and the insert can be measured (Li *et al*, 1993; Li *et al*, 1994; ISO 3685).

The performance of cutting tool inserts can be quantified in different ways. ISO 3685 recommends that the criterion for performance be the tool life. Tool-life is defined as the duration of time necessary for the span of some wear feature to reach a pre-decided value. Possible wear feature measurements are the depth of the flank wear V or the crater depth K as shown in fig. 5-3. For ceramics ISO 3685 recommends either a maximum flank wear width of 0.6 mm or an average flank wear of 0.3 mm as the pre-decided cut-off point for tool-life. With the ISO recommended work piece material (steel or cast iron), notch and crater wear should not occur on ceramic cutting tools (in the experimental work of this work, however, a ceramic rod of Siffer' is used as a workpiece material).

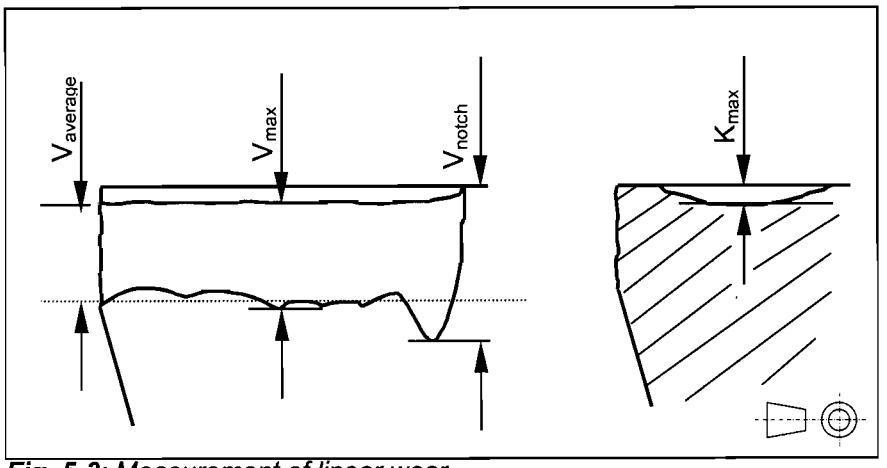

***Fig. 5-3**: Measurement of linear wear.*

5.4 Models

The Archard wear law is commonly used to describe to wear, particularly abrasive wear (Hutchings, 1992):

$$\frac{\delta Q}{\delta S} = \frac{k_A}{H} N \qquad (5\text{-}1)$$

where Q is the volume of material worn away after sliding a distance S. N is the normal force, H is the hardness (no particular hardness measurement value recommended) of the softer material and k_A is a coefficient that takes all other factors into account. The ratio $\delta Q/\delta S$ is commonly known as the specific wear rate.

Axén and Jacobson (1994) reformulated the Archard wear law to develop a model for the abrasive wear of composite materials. They defined wear resistance Ω as

$$\Omega = \frac{N}{\delta Q / \delta S} \qquad (5\text{-}2)$$

With this definition Archard's wear law can be reformulated as

$$\frac{\delta Q}{\delta S} = \frac{N}{\Omega} \qquad (5\text{-}3)$$

Axén and Jacobson propose two possible modes for composite wear. Firstly, equal wear mode in which two phases wear down at the same linear rate. Secondly, equal pressure wear mode in which both the hard and soft phase carry the same pressure. Equal wear and equal pressure mode should respectively give the lower and upper bounds of the wear rate, with the actual wear for a composite lying somewhere in between. For equal wear mode Axén and Jacobson derived the linear equation

$$\Omega_{Composite} = g_{Hard}\Omega_{Hard} + g_{Soft}\Omega_{Hard} \qquad (5\text{-}4)$$

and for equal pressure mode they derived the inversely additive equation.

$$\Omega_{Composite} = \frac{1}{\frac{g_{Hard}}{\Omega_{Hard}} + \frac{g_{Soft}}{\Omega_{Soft}}} \qquad (5\text{-}5)$$

where g_{hard} and g_{soft} is respectively the area fractions of the exposed hard and soft phases. For composites with randomly distributed phases the area fractions of phases are equal to the volume fractions, i.e. g = f. By combining equation 5-4 and 5-3 the wear under conditions of equal linear penetration can be derived as the inversely additive equation

$$\frac{\delta Q}{\delta S} = \frac{N}{f_{Hard}\Omega_{Hard} + f_{Soft}\Omega_{Hard}} \qquad (5\text{-}6)$$

where f is the volume fraction of the phases. By combining equations 5-5 and 5-3, the wear under equal pressure can be derived as the linearly additive equation

$$\frac{\delta Q}{\delta S} = N\left(\frac{f_{Hard}}{\Omega_{Hard}} + \frac{f_{Soft}}{\Omega_{Soft}}\right) \qquad (5\text{-}7)$$

Fig. 5-4 illustrates the trend of the bounds for the specific wear rate given by equations 5-6 and 5-7.

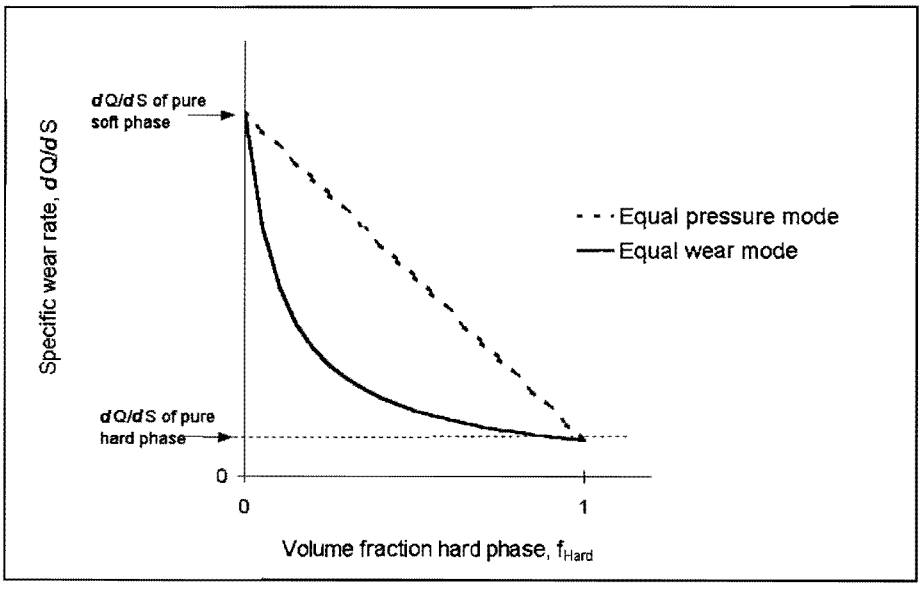

***Fig. 5-4**: Equal wear and equal pressure composite wear modes compared.*

The relations (equations 5-1 to 5-7) and of Archard and of Axén and Jacobson only describe the instantaneous wear rate and the coefficient k_A and wear resistance Ω are not constant, but change with time as wear progresses. In practice, wear typically follows the trend illustrated in fig. 5-5 (Jarvis, personal communication; Blau, 1989).

In the experimental work of this thesis no force measurements were taken. The relationship given by Singh and Vajpayee (1980) is therefore rather useful for interpretation of results. They state that the normal force on a cutting tool follows the simple relationship

$$N = k_{SV1}V + k_{SV2} \qquad (5\text{-}8)$$

where k_{SV1} and k_{SV2} are constants. At the least this relationship shows that the normal force on the tool shows a linear increase, and not, for instance, a sudden exponential jump at any stage.

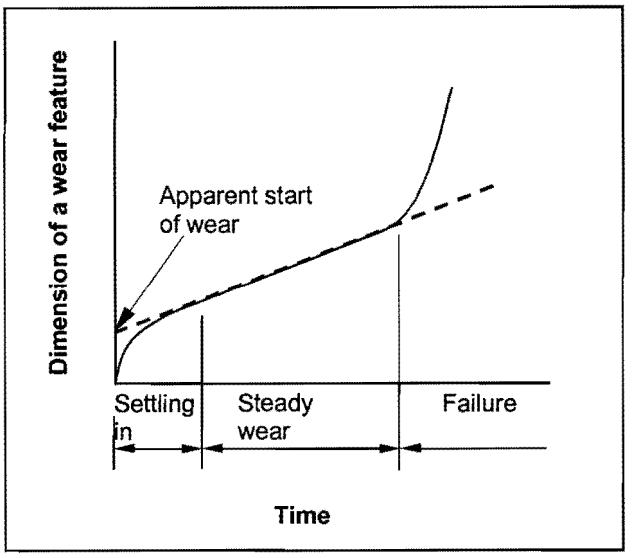

***Fig. 5-5**: Typical course of wear.*

5.5 The influence of hardness and toughness on wear

Hardness and toughness are the two most important factors in wear resistance (Hickman, personal communication). This relationship can be quantified by Baldoni *et al*'s (1986) wear resistance indicator $K_{IC}^{3/4}H^{1/2}$ (K_{IC} being mode I fracture toughness and H hardness) which indicates abrasive wear resistance. Mode I fracture toughness, K_{IC} ('K one C', i.e. mode I fracture toughness) and not K_c ('K C'), is specified but it is unclear if Baldoni *et al* actually used K_{IC} values. Baldoni *et al* seem to have used Knoop hardness. It is unclear how accurate the wear resistance indicator will be with other forms of toughness and hardness measurements, like it used in this work. In this work it is used with Vickers' hardness, H_V and Vickers' crack length toughness K_C, i.e. as $K_C^{3/4}H_V^{1/2}$.

Toughness can be determined from indentation crack length, for which several equations exist (McColm, 1990). In their work on diamond-alumina Noma and Sawaoka (1984 and 1985) used the relation of Lawn *et al* (1980):

$$K_C = 0.0070\, E^{1/2} H_V^{1/2} d^2 c^{-3/2} \qquad (5\text{-}9)$$

with the dimensions c and d as defined in fig. 5-6. (If c and d are in m and E and H_V is in Pa then K_c is in $Pa.m^{½}$.) As Noma and Sawaoka used this equation for a similar material, it seems reasonable to use it in

this work as well. The Young modulus (E) for the composites in this work is estimated as 490 GPa (appendix A4).

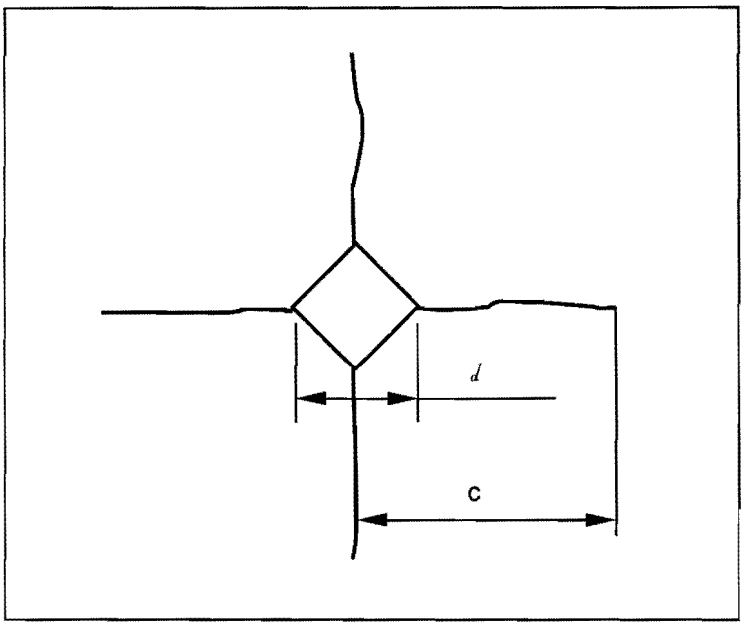

***Fig. 5-6**: Indentation dimensions used in toughness measurement.*

5.6. Wear and wear related properties of relevant materials

5.6.1 Untoughened alumina

Alumina exhibits increased hardness with smaller grain size as illustrated in fig.5-7.

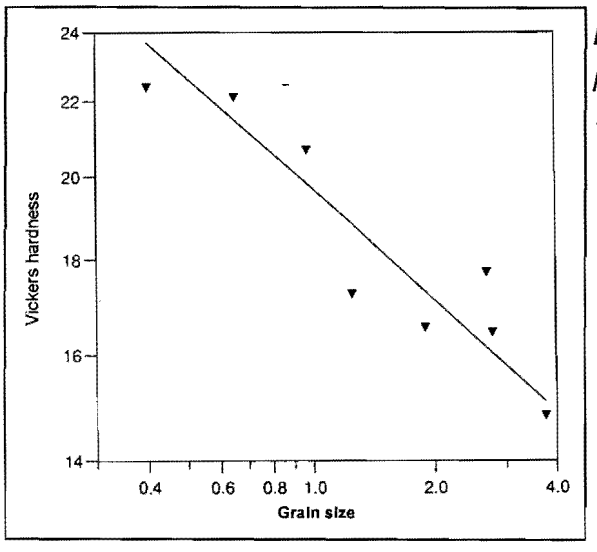

***Fig. 5-7**: Grain size dependence of the Vickers hardness (at 10 kg f) of alumina (Krell and Blank, 1995).*

Pure alumina or alumina only containing sintering aids is not very resistant to thermal loading (differential heating) due to its relatively low thermal conductivity, which drops of between 25 °C and 400 °C (fig. 5-8). Alumina for cutting use is normally toughened with some additive, like zirconia, although untoughened alumina is sometimes used in industry (Toshiba marketing pamphlet, Dörre and Hübner, 1984).

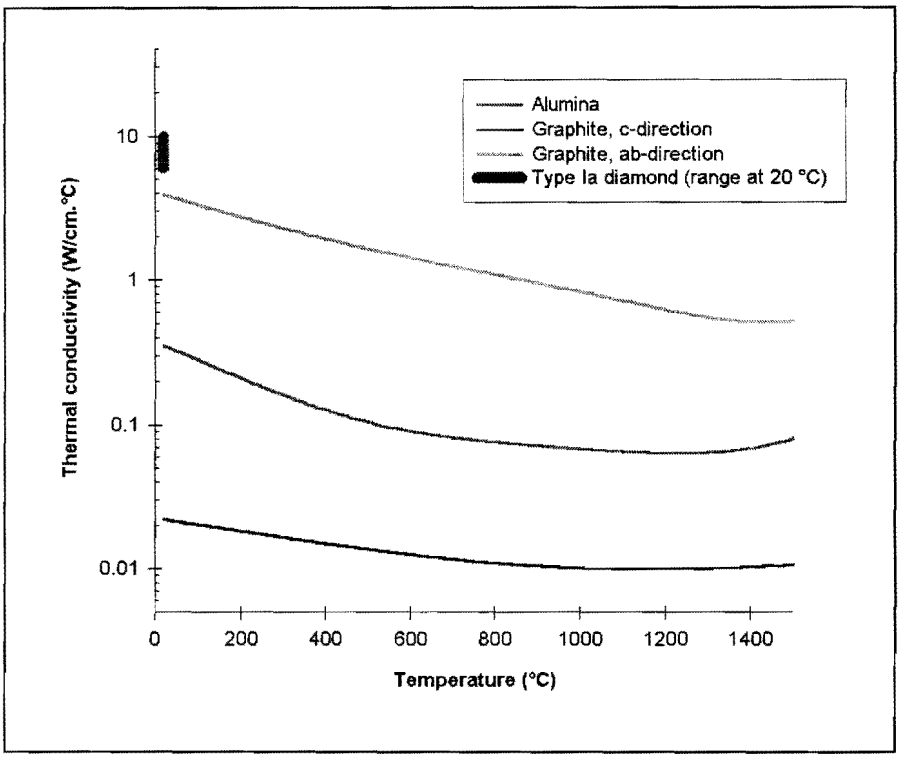

***Fig. 5-8**: The thermal conductivities of alumina, diamond and graphite as a function of temperature. Data from Dörre and Hübner (1984) and Pierson (1993). No data for any form of diamond at higher temperature than shown are available.*

Alumina in general displays good resistance to chemical loading by ferrous alloys. Some reactions occur when cutting oxides of calcium, magnesium and silicon and with titanium alloys (Stachowiak and Stachowiak, 1994).

Typical wear features of non-toughened alumina are shown in fig. 5-9. Alumina shows relatively little cratering in turning, but it shows broad flank wear. Like some other ceramics alumina has its most optimal wear at high speed, typically above 100 m/min, as fig. 5-10 shows (Dörre and Hübner, 1984).

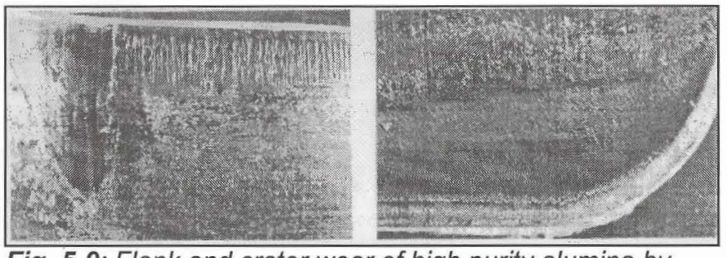

***Fig. 5-9**: Flank and crater wear of high purity alumina by abrasion, presumably after cutting metal. ×8.5. (Dörre and Hübner, 1984).*

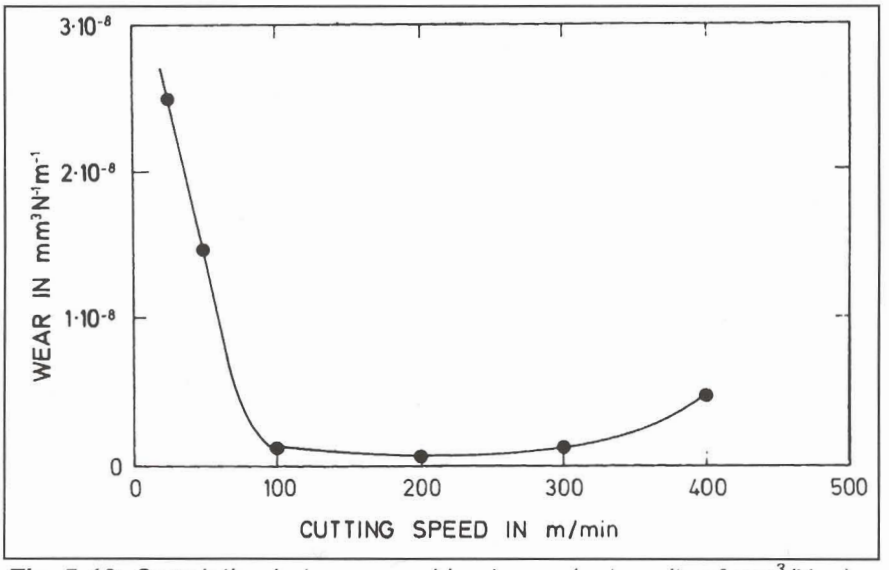

***Fig. 5-10:** Correlation between combined wear (note units of $mm^3/N.m$) and cutting speed of high purity alumina (Dörre and Hübner, 1984), presumably on cast iron or steel.*

5.6.2 Diamond-alumina composites

Reinforcement of matrices for cutting purposes with the inclusion of inert, non-whisker, non-platelet particles is not common. (In this sense 'inert' means materials that do not change in composition or phase during processing like zirconia does). For instance, Chuanzhen and Xing (1996) developed alumina (matrix) composites with silicon carbide enforcement in the form of both simply shaped, relatively spherical particles and whiskers. However they only subjected their whisker containing composites to cutting tests, presumably because of its toughness being double that of the composites with simple particles (8.1 $MPa.m^{½}$ versus 4.9 $MPa.m^{½}$).

In sharp contrast with alumina, diamond has excellent thermal conductivity (fig. 5-8), the highest of any solid at room temperature. For a finely dispersed, isotropic composite, with no thermal barrier between phases, thermal conductivity k is linearly additive with respect to volume fraction f, i.e.

$$k_{Composite} = f_{Diamond} k_{Diamond} + f_{Alumina} k_{Alumina} \qquad (5\text{-}10)$$

Addition of diamond therefore has the potential of enhancing an alumina matrix's thermal conductivity. This would result in less sharp temperature gradients and improve the ability to resist thermal loading. However, there can be some doubt about to what extent the ideal situation of equation 5-10 would be followed in reality. Even in the case of perfect mechanical contact between phases a thermal barrier can exist between phases. Hasselman *et al*'s work (1994) on a diamond-cordierite composite indeed showed that the above ideal additive effect for composites was not followed in their composites: Composite thermal conductivity was approximately a factor of ten smaller than that predicted by equation 5-10. In the case of the diamond-alumina of this work the possible formation of a graphite layer between diamond and alumina therefore provides two possible mechanisms for resistance to conduction of heat:

1) Two phase boundaries (diamond to graphite and graphite to alumina, instead of only diamond to alumina) which leads to two possible phase to phase thermal barriers.

2) Depending on the predominant orientation in the graphite layer, the graphite layer itself can have low thermal conductivity. In the worst possible scenario the graphite layer can form on the diamond with its ab-direction parallel to the diamond surface. This would imply heat transfer in the c-direction, in which thermal conductivity is very low (fig. 5-8). (It is more likely, however, that the graphite would be isotropic and that its thermal conductivity would be intermediate to that of the c and ab-directions. Thermal conductivity in the ab-direction is good, better than alumina, as can be seen in fig. 5-8).

Noma and Sawaoka (1985a and 1985b) manufactured diamond alumina composites and determined their hardness and toughness. Interestingly, they intentionally and extensively graphitised the diamond in their composites to take advantage of a toughening effect of the conversion of diamond to graphite. Grain size in their alumina matrix was relatively coarse, being > 2 μm. In Noma and Sawaoka's results it seems that hardness was sacrificed with increasing diamond content but that hardness was roughly independent of graphitisation (fig. 5-11). Toughness achieved as functions of diamond content and increased graphitisation (longer heat treatment leading to more graphitisation, also compare fig. 4-5) is seen in fig. 5-12 and 5-13. The obvious toughening mechanism would be microcrack toughening due to volume expansion (the specific volume of carbon particles changes from the 0.32 cm^3/g of diamond to the 0.44 cm^3/g of graphite). However, Noma and Sawaoka also observed an increase in the aspect ratio (ratio of the length to width) of carbon particles, and they suggest crack deflection by this change as the toughening mechanism. (Noma and Sawaoka's experimental conditions are summarised in table 4-3.)

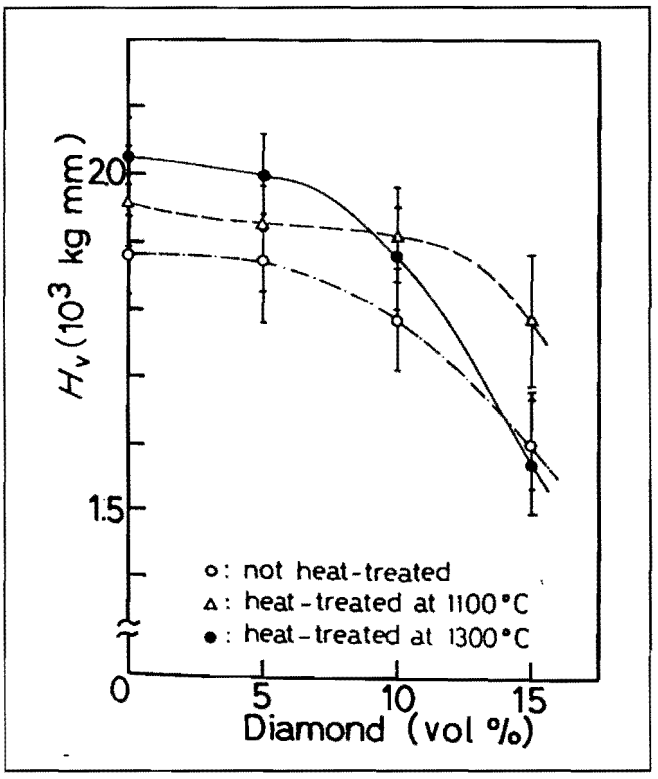

***Fig. 5-11**: Hardness as a function of diamond content after post densification heat treatment of 6h. Indentor load 10 kg. From Noma and Sawaoka (1984)*

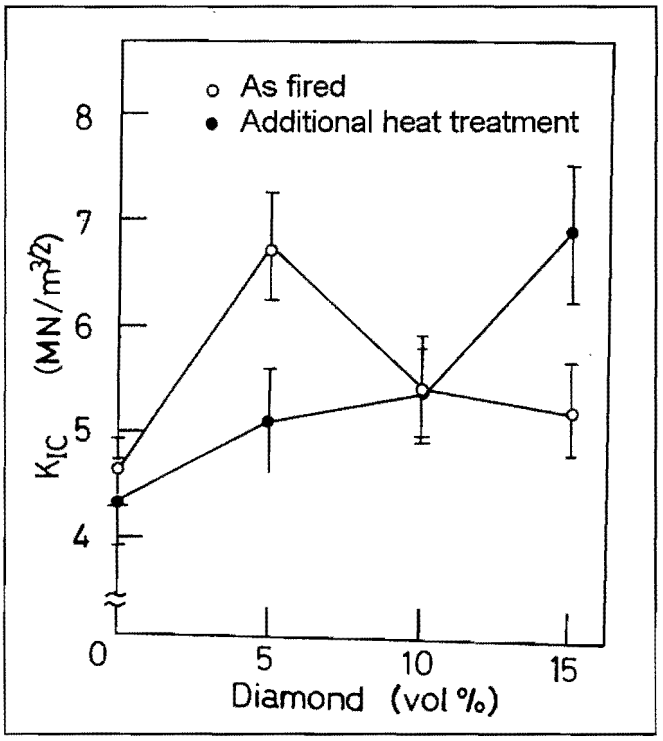

***Fig. 5-12**: Variation of fracture toughness with diamond content. Method of toughness measurement not given. Heat treatment was 6 h at 1 300 °C. From Noma and Sawaoka (1985).*

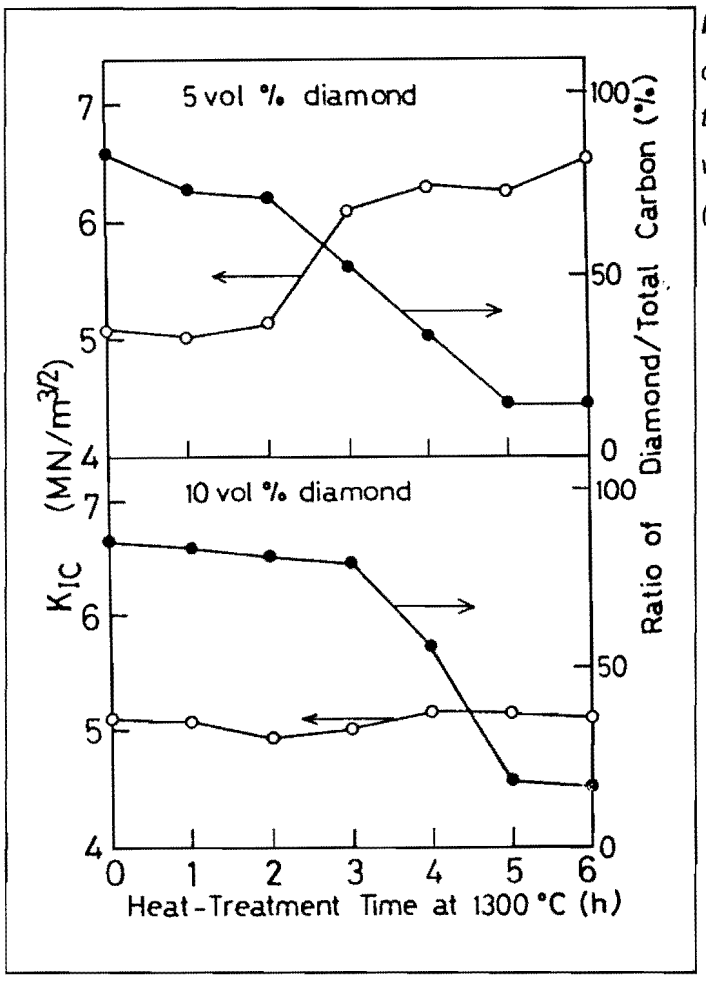

***Fig. 5.13**: Variation of fracture toughness and degree of graphitisation with post-firing heat treatment. Fracture toughness by indentation with a 30 kg load. From Noma and Sawaoka (1985).*

The only available literature on the wear of actual diamond-alumina composites is that of Chu *et al* (1992). They manufactured a diamond-alumina composite by dry pressing followed by hot pressing at 1 550 °C. The resultant composite's friction coefficient was compared with that of diamond and zirconia toughened alumina. An increase in the coefficient of friction implied an increase in wear. However, their test on a magnetic disk is extremely mild compared to the wear test method employed in this work. In the face of the lack of other wear data on diamond-alumina composites their data are included and given in fig. 5-14. Diamond-alumina is seen to have an advantage in having friction coefficients of approximately less than halve of that of zirconia-alumina.

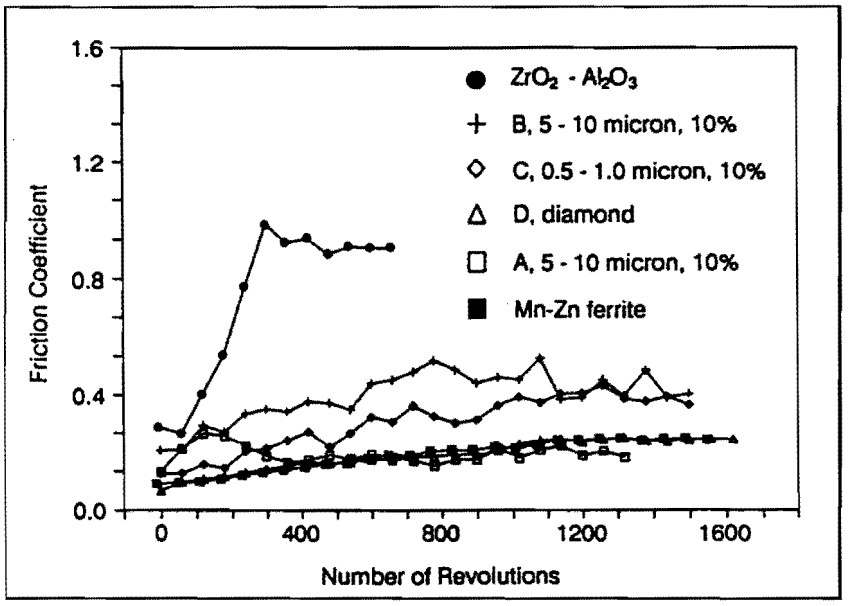

***Fig. 5-14**: The friction coefficient of a diamond-alumina composite on a magnetic storage disk compared to some other materials. Indicated sizes and percentages in the legend refer to the size and volume percentage of diamond (Chu* et al, *1992).*

Chapter 6: Preparation of Compacts

6.1 Raw materials

The following powders were used.

- Sumitomo AKP-53 (α-alumina) as primary alumina constituent or as seeding in predominantly α-alumina suspensions.
- Sumitomo AKP-50 (α-alumina) as primary alumina constituent.
- Degussa alumina (γ-alumina) as primary alumina constituent.
- Grade 2 natural diamond (acid washed).
- Degussa titania as grain growth inhibitor in the alumina matrix.

Powders are characterised in detail by Msibi (1997).

6.2 Suspension of powder

Firing experiments were conducted in parallel with the development of suspension preparation routes, with the result that different routes were used during the project. Suspension preparation generally followed the sequence:

1) pH adjustment of suspending solution water.
2) Addition of dispersant.
3) Addition of powder.
4) Sonification.

Some of the steps were not used in every route; details of individual preparation routes are given in table 6-1.

Not detailed in table 6-1 is route CP. Route CP only required the mixing of suspensions prepared by routes Pα or Pγ and C to the required ratio of diamond to alumina, followed by additional sonification.

Preparation by route pH$\alpha\Diamond$ entailed adding powder (which tends to bring the pH down) to the suspension while maintaining pH 11. It was not very reproducible due the difficulty of measuring pH in a viscous suspension over prolonged periods of time.

***Table 6-1**: Preparation of suspensions.*

		Route pHα	Route HP	Route pHα◊	Route Pα	Route Pγ	Route C
Total solids loading (% v/v)		<25[#]	30	<30[‡]	30	10	30
Dispersal method		pH 4 (Nitric acid)	Hydropalat 3204	pH 11 (Ammonia)	Propionic acid	Propionic acid	1 % w/w CTAB[§]
Dispersant/Water (% w/w)		Not applicable	1.3	Not applicable	0.85	0.85	0.75[*]
Solid constituents	AKP-50	✓	×	×	×	×	×
	AKP-53	×	✓	✓	✓	✓	×
	Degussa alumina	×	×	×	×	✓	×
	Diamond	×	✓	✓	×	×	✓
	Titania	In some cases	✓	✓	✓	✓	×
Mixing procedure[†]	pH pre-adjustment	pH 4 with nitric acid	×	pH 11 with ammonia solution	pH 4 with nitric acid	pH 4 with nitric acid	pH 4 with nitric acid
	Addition of dispersant	Not applicable.	✓	Not applicable.	✓	✓	✓
	Addition of titania	In some cases	✓	✓	✓	✓	×
	Addition of α-alumina seeds	×	×	×	×	✓	×
	Addition of primary constituents	Alternate addition of small amounts of alumina and ammonia solution while keeping the pH close to 4 by the addition of nitric acid	Dry mixture of alumina and diamond	Alternate addition of small amounts of alumina and diamond and ammonia solution while keeping the pH close to 11 by the addition of ammonia solution	α-alumina	γ-alumina	Diamond
	Sonification	✓	✓	✓	✓	✓	✓
	pH readjustment	pH readjusted to 4 with nitric acid	×	pH readjusted to 11 with ammonia solution	×	×	×

[#] The total amount of solids used was calculated as $^1/_3$ of the initial liquid volume. After addition of nitric acid solution solids loading was therefore less than 25 % v/v.
[‡] The total amount of solids used was calculated as $^3/_7$ of the initial liquid volume. After addition of ammonia solution solids loading was therefore less than 30 % v/v.
[§] Cetyltrimethylammonium bromide.
[*] I.e. 0.75 % of a 1 % w/w solution of CTAB.
[†] The mixing procedure followed the order (from top to bottom) indicated.

6.3 Consolidation of suspensions

Suspensions were filter pressed by either the pressurised air or the direct force device depicted in fig 10-1 and 10-2.

In the pressurised air device pressure is supplied by compressed gas. Maximum working pressure for this press is 5 MPa, which was also the pressure used for the preparation of compacts. Two sizes of inserts were used: 35 and 8 mm diameter, which allowed the formation of compacts of the corresponding size. Filtration time for compacts that are evaluated in this work was 2 hours.

In the direct force device the load is supplied mechanical with a small press. The pressure (as experienced by the suspension) used for preparation was 20 MPa. Filtration time varied, but a minimum of 20 minutes was used successfully for AKP-53 containing suspensions, and 60 minutes for Degussa alumina containing suspensions.

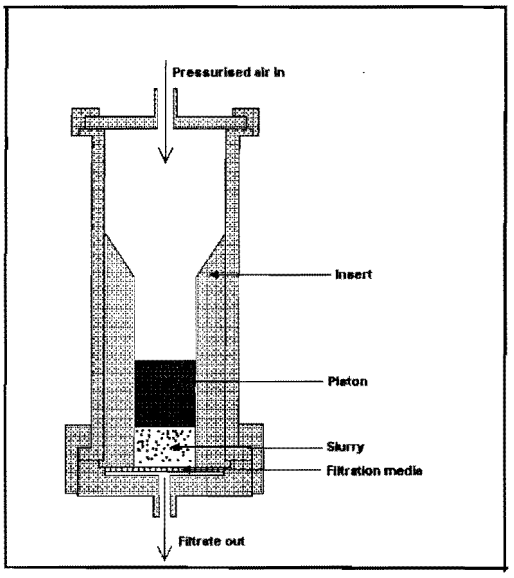

***Fig. 10-1**: The pressurised air device.*

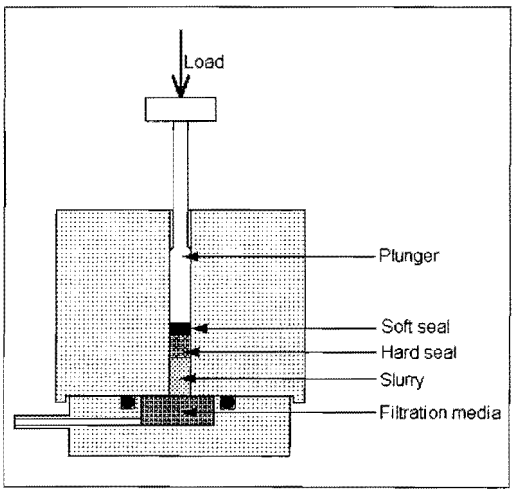

***Fig. 10-2**: The direct force device.*

6.4 Firing

6.4.1 Introduction

An attempt was made to duplicate the results of Yeh and Sacks (1988a) (section 3.2, page 19), as they achieved high densities by sintering at low temperature in air. These attempts were unsuccessful and afterwards densification was only done by HIPping.

6.4.2 Sintering

Suspensions were prepared for sintering by route pHα. Titania (1 % m/m) was added to some samples. For sintering runs only green body formation by the pressurised air device were used. The resulting compacts were sintered in air by heating at 250 °C/h to the dwell temperature. Dwell time was 2 hours followed by natural cooling in the furnace.

6.4.3 HIPping

Encapsulation (in titanium) for HIPping and HIPping itself was conducted by Mattek[‡]. As such, precise control of the conditions was limited to the specifications given to Mattek. Specifications were as follows:

- The pre-pressure was to be as great as possible, which amounted to 60 bar.
- The dwell temperature and pressure were to be reached as rapidly a possible.
- The dwell pressure was to be as high as possible, which amounted to 150 ± 2 MPa.
- The dwell time was to be 30 minutes.
- The compacts were to be left to cool down naturally in the HIP vessel.

A variety of mechanical methods were used to remove the titanium HIPping capsules, but immersion in warm concentrated hydrofluoric acid proved the most efficient method of removal.

[‡] Mattek, CSIR, Pretoria, South Africa.

Chapter 7: Routine characterisation

7.1. Introduction

Chapters 7, 8, 9 and 10 give analyses of the fabricated compacts. While the experimental work of chapters 8, 9 and 10 required development of methods, analyses in which established and routine methods used are presented in this chapter.

7.2. Mercury porosimetry on green compacts

To test the integrity of samples prepared with nanosized powders and by pressure filtration a non-diamond containing green compact prepared with the pressurised air press (section 6-3, page 50) was subjected to mercury porosimetry[‡]. At that stage of this project work was still conducted with AKP-50. Data for the mercury porosimetry run are given in fig. 7-1.

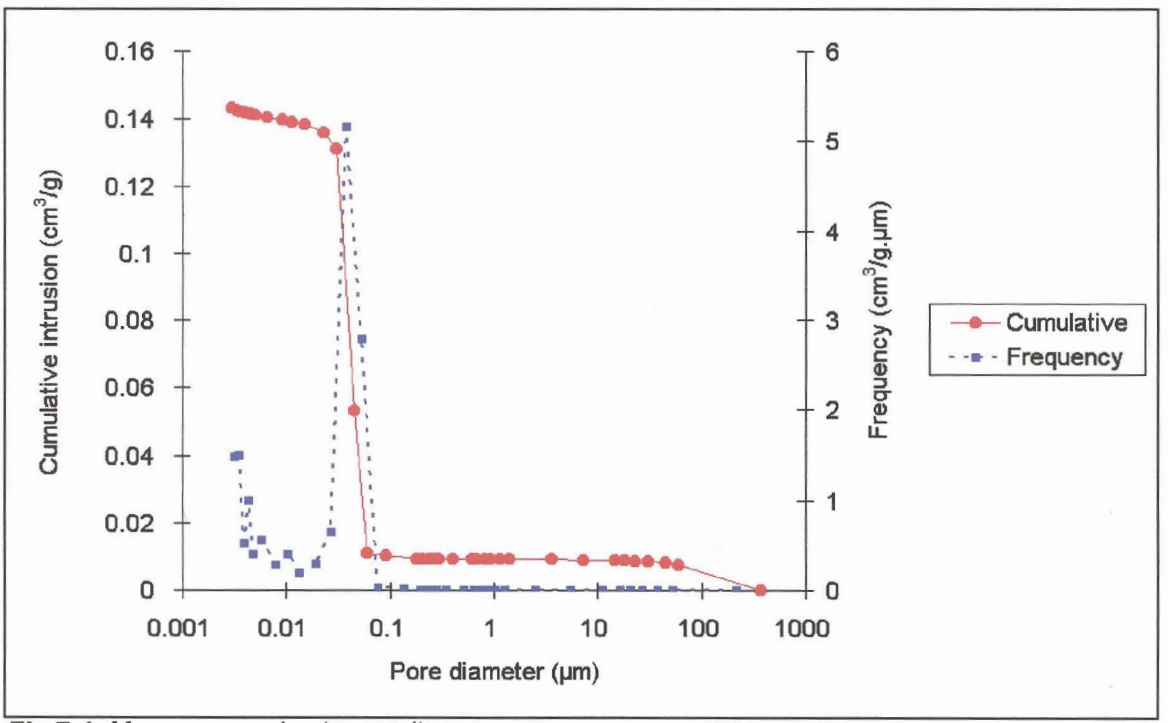

***Fig.7-1**: Mercury porosimetry results.*

[‡] Atomic Energy Corporation, Pelindaba, South Africa.

7.3 Fired density

Densities were determined by immersion in water. With repeated measurements values did not vary more than ± 1 relative density percentage points for each sample.

Results for sintering are reported in fig. 7-2.

The densities achieved by HIPping, together with relative amounts of constituents are given below (table 7-1). All α-alumina samples densified to almost their full relative densities. There is no correlation between HIPping temperature and density.

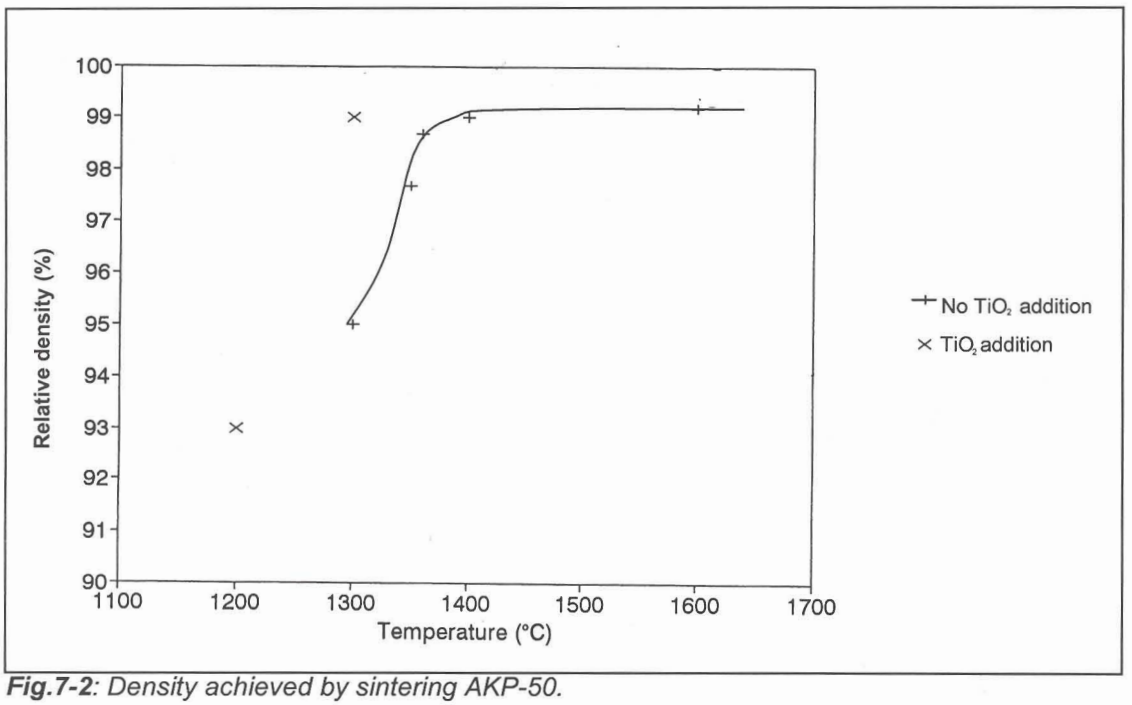

***Fig.7-2**: Density achieved by sintering AKP-50.*

***Table 7-1**: Densities achieved.*

Sample.	Relative density (%)
0◊-α-CP-H1400	99
15◊-α-CP-H1400	97
15◊-α-CP-H1350	98
0◊-α-Pα-H1350	98
0◊-α-HP-H1300	99
15◊-α-HP-H1300	99
15◊-α-pH-H1300	96
15◊-α-HP-H1300	100
15◊-α-HP-H1250	99
15◊-α-pH-H1250	99
0◊-α-CP-H1250	100
0◊-α-Pα-H1200	99
15◊-α-CP-H1200	99
0◊-γ-Pγ-H1200	83
0◊-γ-Pγ-H1250	96

7.4. Raman analysis

The Raman spectra[‡] in fig 7-3 were obtained with freshly fractured surfaces. At least three different points were analysed on each sample and for each sample a typical spectrum is shown. Note that the area covered by a single measurement is in the order of 0.5 mm and therefore includes several exposed diamond particles. It is not possible to focus on a single diamond particle.

[‡] Institute for Applied Materials, Faculty of Science, University of Pretoria, South Africa.

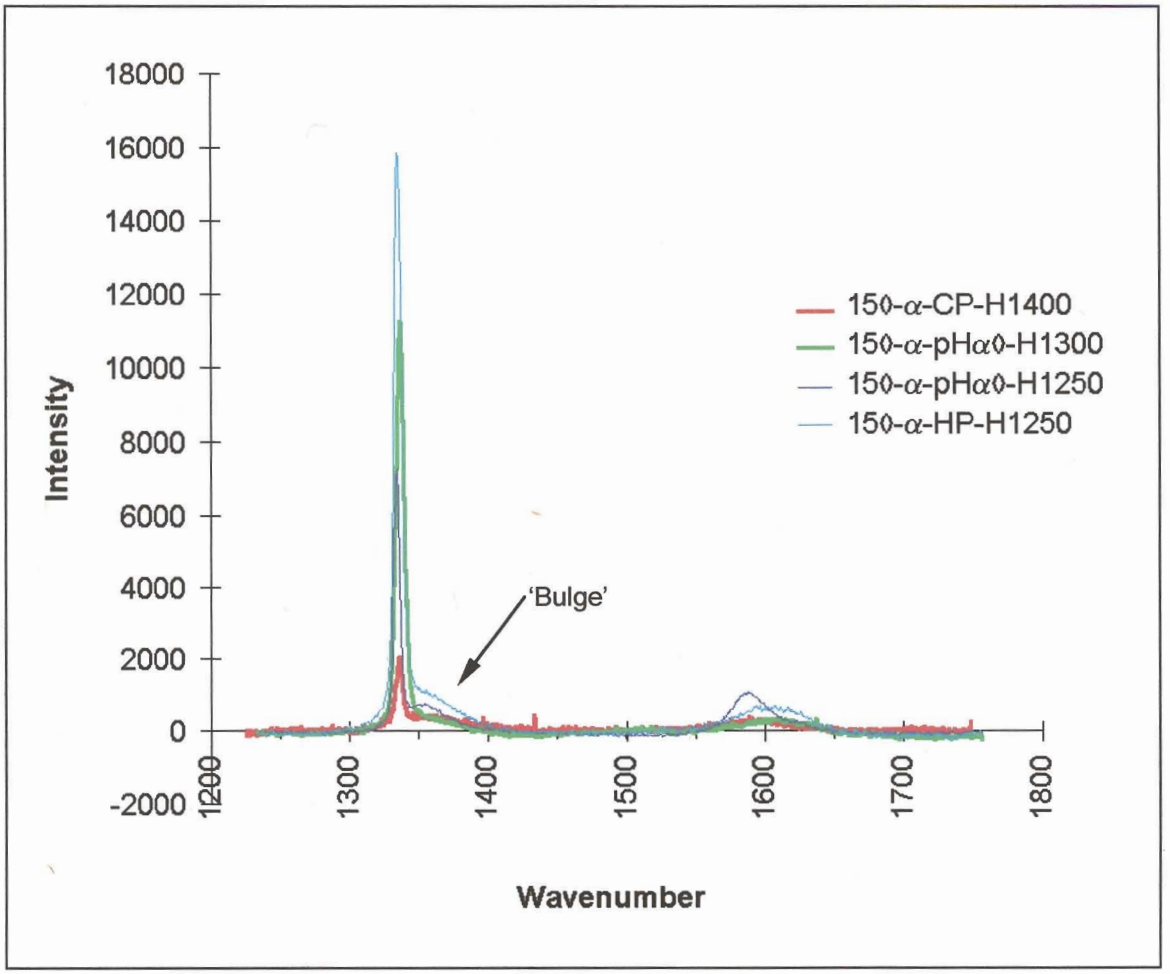

***Fig. 7-3**: Raman spectra for the analysed diamond containing samples. The indicated 'bulge' is discussed in section 11.1.3.*

Chapter 8: Fired microstructure

8.1 Introduction

8.1.1 Lack of micrographs of polished and etched samples

Ideally, work of this nature should also include images of polished and etched surfaces, which should give a representative image of grain size. Unfortunately, this was not possible. Table 8-1 gives the steps used in surface preparation for each sample that was used with some success on both diamond containing and non-diamond containing samples. Fig. 8-1 and fig. 8-2 show the finishes obtainable with this procedure. Thermal etching would have damaged the diamond particles and chemical etching did not achieve the desired effects: Chemical etching for 20 minutes with 40 % w/w hydrofluoric acid as recommended by Petzow (1976) produced the selective etching seen in fig 8-3. For these reasons only fracture surfaces are presented here.

***Table 8-1**: Surface preparation steps.*

Time (minutes)	Particle type	Particle size	Surface	Surface speed (cm/s)
~ 1	SiC	180 grit	Sanding paper	< c. 120
~ 1	SiC	220 grit	Sanding paper	< c. 120
~ 1	SiC	320 grit	Sanding paper	< c. 120
~ 1	SiC	400 grit	Sanding paper	< c. 120
~ 1	SiC	600 grit	Sanding paper	< c. 120
~ 1	SiC	800 grit	Sanding paper	< c. 120
5	Diamond	9 μm	Polishing cloth	< c. 105
5	Diamond	3 μm	Polishing cloth	< c. 105
5	Diamond	1 μm	Polishing cloth	< c. 105

8.1.2 Identification of diamond

Diamond particles can be distinguished as micron-sized particles in the micrographs, but they are also identified in black on the maps attached to micrographs showing diamond containing samples.

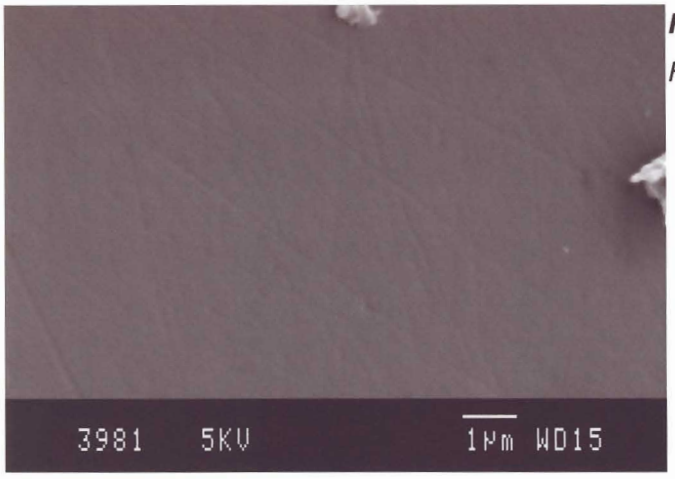

***Fig. 8-1**: A non-diamond containing sample (0◊-α-Pα-H1400) after polishing and before any etching.*

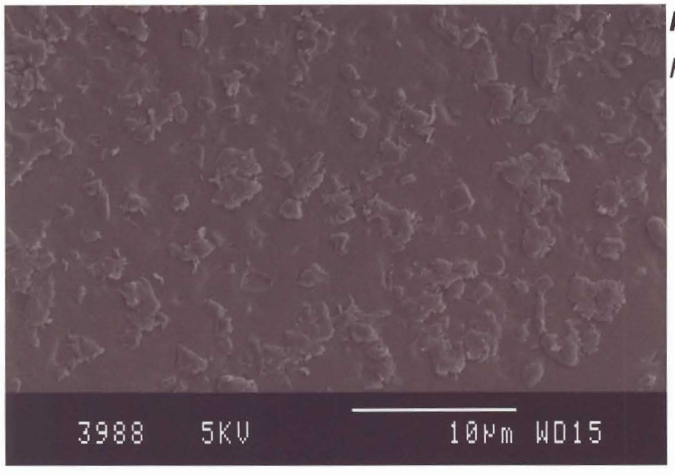

***Fig. 8-2**: A diamond containing sample (15◊-α-CP-H1400) after polishing and before any etching.*

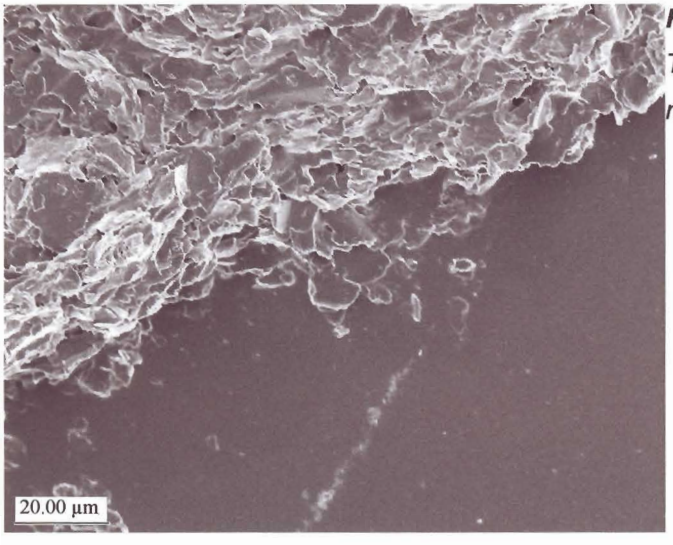

***Fig. 8-3**: The same as in fig. 8-1 after chemical etching. The etchant attacked the area in the upper half of the micrograph while area in the lower half is unaffected.*

8.1.3 Grain size estimation

By counting the number of times a line across a micrograph of a fracture surface intersects grains a crude estimation of grain size can be made. An average grain size $\bar{d}_{grain}$ would then be given by

$$\bar{d}_{grain} = \frac{[\text{Length of line}]}{[\text{Number of grains}]} \qquad (8\text{-}1)$$

As an example, consider fig. 8-4. The line spans 4.0 µm and crosses the 20 grains indicated. The average grain size for this sample is therefore 200 nm. (Ideally estimation should have been performed with properly polished and etched surfaces as, for example, per ASTM E 112-82. This was not possible for reasons already explained in paragraph 8.1.1.)

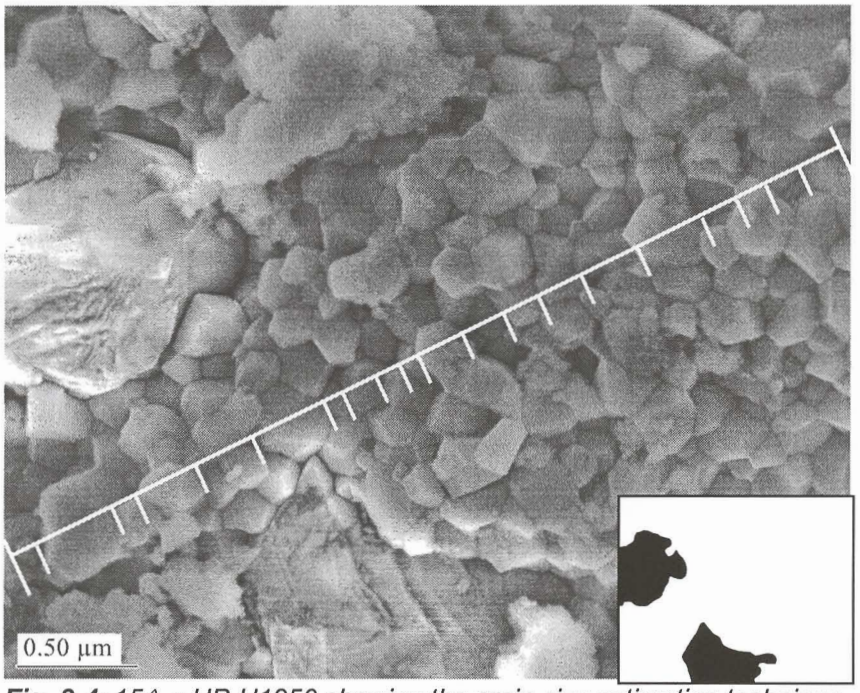

***Fig. 8-4**: 15◊-α-HP-H1250 showing the grain size estimation technique used.*

8.1.3 Equipment

All micrographs presented in this chapter were obtained with an ultrahigh resolution field emission SEM[‡] (scanning electron microscope) except fig. 8-1 and 8-2 which were obtained with a conventional (SEM)[†].

[‡] Jeol 6000, Laboratory for Microscopy and Microanalysis, Faculty of Science, University of Pretoria, South Africa.

[†] Jeol 840, as above.

8.2 Observations

Artificial fracture surfaces judged to be representative of each sample are given. For comparison, sets of micrographs are grouped on pages according the scheme given in table 8-2.

Average grain size as a function of HIPping temperature is given in fig. 8-24.

***Table 8-2**: Ordering of micrographs.*

Sample	Page	Micrographs	Remarks
0◊-α-Pα-H1400	60	Fig. 8-5	Both non-diamond containing
0◊-α-Pα-H1200		Fig. 8-6	
15◊-α-CP-H1400	61	Fig. 8-7	Same area
		Fig. 8-8	
		Fig. 8-9	
15◊-α-pH-H1300	62	Fig. 8-10	Same area
		Fig. 8-11	
		Fig. 8-12	
15◊-α-HP-H1250	63	Fig. 8-13	Same area
		Fig. 8-14	
		Fig. 8-15	
15◊-α-pH-H1250	64	Fig. 8-16	Same area
		Fig. 8-17	
		Fig. 8-18	
15◊-α-CP-H1250	65	Fig. 8-19	Same area
		Fig. 8-20	
		Fig. 8-21	
15◊-α-pH-H1300	66	Fig. 8-22	Close-up of diamond-alumina interface
		Fig. 8-23	

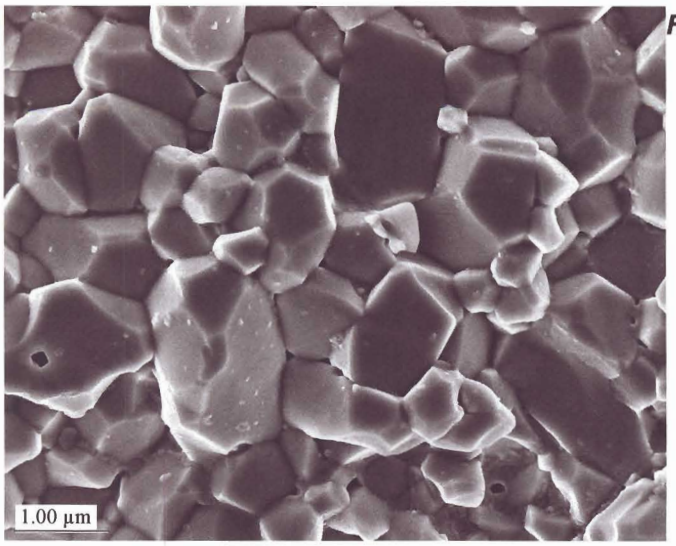

***Fig. 8-5**: 0◊-α-Pα-H1400.*

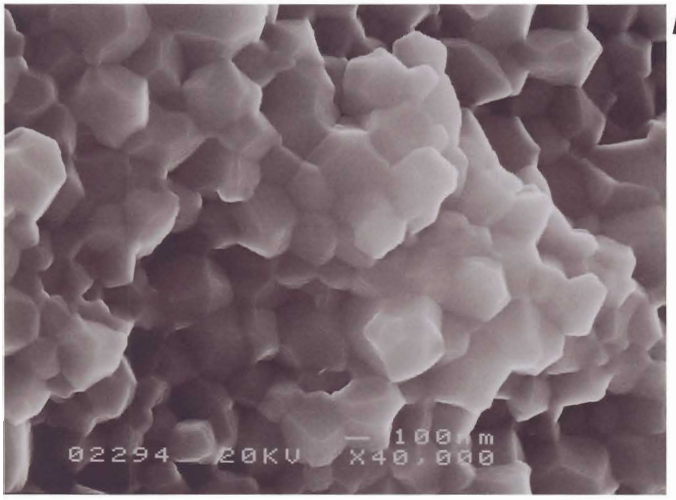

***Fig. 8-6**: 0◊-α-Pα-H1200.*

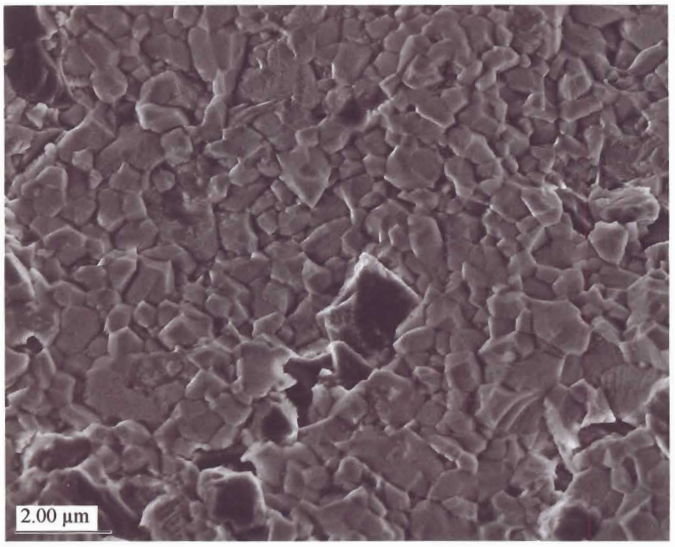

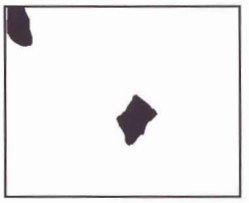

***Fig. 8-7**: 15◊-α-CP-H1400.*

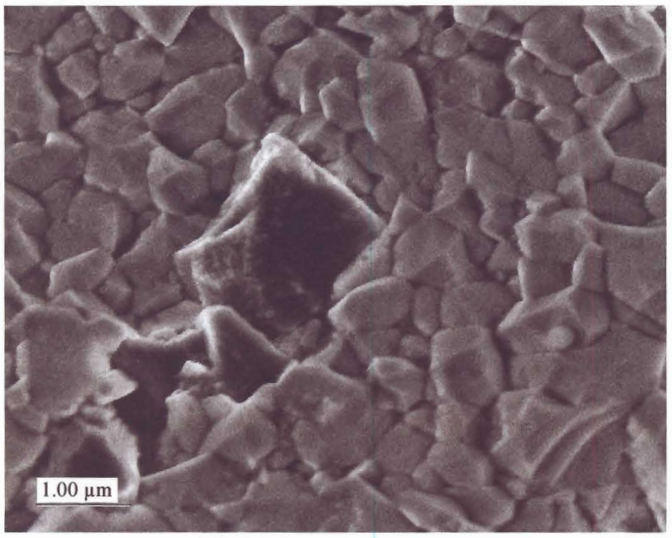

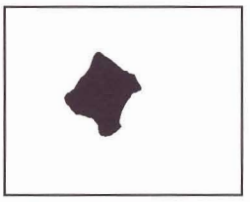

***Fig. 8-8**: 15◊-α-CP-H1400.*

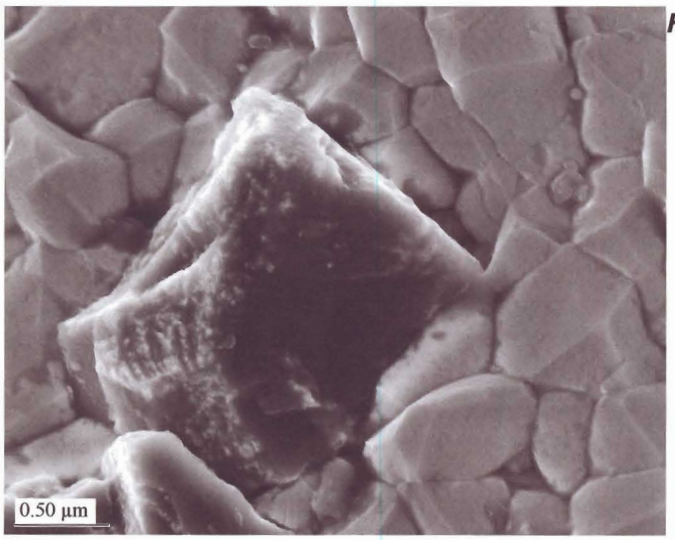

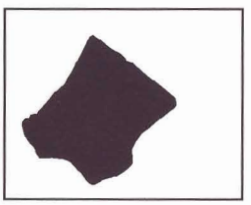

***Fig. 8-9**: 15◊-α-CP-H1400.*

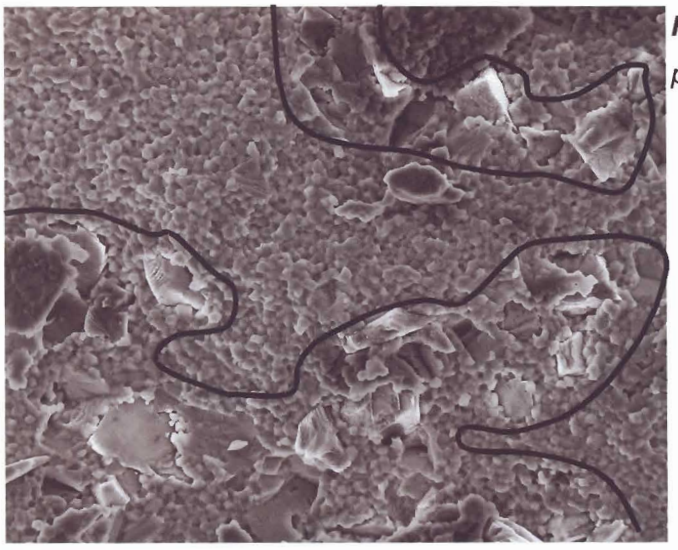

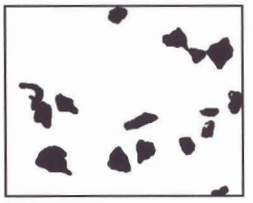

***Fig. 8-10**: 15◊-α-pH-H1300. Note grouping of diamond particles.*

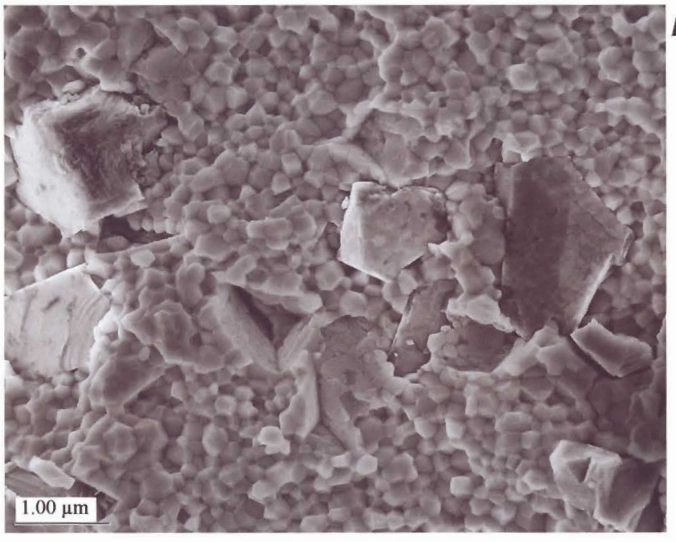

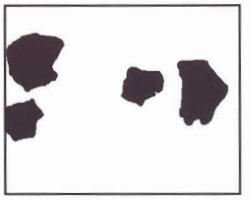

***Fig. 8-11**: 15◊-α-pH-H1300.*

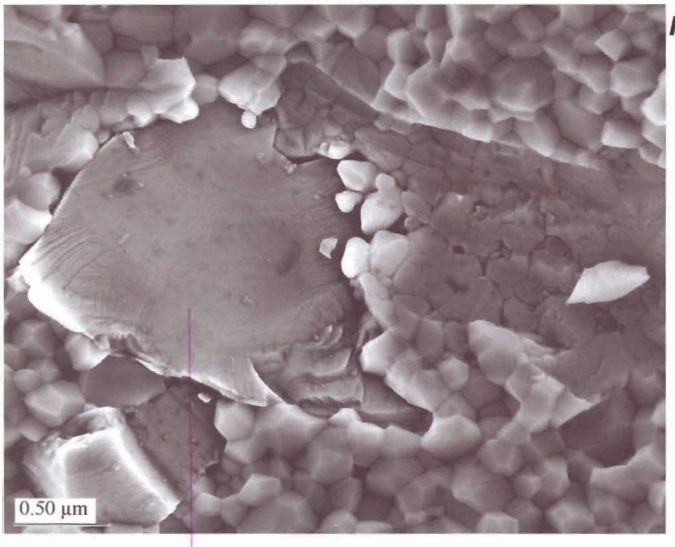

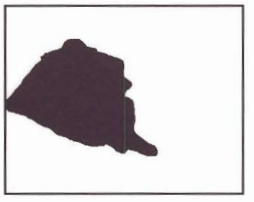

***Fig. 8-12**: 15◊-α-pH-H1300.*

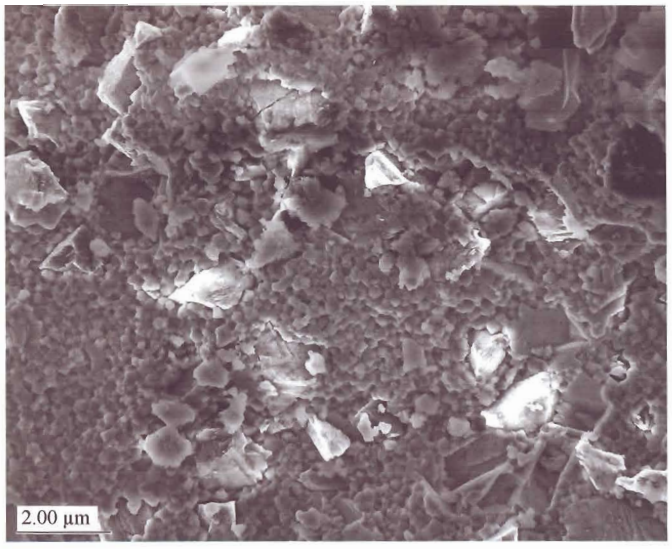

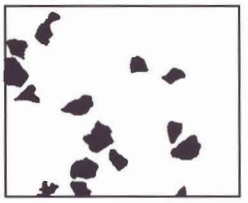

***Fig. 8-13**: 15◊-α-HP-H1250.*

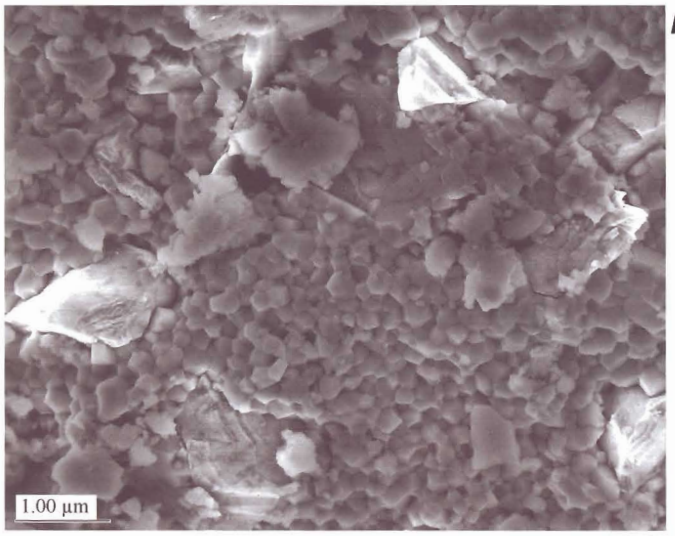

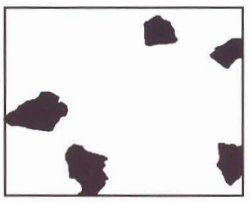

***Fig. 8-14**: 15◊-α-HP-H1250.*

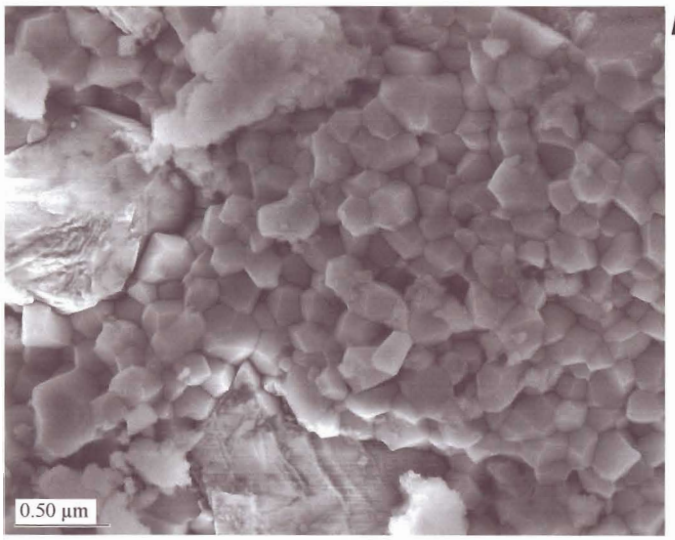

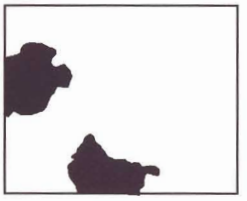

***Fig. 8-15**: 15◊-α-HP-H1250.*

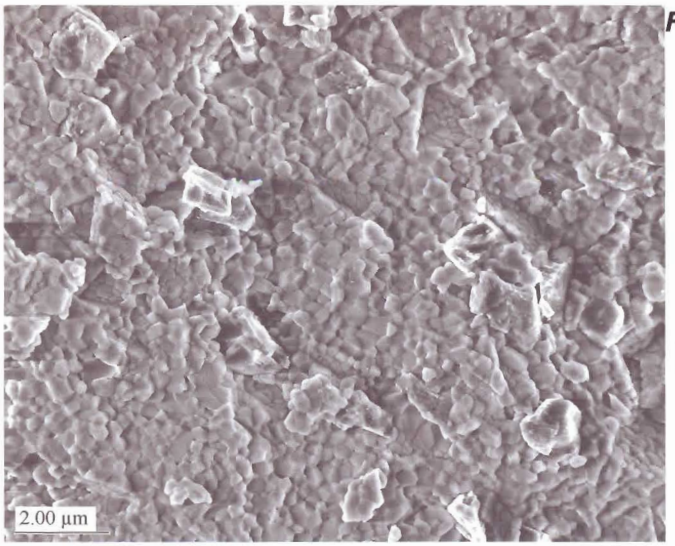

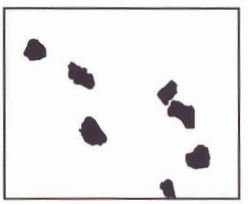

Fig. 8-16: *15◊-α-pH-H1250.*

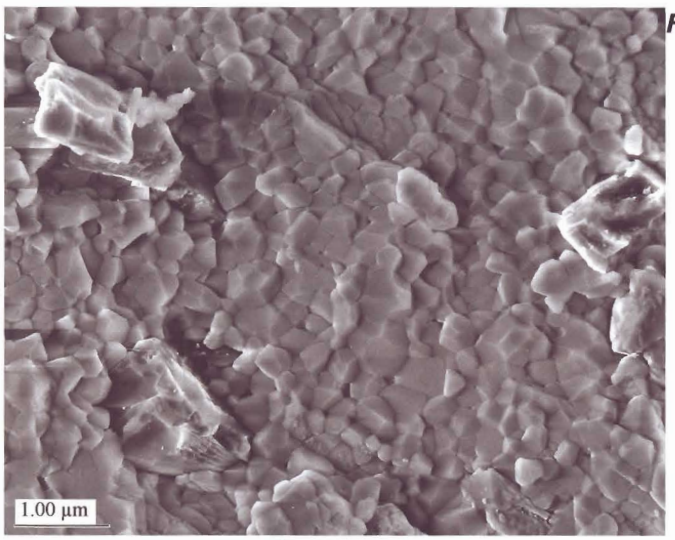

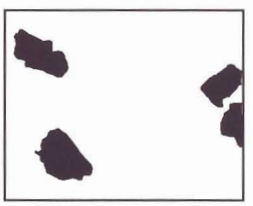

Fig. 8-17: *15◊-α-pH-H1250.*

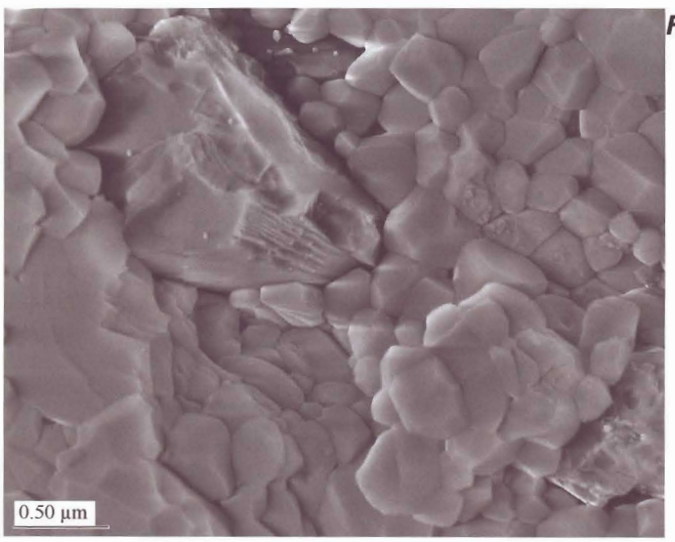

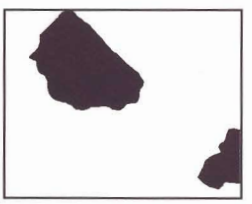

Fig. 8-18: *15◊-α-pH-H1250.*

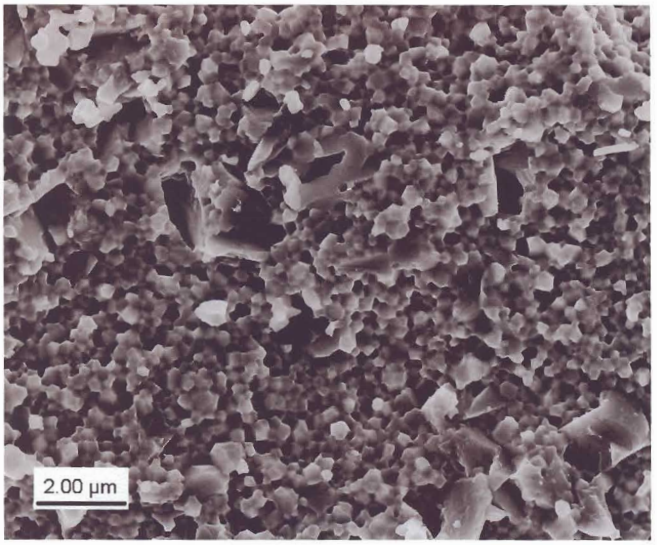

Fig. 8-19: *15◊-α-CP-H1250.*

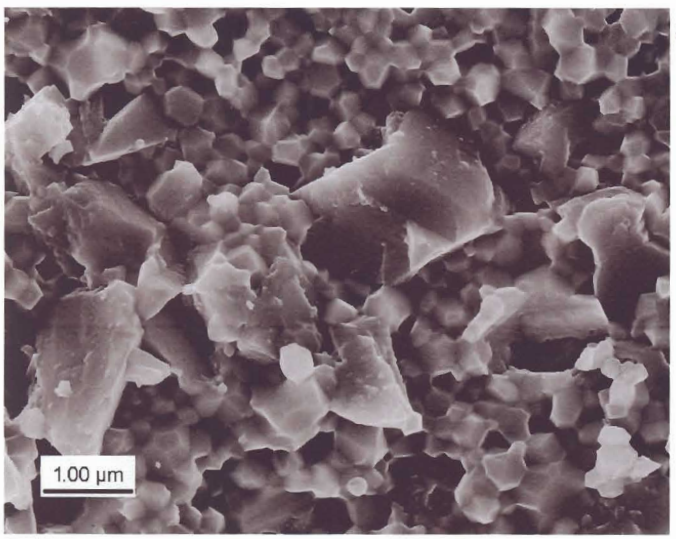

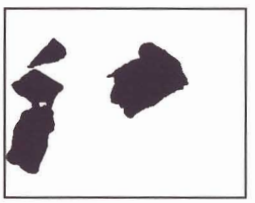

Fig. 8-20: *15◊-α-CP-H1250.*

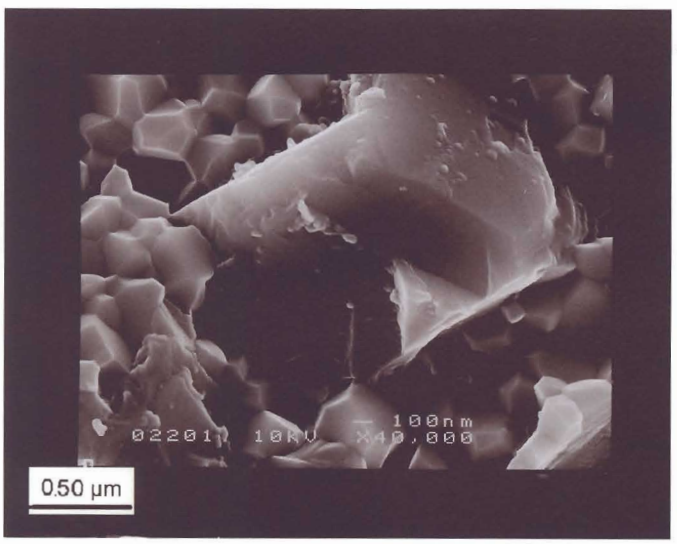

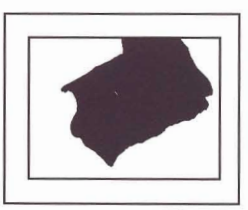

Fig. 8-21: *15◊-α-CP-H1250.*

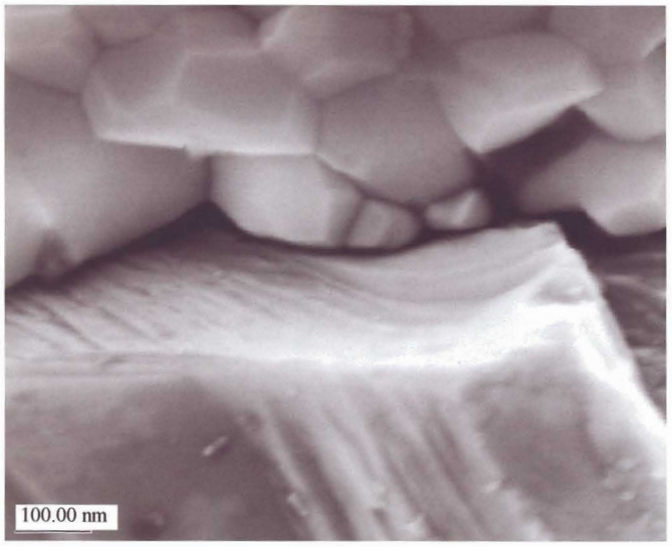

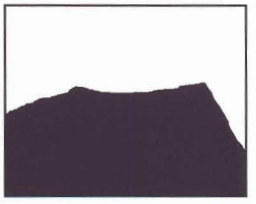

***Fig. 8-22**: 15◊-α-pH-H1300.*

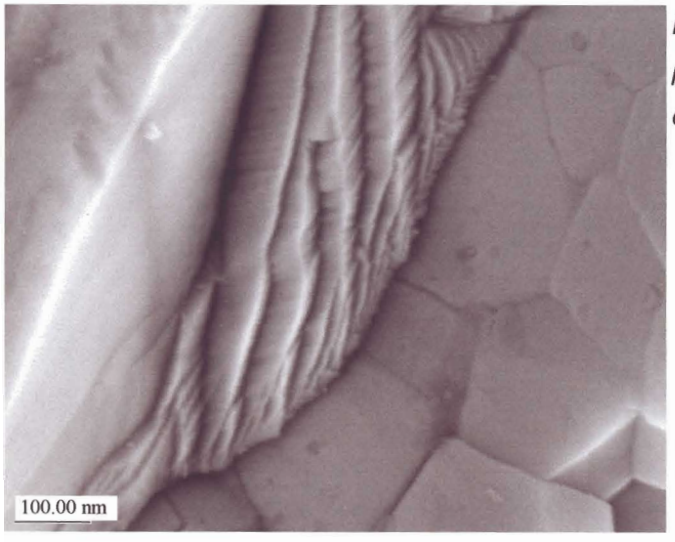

***Fig. 8-23**: 15◊-α-HP-H1300. The stepped surface is probably diamond, although this is not typical of the diamond particles used.*

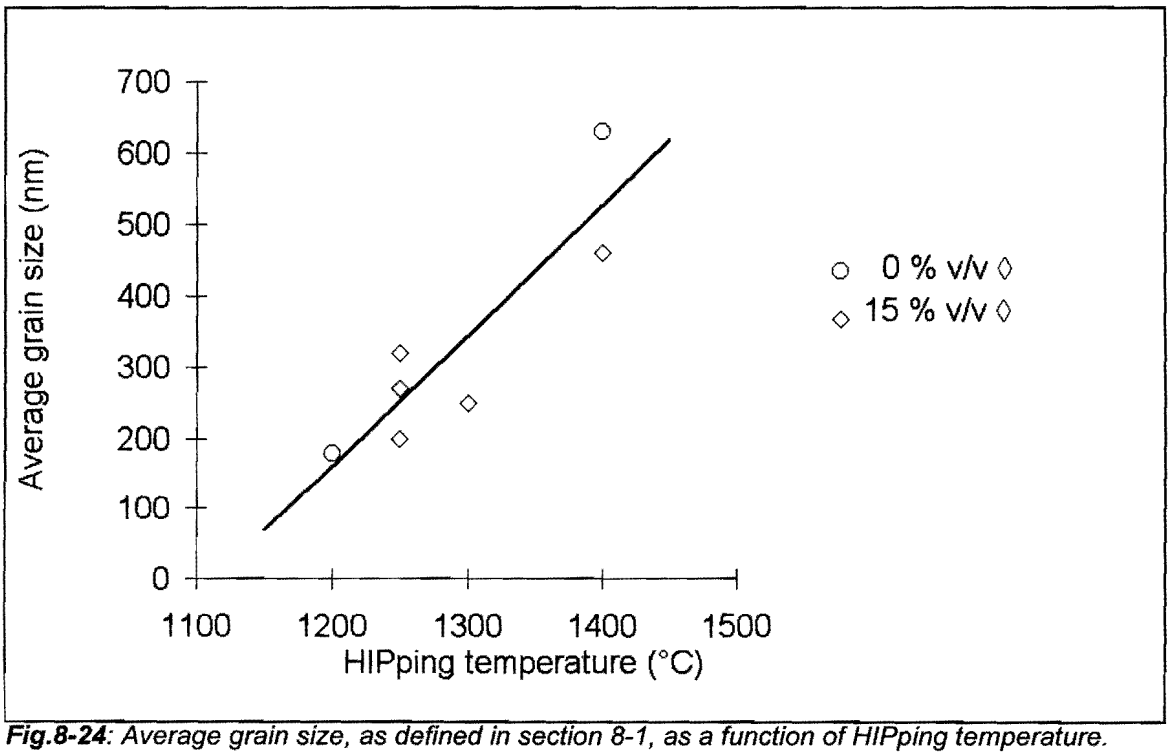

***Fig.8-24**: Average grain size, as defined in section 8-1, as a function of HIPping temperature.*

Chapter 9: Hardness and toughness

9.1 Techniques

Although surfaces can be relatively rough for hardness measurement by indentation, finishes needs be smoother for toughness measurement by the same technique, as cracks need to be differentiated. Accordingly, surfaces were polished as for microscopy (table 8-1, page 68). The micrography arrangement that was used is shown in fig. 9-1. All actual measurements were made on the PC screen, as this was deemed to give the best resolution. (The video monitor was only used as a focussing aid, which was neccesary as the 'Snappy' only updates the PC image every half a second; the video monitor image is live.) Identical conditions of resolution and magnification were used for measurements. Where in doubt the location of the end of cracks was confirmed by observation at the microscope itself.

It should be noted that the use of a video camera and a 'Snappy' is a low cost alternative to proper digital photography equipment. It does not give images of high quality (as can be seen in fig.9-4 to 9-9). The accuracy of hardness and toughness values reported here is adversely affected by the low quality of micrography.

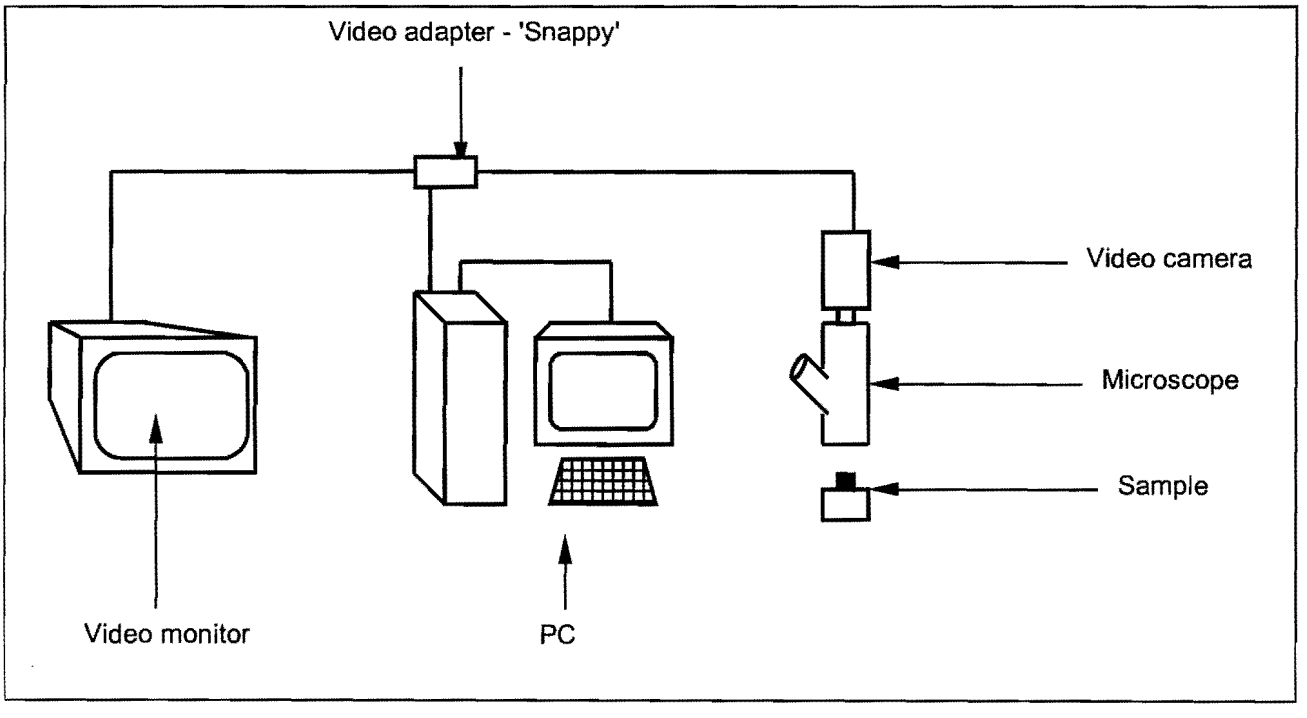

***Fig. 9-1**: Micrography set-up for crack length measurements.*

The lengths of the diagonals, d were measured under the same conditions as the crack length. The edges of the indent were not always well defined and the error in the

measurement of the diagonal length, d, is judged from repeated measurements to be approximately $^{+4.4\ \mu m}/_{-4.4\ \mu m}$. This translates to quite a large possible error in the reported hardness values (fig. 9-2).

The value of c needed in equation 5-12 (page 39) was taken from the average of the four values of c that each indentation has. The hardness and toughness of each sample was determined from the average of three indentations' hardness and toughness measurements.

Indentor load was 10 kg throughout. This was also the load used by Noma and Sawaoka (1984 and 1985).

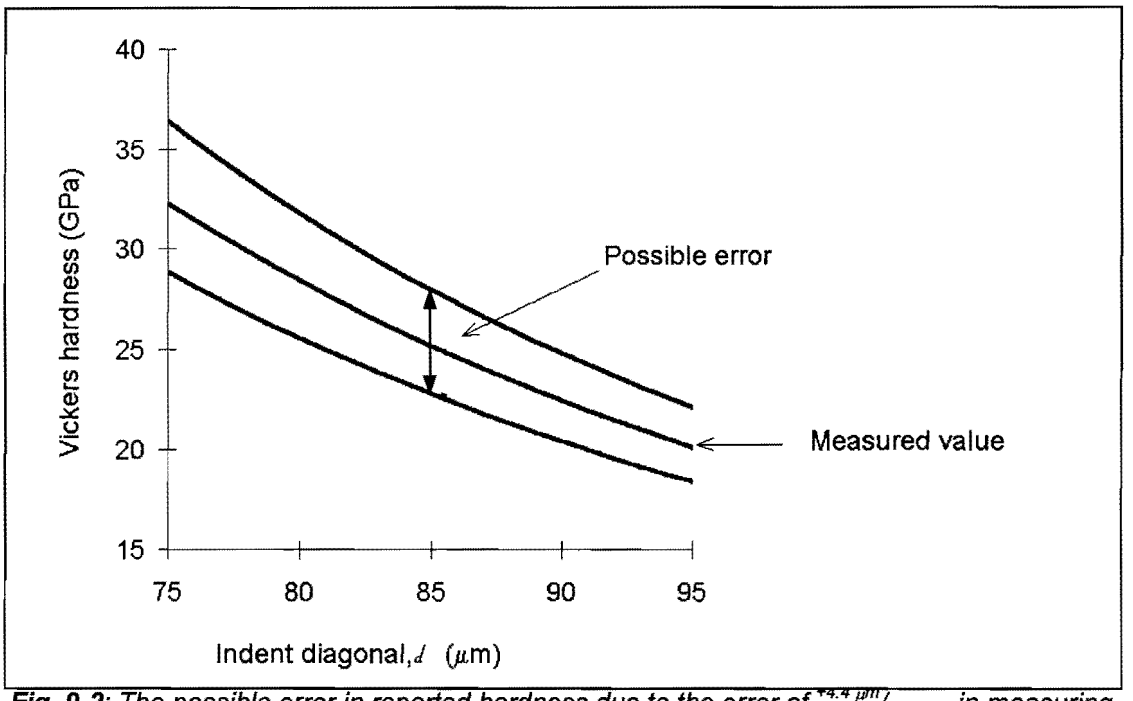

***Fig. 9-2**: The possible error in reported hardness due to the error of $^{+4.4\ \mu m}/_{-4.4\ \mu m}$ in measuring indent diagonal size. E.g. if the indent diagonal is measured as 85 μm the reported hardness would be 25 GPa but due to the error in measurement actual hardness may be any value between 22.5 and 27.5 GPa.*

9.2 Results

The recorded values of d and c and the calculated hardness and toughness are reported in table 9-1. Hardness was calculated as the pressure exerted on the indent surface area, i.e.

$$H_V = \frac{9.81M}{\frac{(10^{-6}d)^2}{2\cos 22^\circ}} \qquad (9\text{-}1)$$

with H_V in Pa if the indentor load M is given in kg and d is given in µm, 22° being the angle between the surfaces of the indentor's tip and the surface of the sample. Toughness was calculated from equation 5-12. The Young modulus (E) for the diamond containing samples, which is required for toughness calculation (equation 5-9, page 40), is estimated in appendix A4.

Examples of indentations for each of the three types of material (Toshiba LX11, non-diamond containing alumina, and diamond-alumina composite) are shown in fig. 9-3 to 9-8. Note that the crack lengths were not measured at the magnification or resolution of fig. 9-3 to 9-8 but were measured on the PC screen. If crack lengths were to be measured from the micrographs as they are printed here they will not correspond to those reported in table 9-1.

The Toshiba LX11 can be used as a crude control for the toughness measurement, as some indication of its toughness is available. Toshiba replaced their grade LX10 with grade LX11. Grade LX10 is unobtainable, although specifications (from a pamphlet of Toshiba) are only available for LX10. According to the local suppliers (Toolquip), LX11 is an improved version of LX10. It can therefore not be expected to be very different from that of LX11. Also, the measured density of 4.3 g/cm^3 for the LX11 insert used corresponded to the 4.30 g/cm^3 given for LX10. The specified toughness for LX10 is 3.3 MPa.m^{½}, with no indication of the method used. This value is reasonably close to the value of 2.7 MPa.m^{½} measured for LX11.

***Table 9-1**: Results from indentation.*

Sample	d (μm)	Average c (μm)	Estimated E (GPa)	Hardness (GPa)	Fracture toughness (MPa.m^{½})	Average hardness (GPa)	Average toughness (MPa.m^{½})
LX11	85	145	390	25	2.9	26	2.7
	83	153		27	2.6		
	83	155		27	2.5		
15◊-α-CP-H1400	83	109	460	27	4.6	26	4.2
	85	128		25	3.7		
	83	117		27	4.2		
0◊-α-Pα-H1400	89	174	390	23	2.3	24	2.1
	87	180		24	2.1		
	87	185		24	2.0		
15◊-α-CP-H1250	83	140	460	27	3.2	27	2.7
	83	166		27	2.5		
	83	169		27	2.4		
15◊-α-pHα◊-H1250	87	145	460	24	3.2	22	3.3
	94	153		21	3.2		
	91	137		22	3.6		
15◊-α-HP-H1250	85	135	460	25	3.5	25	3.8
	85	112		25	4.6		
	85	136		25	3.4		

Table 9-1 *continued.*

Sample	d (μm)	Average c (μm)	Estimated E (GPa)	Hardness (GPa)	Toughness (MPa.m^{½})	Average hardness (GPa)	Average toughness (MPa.m^{½})
15◊-α-HP-H1300	89	147	460	23	3.2	24	2.8
	85	160		25	2.7		
	87	169		24	2.5		
0◊-α-Pα-H1350	89	235	390	23	1.5	24	1.5
	87	222		24	1.5		
	87	217		24	1.6		
0◊-α-Pα-H1200	85	216	390	25	1.6	26	1.7
	83	205		27	1.7		
	83	192		27	1.8		

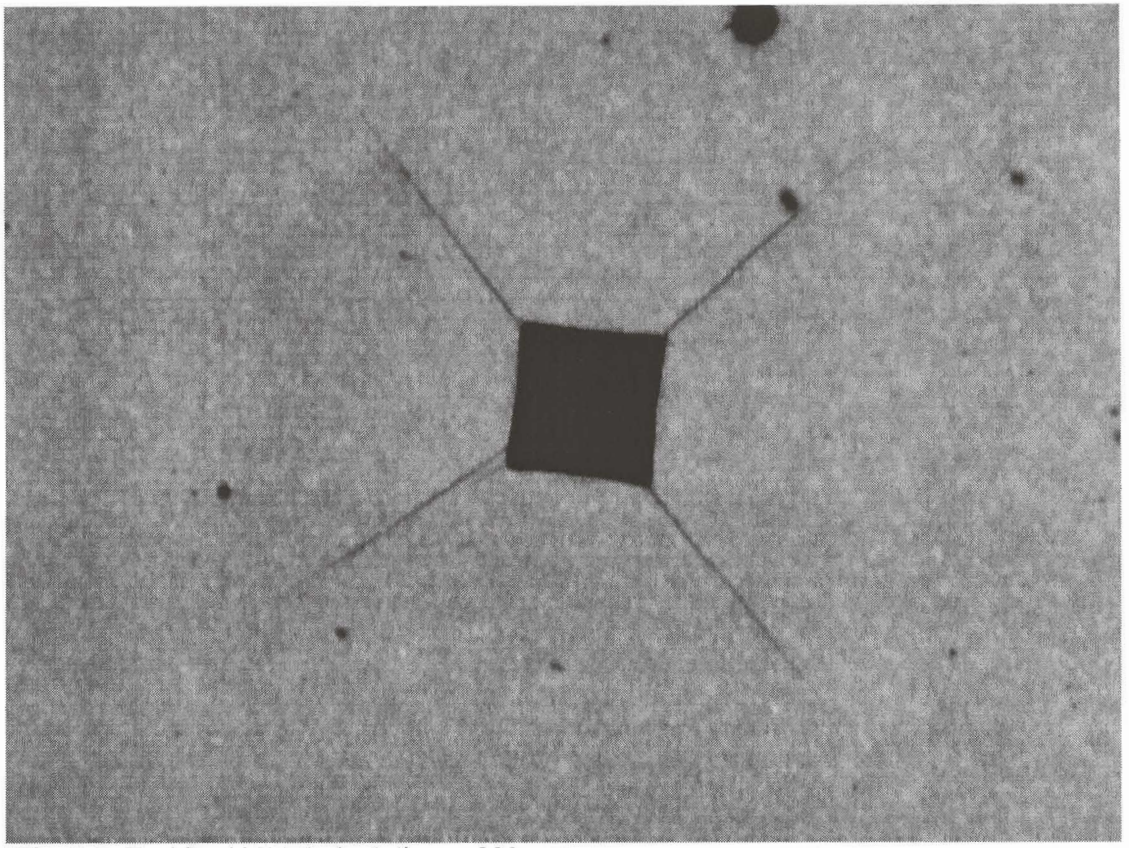

***Fig. 9-3**: Toshiba LX11. Indentation. × 300.*

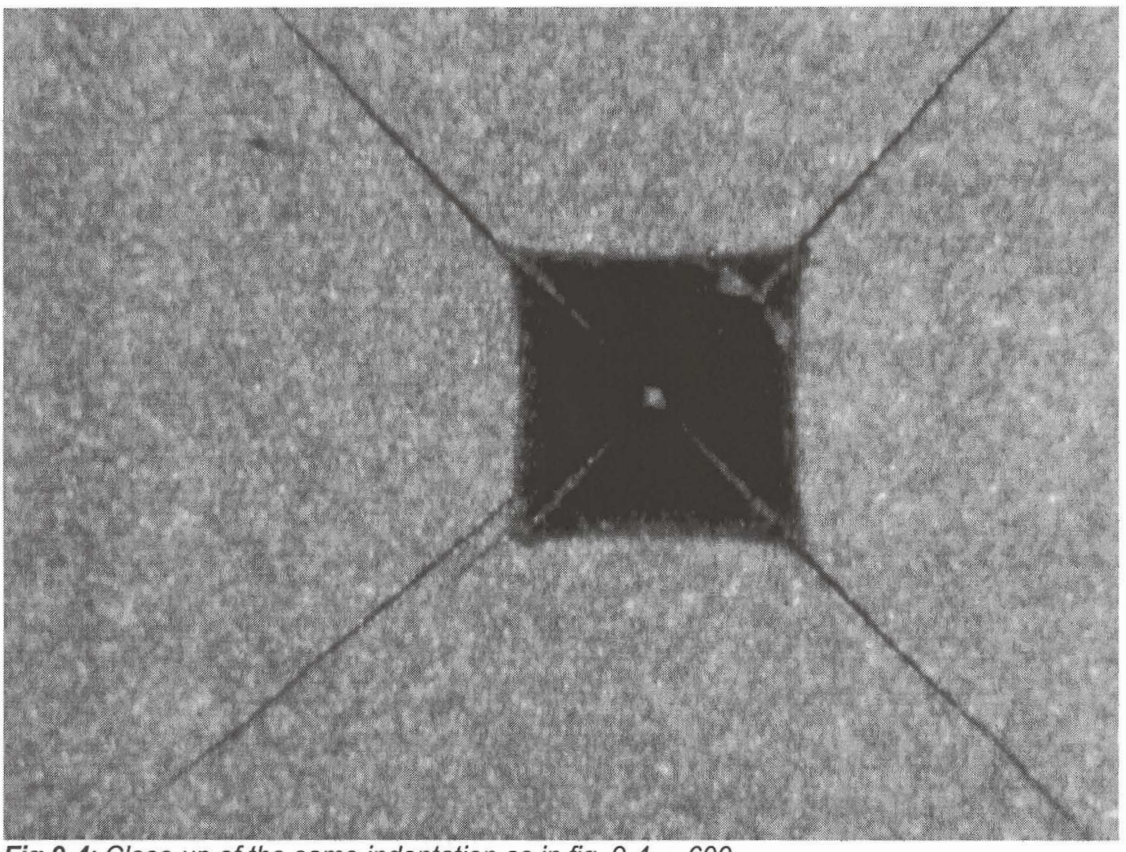

***Fig 9-4**: Close up of the same indentation as in fig. 9-4. × 600.*

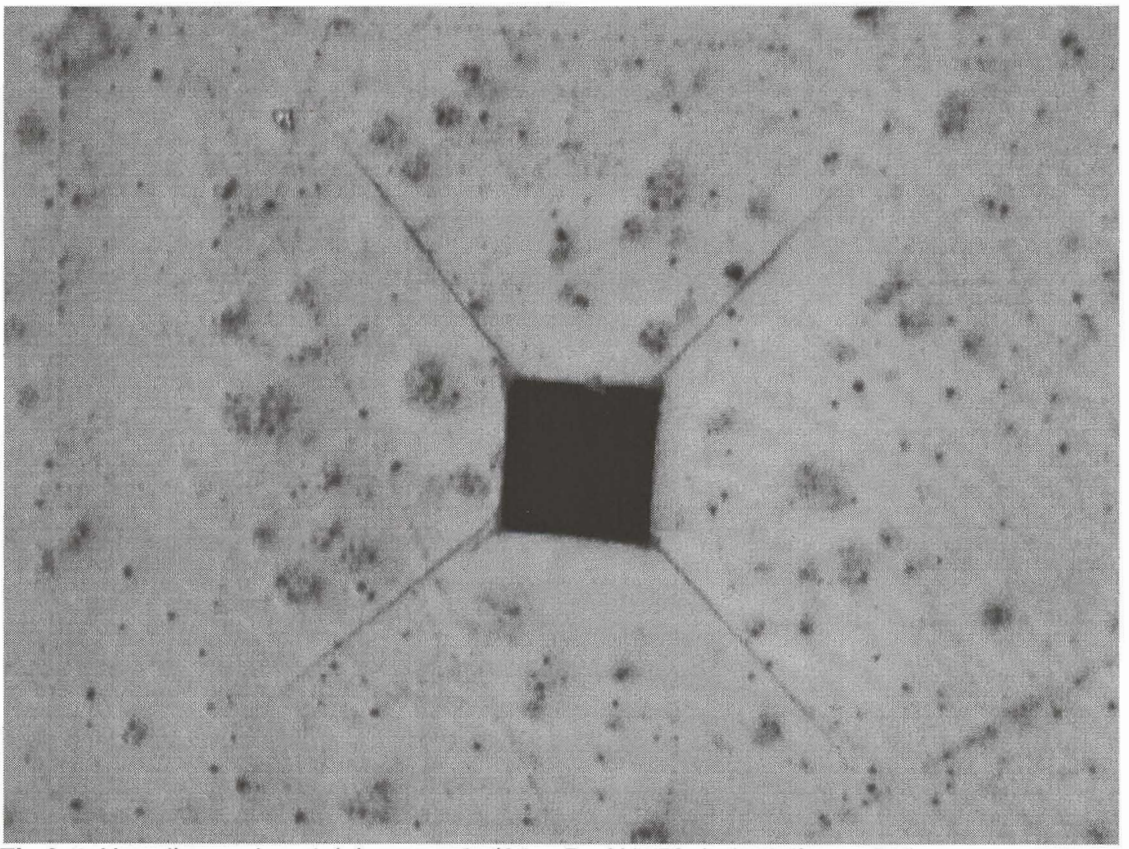

***Fig 9-5**: Non-diamond containing sample (0◊-α-Pα-H1350. Indentation. × 300.*

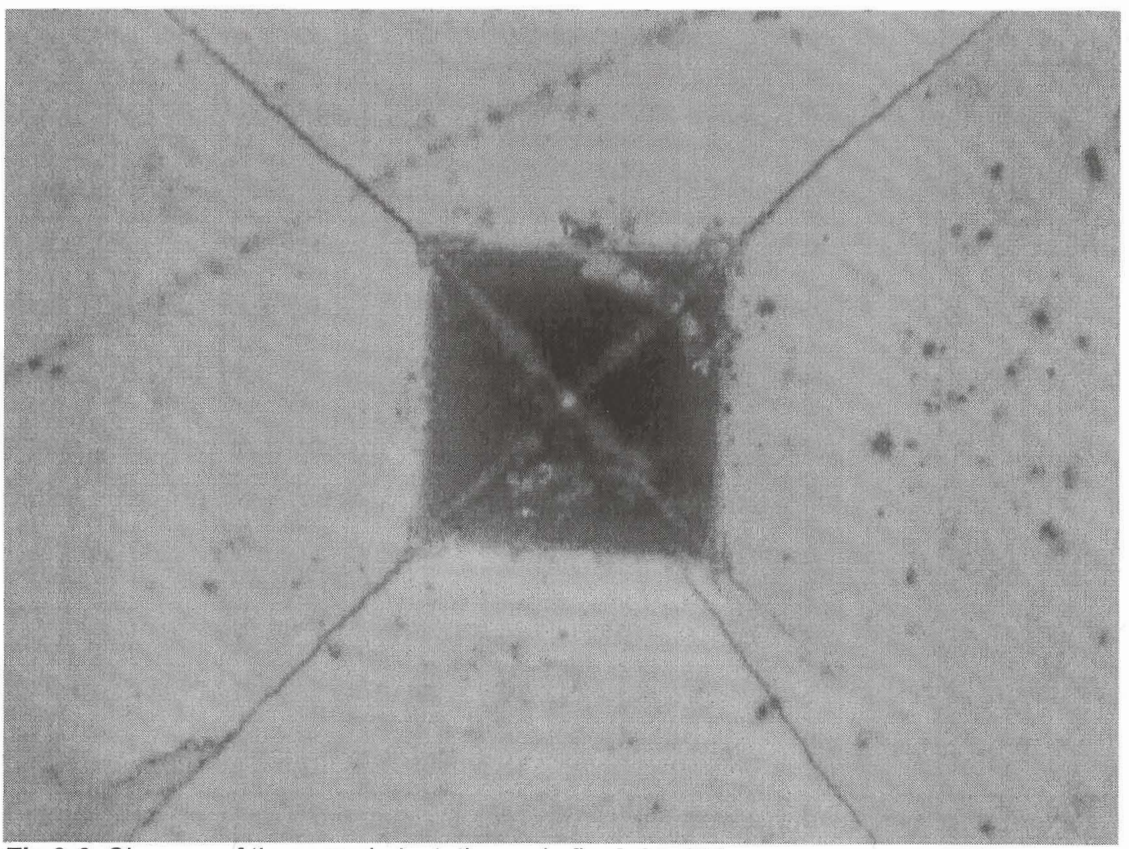

***Fig 9-6**: Close up of the same indentation as in fig. 9-6 × 600.*

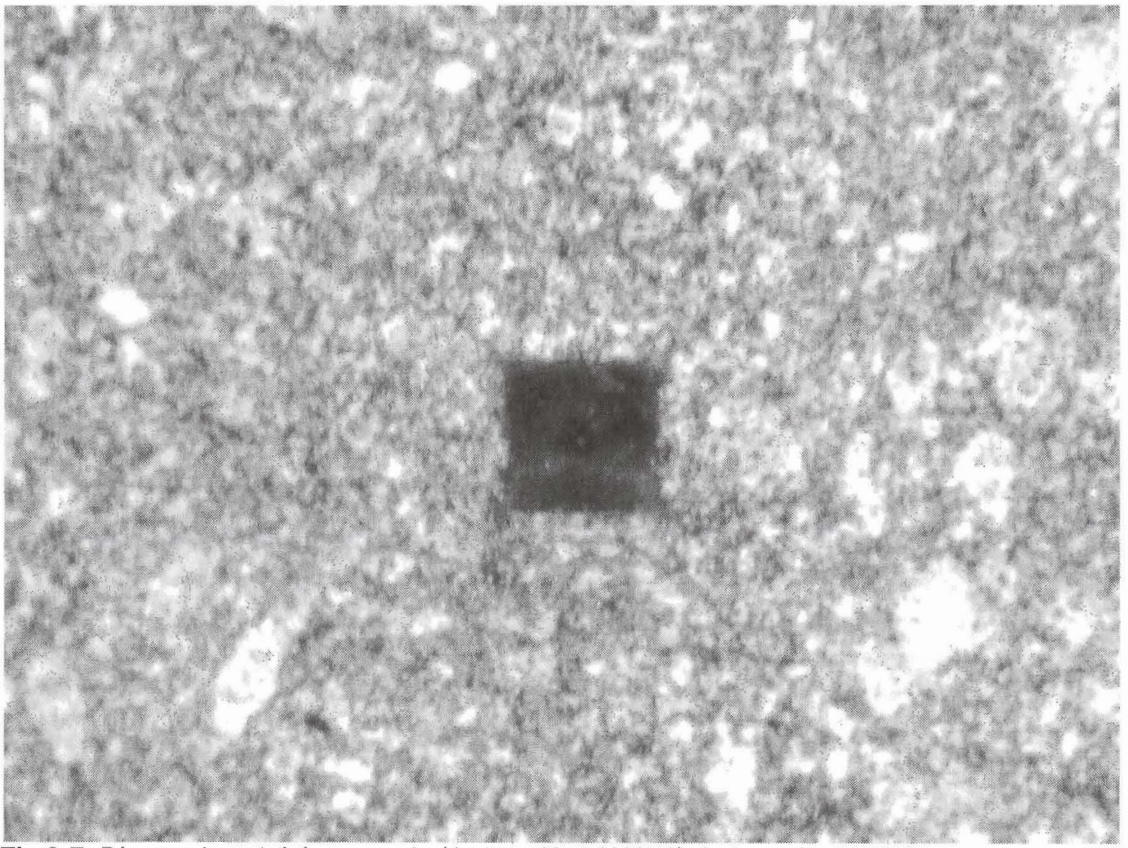

Fig 9-7: Diamond containing sample (15◊-α-pHα◊-H1250). Indentation. × 600.

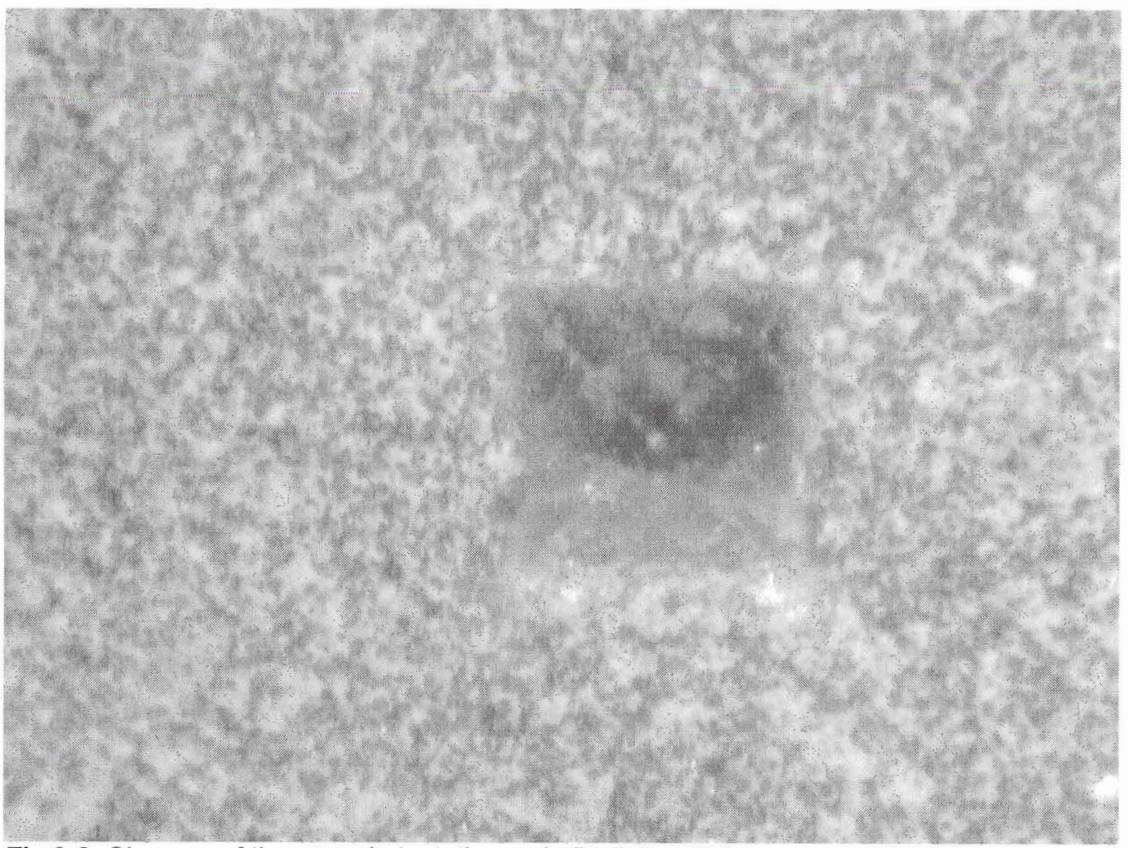

Fig 9-8: Close up of the same indentation as in fig. 9-8. × 600.

Chapter 10: Wear testing

10.1 Techniques

Wear performance was evaluated by a cutting test with a commercial lathe. The test material was a standard rod of so-called 'Siffer'[†]. The samples were shaped to the required dimensions with commercial tool sharpening equipment. Again the commercially available Toshiba LX11 was chosen as reference material. Ideally the wear performance of alumina -diamond should approach the performance of LX11 as LX11 is also an alumina composite, albeit an alumina-zirconia composite. LX11 also proved useful to set the conditions for the wear tests. Of the possible dimensional wear measurements illustrated in fig. 5-3 (page 38), only maximum flank wear V_{max} was measured.

Parameters for the test were as follows (terminology is illustrated in fig. 5-1, page 34).

Surface speed:	15 $^{+0.5}/_{-0}$ m/min.
Depth of cut:	2 mm.
Tool nose radius:	0.8 mm
Tool nose clearance:	6°.
Approach:	45°
Rake angle:	0°
Feed rate:	0.1 mm/revolution

Although it may not appear so from fig. 10-1 to 10-4 (showing the progress of wear), the precise boundaries between the flank wear scar and the unworn face were unclear (lighting conditions for fig. 10-1 to 10-4 were not the same as for wear scar observation). Furthermore, distinction between flank wear zones and notch wear zones were open to individual interpretation. The length of maximum flank therefore depended on (possibly subjective) visual inspection. To eliminate at least some experimental variation, only the measurements of one observer, A. R. Ravenhill[‡] are quoted.

10.2 Results

Wear followed the trend illustrated in fig. 5-5 (page 40) but samples were not tested up to failure and the setlling-in behaviour was not observed in any samples. This meant that wear rate and apparent starting wear (fig. 5-5) was not observed. Wear rates and apparent starting wear were therefore determined by simple linear regression and are noted in table 10-1. The complete set of wear test data are presented in appendix A5.

[†] 'Siffer' is an in-house testing material used exclusively by De Beers.

[‡] Synthesis Division, Diamond Research Laboratory, Industrial Diamond Division, De Beers, Johannesburg, South Africa.

The progress of the wear for sample 0◊-α-Pα-H1200 is shown in fig. 10-1 to 10-4. Although this is a non-diamond containing sample the wear progress shown is typical of both diamond containing and non-diamond containing samples. Note that wear measurements were made with measuring toolmaker's microscope on site and not on the micrographs themselves, with the result that the length of maximum flank given in table 10-1 would not exactly correspond to the flank wear length visible in the given micrographs (fig. 10-1 to 10-4).

***Table 10-1**: Average wear rates and apparent starting wear.*

Reference no.	Wear rate (µm/s)	Apparent starting wear (µm)
LX11	0.5	90
0◊-α-CP-H1400	6.0	208
15◊-α-CP-H1400	19.3	301
15◊-α-CP-H1350	12.9	135
0◊-α-Pα-H1350	7.0	110
0◊-α-HP-H1300	2.0	76
15◊-α-pH-H1300	1.5	190
15◊-α-HP-H1300	4.4	186
15◊-α-HP-H1250	13.0	-107
15◊-α-pH-H1250	7.7	147
15◊-α-CP-H1250	7.4	174
0◊-α-Pα-H1200	2.5	108
15◊-α-CP-H1200	8.9	104

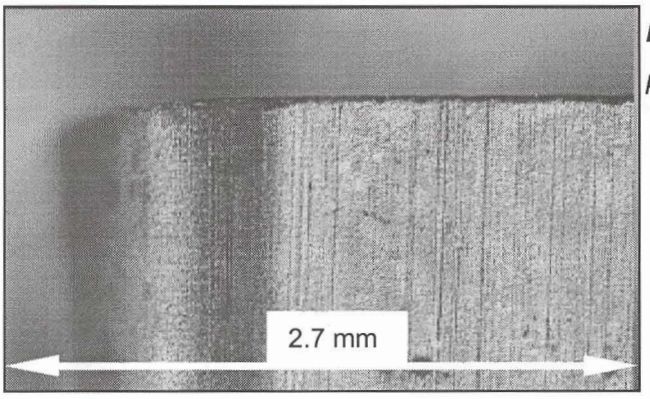

***Fig. 10-1**: Sample 0◊-α-Pα-H1200 as prepared for cutting test.*

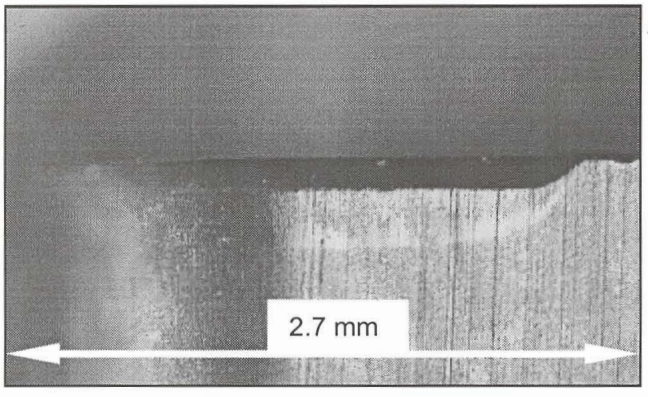

***Fig. 10-2**: Sample 0◊-α-Pα-H1200 after 10 seconds' cutting of cutting Siffer.*

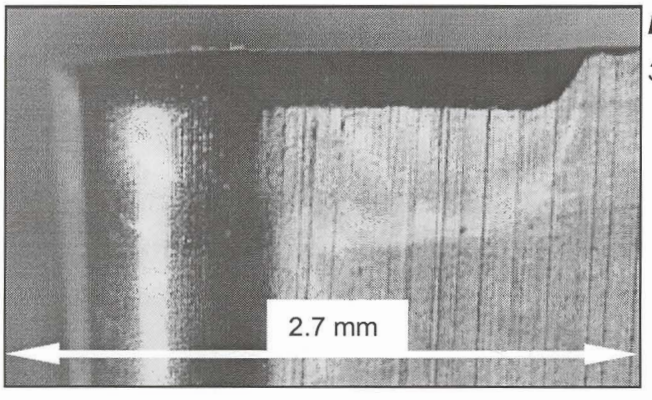

***Fig. 10-3**: Sample 0◊-α-Pα-H1200 after 30 seconds' cutting of cutting Siffer.*

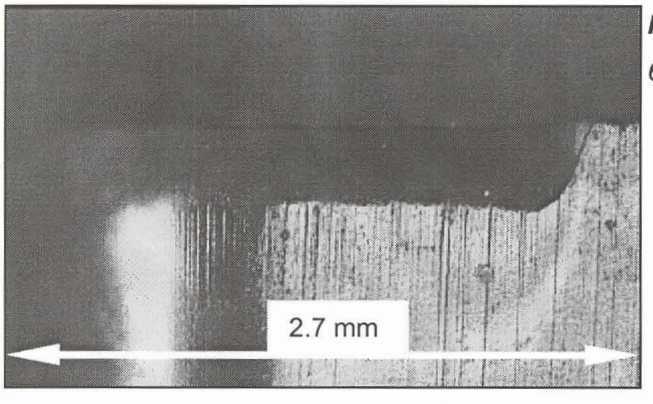

***Fig. 10-4**: Sample 0◊-α-Pα-H1200 after 60 seconds' cutting of cutting Siffer.*

Chapter 11: Discussion

11.1 Interpretation of results

11.1.1 Green processing

Although other methods of green processing, i.e. dry pressing, slip casting and centrifugal casting, were not used in this work, literature shows that filter casting is the preferred green processing route for the processing of nanocomposites (at least in a laboratory environment). Dry pressing generally gives compacts of poorer quality than 'wet' processing routes, while slip casting and centrifugal casting is impractical compared to filter casting.

Some of the practical problems with filter casting presented in literature may not have been noticed in this work. These are recovery strain (samples were too small to observe any recovery) and separation of particle sizes (powders used had fairly narrow particle size distributions). Separation of the suspensions components (diamond and alumina) during filtration would have been discovered if it did occur, but were not observed as long as fresh (not older than c. 6 h) suspensions were used.

In the mercury porosimetry run (section 7.1, page 52) the greatest frequency of pores occurred at pore sizes of c. 50nm, which is of the same order of size as the particle. This is to be expected of fairly monosized particles, since the size of voids between particles would be of the same order as the size of the particles. No peaks occurred at larger pore sizes, indicating that no large cracks were present.

11.1.2 Firing

The sintering results of Yeh and Sacks (100 % relative density at 1 150 °C in air with AKP-50, section 2.2, page 19) could not be duplicated. With similar conditions 99 % relative density could only be obtained at 1400 °C (fig. 7-2, page 53). The addition of titania improved the situation, with 99 % relative density occurring at 1300 °C.

It is difficult to compare HIPping results of this work with HIPping results from literature (page 26), as the starting conditions (green compact preparation history and especially pre-HIP heat

treatment history) of compacts are not comparable. Nonetheless HIPping conditions used in this work (section 6.4.3, page 51) does not seem to be too excessive compared to those from literature (page 26).

11.1.3 Graphitisation

Although it is impossible to obtain reliable quantitative results from Raman spectroscopy without extensive research into the specific case, there should at least be some relationship between peak intensities and the degree of graphitisation. For instance, smaller intensities at the diamond wavenumber and higher intensities at the graphite and amorphous wavenumbers might correspond to a higher degree of graphitisation. Features on the spectra obtained (fig. 7-3, page 55) and the spectra of Knight and White (1989) (fig. 4-6 to 4-9, page 34) are compared in table 11-1.

The 'bulge' to the right of the diamond peak (indicated in fig. 7-3) might be either attributable to the formation of amorphous carbon (typified by a weak peak at c. 1350, compare fig. 4-8) or due to a possible shift on the diamond peak in the presence of alumina (compare fig. 4-9). Since the 'bulge' is more prominent with the samples HIPped at 1 250 °C, where one might expect less graphitisation and less diamond to amorphous carbon transition, it could rather be indicative of the closeness of contact between diamond and alumina (similar to that occurring with vapour deposited diamond on alumina) in these samples, than the presence of amorphous carbon (unless amorphous carbon also forms during vapour deposition of diamond on alumina, although this possibility was not mentioned by Knight and White).

The slight 'bump' occurring with all samples at a wavenumber of 1580 is very likely due to formation of graphite (which has a peak at 1580, compare fig. 4-7).

There is evidence for graphitisation in all samples, but it is difficult to rank samples according to degree of graphitisation. For instance, on the evidence of the strength of the diamond peaks, it would seem that 15◊-α-CP-H1400 (i.e. the sample with the hottest HIPping) experienced the most graphitisation but it also has the one of smallest graphite 'bumps'.

***Table 11-1**: Comparison of Raman spectra.*

		Feature →	Diamond peak	'Bulge' on the right of the diamond peak	Graphite 'bump'
		Wavenumber →	1 332	1 332-1 380	c. 1 580
		Mode of comparison →	Intensity	Ranking	Intensity
HIPping temperature (°C)	Preparation route				
1 400	CP		4 000	4th	310
1 300	pHα◊		11 000	3rd	310
1 250	pH53		7 000	2nd	1 100
1 250	HP		16 000	1st	600

11.1.4 Fired microstructure

The general quality of compacts are good, as far can be seen from fracture surfaces. Alumina grains are small and size distributions are narrow. Diamond particles are well dispersed throughout the examined samples, with the exception of the grouping seen in 15◊-α-pHα◊-H1300 (fig. 8-10, page 62), which is almost certainly due to diamond agglomeration carried over from green compact formation. Fig. 8-23 and 8-24 (page 66) shows interfaces between diamond and alumina that are characteristic of all samples: The diamond particles are seen to fit closely into the alumina matrix. No obvious graphite could be distinguished on diamond surfaces, even though it must have been present as shown by the Raman spectroscopy.

As can be expected, grain size increases with HIPping temperature (fig. 8-24, page 67). The presence or absence of diamond would not seem to have an effect on grain size, as the alumina grain size in non-diamond containing samples followed the same trend as the diamond containing samples (fig. 8-24). Not enough data are available to draw conclusions as to the effect of the green processing route.

11.1.5 Hardness and toughness

In non-diamond containing samples, hardness was slightly above the relationship with grain size given by Krell (1995) (fig. 5-6) as shown below in fig. 11-1.

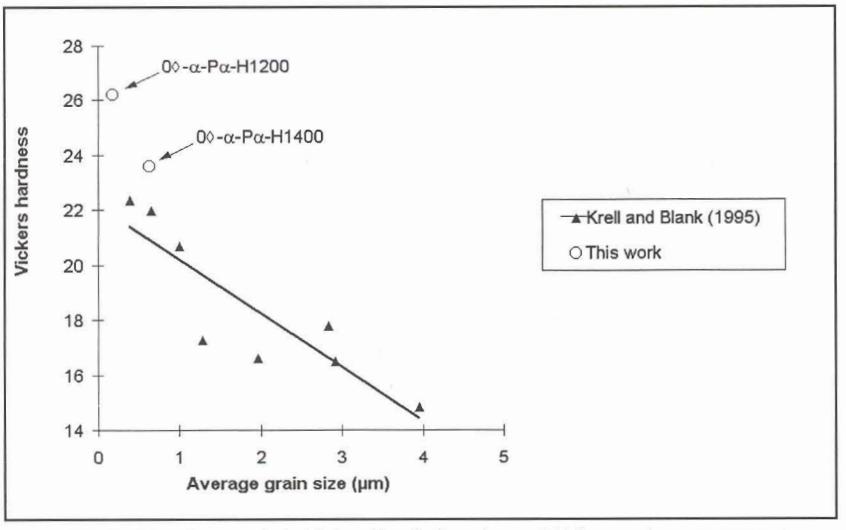

***Fig. 11-1**: Hardness (at 10 kg f) of alumina of this work compared with Krell and Blank's (1995) values.*

Whereas in the work of Noma and Sawaoka (1984 and 1985) hardness decreased with the incorporation of diamond (fig. 5-11, page 46), in this work there was no significant change with the incorporation of diamond. Hardness varied between 22 and 27 GPa (table 9-1, page 71) regardless of diamond content. This is an improvement on the values reported by Noma and Sawaoka (20 GPa and less, fig. 5-11). Hardness of samples fabricated in this work compares favourably with that measured for LX11 (26 GPa). As hardness did not differ much between samples, $K_C^{3/4}H_V^{1/2}$ is in effect an indicator of toughness in this work.

The measured hardness values of this work are probable relatively accurate (subject to the error discussed in section 9.1 on page 68) as are the toughness values of the non-diamond containing samples. However, it is likely that the toughness of diamond containing samples were overestimated. Diamond containing samples could not be polished to the same surface finish as the non-diamond containing samples (compare fig. 9-6, page 74 with fig. 9-8, page 75) with the result that the measured cracks lengths could have been shorter than actual crack lengths. (Note again, however, that micrographs like those of fig. 9-3 to 9-8 were not used for crack length measurement, measurements were made on the PC screen.) Although the toughness of diamond containing samples would appear to be higher than those of the non-diamond containing samples, with toughness of non-diamond containing varying between 1.5 and 2.1 MPa.m^{½} and diamond containing samples varying between 2.7 and 4.2 MPa.m^{½} (table 9-1), this apparent toughening effect of diamond should therefore be interpreted with caution. At any rate, toughness obtained in this work and toughness obtained by Noma and Sawaoka (1985) cannot be compared directly as the toughness of the respective unreinforced matrices differ (probably

mainly due to the difference in matrix grain size in this work being 0.6 μm and less while that of Noma and Sawaoka is in the order of 1.5 μm): In this work toughness obtained with unreinforced samples varied between 1.5 and 2.1 MPa.m^{½} while that of Noma and Sawaoka is 4.5 MPa.m^{½}. However, the maximum improvement in toughness obtained by Noma and Sawaoka is 57 % (see fig. 5-12, page 45) while, in this work, 15◊-α-CP-H1400 has double the toughness of 0◊-α-Pα-H1400 (table 9.1). As 15◊-α-CP-H1400 was certainly not graphitised as much as the samples in Noma and Sawaoka's work, this puts the validity of graphitisation as the mechanism for the toughnening effect by Noma and Sawaoka in some doubt, although, again differences in alumina matrices may invalidate such comparisons.

There are no trends that can reasonably deduced between HIPping temperature or grain size and $K_c^{3/4}H_V^{1/2}$, or as can be seen below in fig. 11-2 and 11-3.

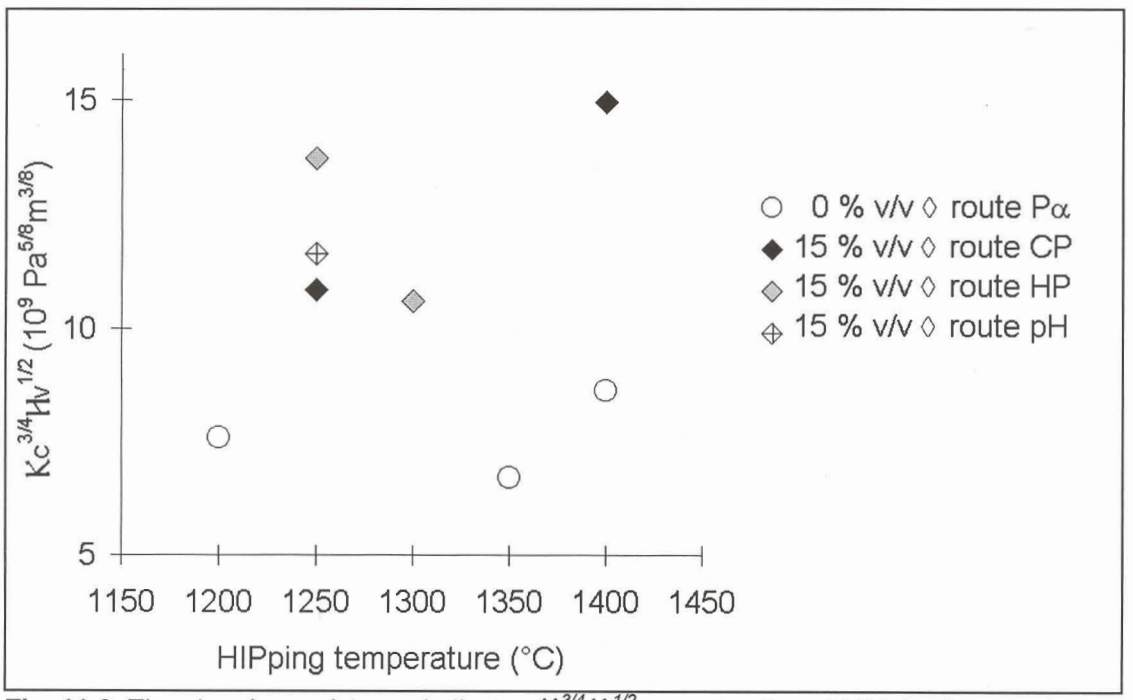

***Fig. 11-2**: The abrasion resistance indicator, $K_c^{3/4}H_V^{1/2}$, as a function of HIPping temperature.*

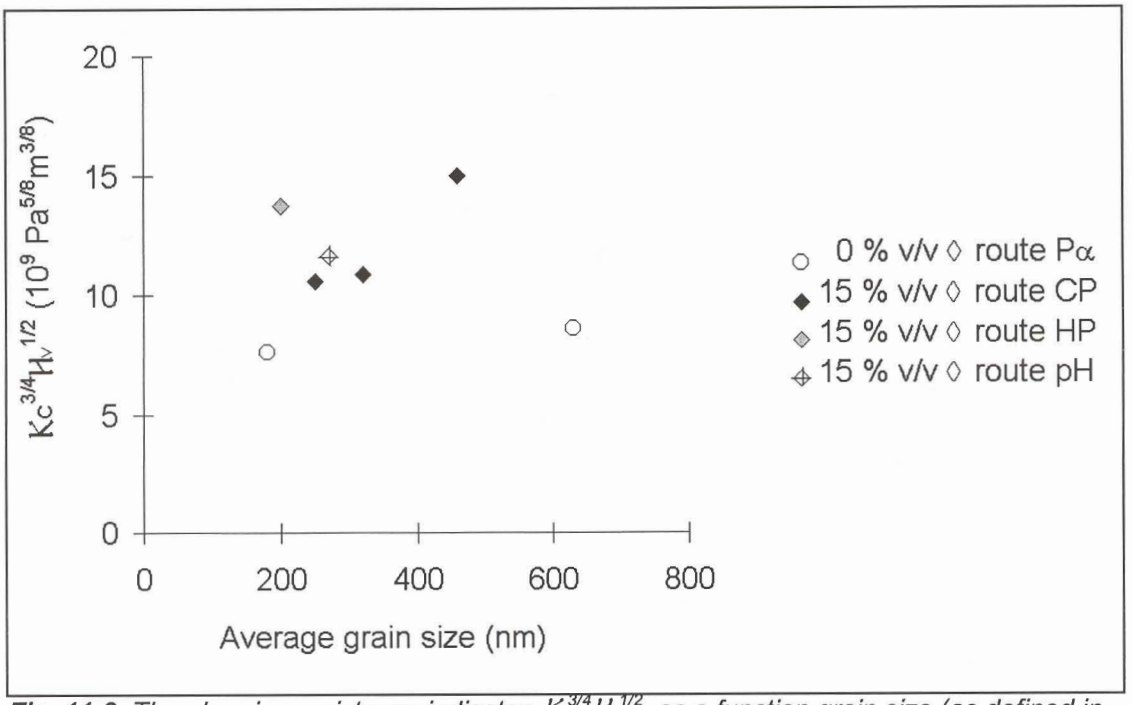

***Fig. 11-3**: The abrasion resistance indicator, $K_c^{3/4}H_V^{1/2}$, as a function grain size (as defined in section 8.1.3).*

11.1.6 Wear

As the 'conclusive' characteristic, the wear performance can depend on many processing parameters or intermediate properties (see fig 1-2, page 3).

No simple relationships exist between HIPping temperature, grain size or green preparation and wear performance; data are randomly distributed for these relationships, which could indicate that experimental conditions during manufacturing of samples were not controlled tightly enough.

Sample 15◊-α-pH-H1300 showed more grouping of diamond particles (fig. 8-10, page 62) than other samples but exhibited the lowest wear rate. This behaviour is not what should be expected, but its low wear need not be connected to its lack of diamond dispersal. On the other hand, no other explanation can be given for this behaviour.

Even more peculiar is the relationship between $K_C^{3/4}H_V^{1/2}$ and wear rate. Whereas $K_C^{3/4}H_V^{1/2}$ is supposed to indicate resistance to abrasive wear (section 5-5, page 40), the wear rate actually increases with increasing $K_C^{3/4}H_V^{1/2}$, as can be seen below in fig. 11-4. Stated differently, this means that the tougher and the harder samples are, the faster they wear.

Some possible explanations for this are the following:

- As $K_C^{3/4}H_V^{1/2}$ indicates abrasive wear resistance, this might mean that the dominating wear mode is not abrasive, which in itself would be surprising.
- Either the measurement of wear rate or toughness (as already pointed out hardness does vary much between samples and $K_C^{3/4}H_V^{1/2}$ is in effect only an indicator of variation of toughness in this work) is suspect.
- Some other property of the wear testing system has a larger influence on the wear rate than toughness.

An additional result from fig. 10-7 is that, if the limited data for unreinforced alumina are extrapolated, it would seem that diamond reinforced alumina would have some advantage above unreinforced alumina of similar $K_C^{3/4}H_V^{1/2}$. However, this could be due to the overestimation of the toughness of diamond containing samples already discussed.

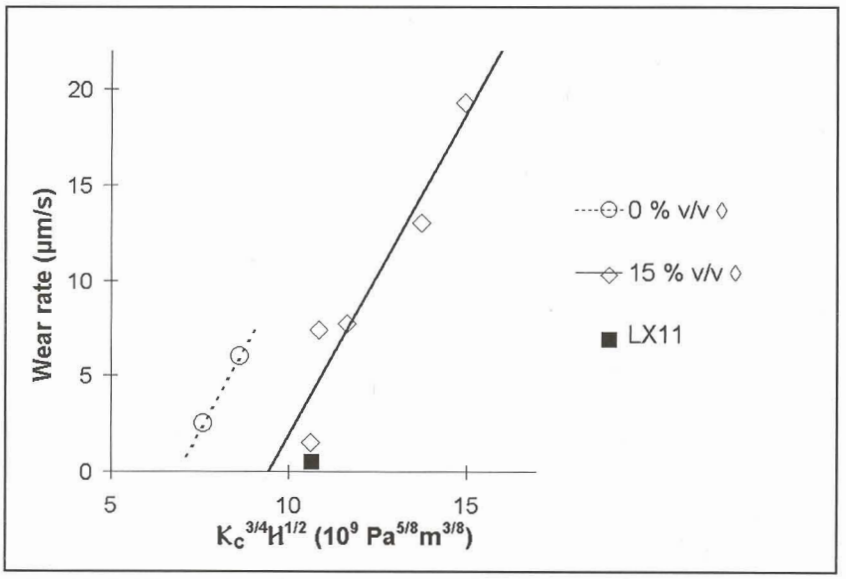

***Fig. 11-4**: The wear rate compared to the abrasion resistance indicator, $K_c^{3/4}H_v^{1/2}$.*

11.2 Conclusion

It would not seem from this research that alumina-diamond would be a feasible material for low wear applications.

This is especially clear from wear tests, in which LX11 outperformed diamond-alumina. Of course, the wear testing method was very aggressive compared to other methods, but it is still unlikely that diamond-alumina would compare better under other wear testing conditions. Even if diamond-alumina can be optimised to compare with something like LX11, or in the unlikely case of improving on it, it is dubious if production would be economical. A cutting tip like LX11 currently sells commercially at a price in the order of R50. It is doubtful if diamond-alumina tips could be produced at such prices, especially with the complicated 'wet' processing involved. Of course, due the difficulty of preparing samples, most test work was done on a relatively few samples. Even if more exhaustive research is done, though it is still unlikely that the overall evidence would change.

However, the emphasis in experimental work in this thesis has been on efforts to limit graphitisation. Graphitisation was perceived as a barrier to adhesion between diamond and alumina. In contradiction with the approach in this work, Noma and Sawaoka (1984 and 1985) actually deliberately graphitised the diamond particles in their composites and claimed this improved toughness. If one would still want to pursue the possibility of diamond-alumina this effect should be looked into.

Furthermore, if only the lower (and conservative) asymptotic mixing law (equal wear mode) of Axén and Jacobson (1994) (fig. 5-4, page 39) is considered, it would seem that the true advantage of composites only comes at much higher concentrations of the harder phase than the 15 % v/v used here in this work. This leaves the possibility of higher diamond concentration leading to better properties than those experienced in this work with its low diamond concentration. One might even imagine alumina merely having a role of only cementing diamond particles together.

Appendix A1: Derivation of equations for consolidated layer growth

A1.1 Consolidated layer growth (Adcock and McDowall, 1957)

The superficial speed v of a clear liquid of viscosity μ moving through a fine textured, rigid, porous bed of depth L_{bed} under a pressure difference of ΔP is given by

$$v = \frac{K\,\Delta P}{\mu L_{bed}} \qquad \text{(A1-1)}$$

where K is the permeability of the bed. It is useful to visualise a collection vessel of the same cross-sectional area as the bed as in fig. A1-1. Then

$$v = \frac{\delta L_{liquid}}{\delta t} = \frac{K\,\Delta P}{\mu L} \qquad \text{(A1-2)}$$

with L_{liquid} the depth of the collected liquid.

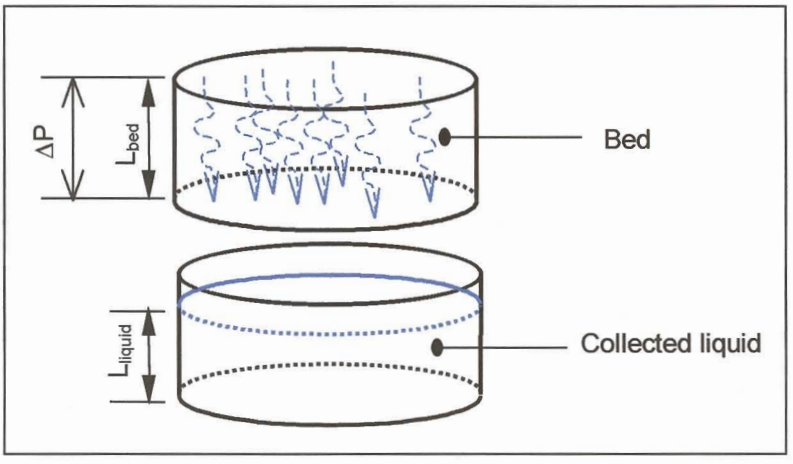

***Fig. A1-1**: A clear liquid moving through a porous bed under the influence of a pressure difference ΔP.*

The rate of liquid movement during filtration of suspensions follows the same relationship as in equation A1-2, with the consolidated layer of removed particles acting as the bed. In contrast with movement of clear liquid through a fixed bed though, the consolidated layer grows with time. More particles from the suspension are forced onto the top of the consolidated layer as filtration progresses. For every depth δL_{sl} of suspending liquid that enters the consolidated layer, the consolidated layer grows by a proportional thickness δL_{cl}. Incorporating this proportionality with equation A1-2:

$$\frac{\delta L_{cl}}{\delta t} = \frac{\delta L_{liquid}}{z\,\delta t} \equiv \frac{\delta L_{sl}}{z\,\delta t} = \frac{K\,\Delta P}{z\mu_{sl}L_{cl}} \qquad \text{(A1-3)}$$

where L_{cl} is the consolidated layer depth (fig. A1-2). Since the suspending liquid is the (clear) liquid moving through the consolidated layer, the suspending liquid viscosity μ_{sl} was substituted for μ to avoid confusion with the suspension viscosity. z is given by

$$z \equiv \frac{Q_{filt}}{Q_{cl}} = \frac{L_{filt}}{L_{cl}} \qquad \text{(A1-4)}$$

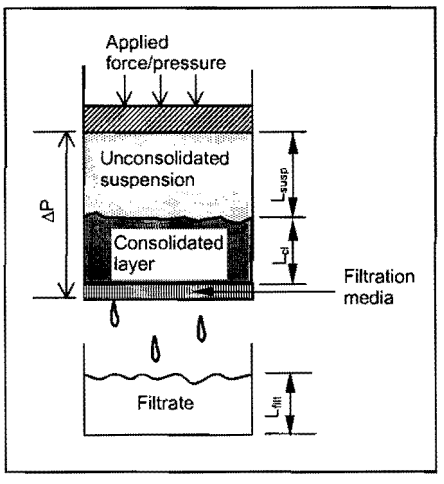

***Fig. A1-2**: Consolidated layer growth.*

Equation A1-3 can be evaluated to give the depth of the consolidated layer L_{cl} at time t:
Integrating:

$$\int_0^{L_{cl}} L_{cl}\delta L_{cl} = \int_0^t \frac{k\,\Delta P \delta t}{z\mu_{sl}} \qquad \text{(A1-5)}$$

giving

$$L_{cl} = \sqrt{\frac{2k\,\Delta P t}{z\mu_{sl}}} \qquad \text{(A1-6)}$$

Alternatively, equation (A1-6) can be modified to give the time needed to consolidate a given depth of suspension. Taking a volume balance

$$L_{cl,\,fin} + L_{filt,\,fin} = L_{susp,\,0} \qquad \text{(A1-7)}$$

with $L_{cl,\,fin}$ and $L_{filt,\,fin}$ respectively the consolidated layer depth and filtrate depths after total consolidation and $L_{susp,\,0}$ the initial suspension depth. Using the z ratio of equation (A1-4):

$$L_{cl,\,fin} + zL_{cl,\,fin} = L_{susp,\,0} \qquad \text{(A1-8)}$$

Rearranging and equating to equation (A1-6).

$$L_{cl,\,fin} = \frac{L_{susp,\,0}}{1+z} = \sqrt{\frac{2k\,\Delta P t_{fin}}{z\mu_{sl}}} \qquad \text{(A1-9)}$$

Rearranging

$$t_{fin} = \frac{z\mu_{sl}L_{susp,0}^2}{2(1+z)^2 k\Delta P} \qquad \text{(A1-10)}$$

which gives the time required to consolidate a load of $L_{susp,0}$ of suspension.

A1.2 The z ratio in terms of suspension volume loading and consolidated layer porosity

The z ratio can be related to the volume loading of the suspension ($1-\varepsilon_{susp}$) and the porosity of the consolidated layer ε_{cl}, as will be done below. This is useful as z itself is generally not known, but the volume loading of the suspension would normally be known and the consolidated layer porosity can generally be estimated as around 40 %.

If the consolidated layer is not compressible, z is independent of the progress of filtration. Taking a volume balance of liquids at the end of filtration, using the same type of visualisation as in fig. A1-1 and A1-2, gives

$$L_{sl\,in\,susp,0} = L_{sl\,in\,cl,fin} + L_{filt,fin} \qquad \text{(A1-11)}$$

or

$$\varepsilon_{susp}L_{susp,0} = \varepsilon_{cl}L_{cl,fin} + L_{filt,fin} \qquad \text{(A1-12)}$$

Taking a total volume balance

$$L_{cl,fin} + L_{filt,fin} = L_{susp,0} \qquad \text{(A1-13)}$$

or

$$L_{filt,fin} = L_{susp,0} - L_{cl,fin} \qquad \text{(A1-14)}$$

Substituting equation A1-14 in A1-12

$$\varepsilon_{susp}L_{susp,0} = \varepsilon_{cl}L_{cl,fin} + L_{susp,0} - L_{cl,fin} \qquad \text{(A1-15)}$$

Solving for $L_{cl,fin}$

$$L_{cl,fin} = \frac{1-\varepsilon_{susp}}{1-\varepsilon_{cl}}L_{susp,0} \qquad \text{(A1-16)}$$

Substituting equation A1-12 in A1-8

$$\frac{1-\varepsilon_{susp}}{1-\varepsilon_{cl}}L_{susp,0} + L_{filt,fin} = L_{susp,0} \qquad \text{(A1-17)}$$

Solving for $L_{filt,fin}$

$$L_{filt,fin} = L_{susp,0}\left[1 - \frac{1-\varepsilon_{susp}}{1-\varepsilon_{cl}}\right] \qquad \text{(A1-18)}$$

Taking (A1-14) / (A1-12)

$$\frac{L_{filt,\,fin}}{L_{cl,\,fin}} = \frac{\varepsilon_{susp} - \varepsilon_{cl}}{1 - \varepsilon_{susp}} \qquad \text{(A1-19)}$$

This gives the z ratio in terms of ε_{susp} and ε_{cl}:

$$z \equiv \frac{Q_{filt}}{Q_{cl}} = \frac{L_{filt}}{L_{cl}} = \frac{\varepsilon_{susp} - \varepsilon_{cl}}{1 - \varepsilon_{susp}} \qquad \text{(A1-20)}$$

A1.3 Derivation of the Carmen-Kozeny equation (Adcock and McDowall, 1957)

For a liquid of viscosity μ, flowing in a narrow circular conduit of diameter d and length L_{cdt}, average linear flow speed in the conduit v' is given by the Poiseuille equation as

$$v' = \frac{d^2}{32\mu L_{cdt}}\Delta P \qquad \text{(A1-21)}$$

Equation (A1-21) is also valid for any a non-circular, cylindrical conduit, with the following modification

$$v' = \frac{m^2}{2\mu L_{cdt}}\Delta P \qquad \text{(A1-22)}$$

where m‡ is given by

$$m = \frac{[\text{Volume capacity of conduit}]}{[\text{Wetted perimeter of conduit}]} \qquad \text{(A1-23)}$$

If the conduit penetrates a bed of material of depth L_{bed} and is twisted as in fig. A1-3, the effective microscopic conduit length L_{cdt} would not be the same as the bulk depth L_{bed} of the bed. To correct this a the tortuosity factor τ is used:

$$\tau = \frac{L_{cdt}}{L_{bed}} \qquad \text{(A1-24)}$$

This also means that

$$\tau = \frac{v'}{v''} \qquad \text{(A1-25)}$$

where v'' is the component of v' in the same direction as L_{bed}. Incorporating (A1-24) and (A1-25) with (A1-22) gives

$$\tau v'' = \frac{m^2}{2\mu\tau L_{bed}}\Delta P \qquad \text{(A1-26)}$$

---

‡ For a round cylinder $m = \frac{\pi d^2}{4} \Big/ \pi d = \frac{d}{4}$. Substitution of this in equation (A1-22) would give the same result as in (A1-21)

which simplifies to

$$v'' = \frac{m^2}{2\mu\tau^2 L_{bed}}\Delta P \qquad \text{(A1-27)}$$

If a set of conduits permeates a bed, giving it a porosity of ε, the superficial flow rate v relates to the conduit flow rate v'' as follows:

$$v = \varepsilon v'' \qquad \text{(A1-28)}$$

Substituting this into (A1-27) gives

$$v = \frac{\varepsilon m^2}{2\mu\tau^2 L_{bed}}\Delta P \qquad \text{(A1-29)}$$

Equation (A1-29) is also found to give v in a set of conduits of uneven cross section if a factor other than 2 is used, that is to say

$$v = \frac{\varepsilon m^2}{\theta\mu\tau^2 L_{bed}}\Delta P \qquad \text{(A1-30)}$$

where θ is the so-called Poiseuille factor.

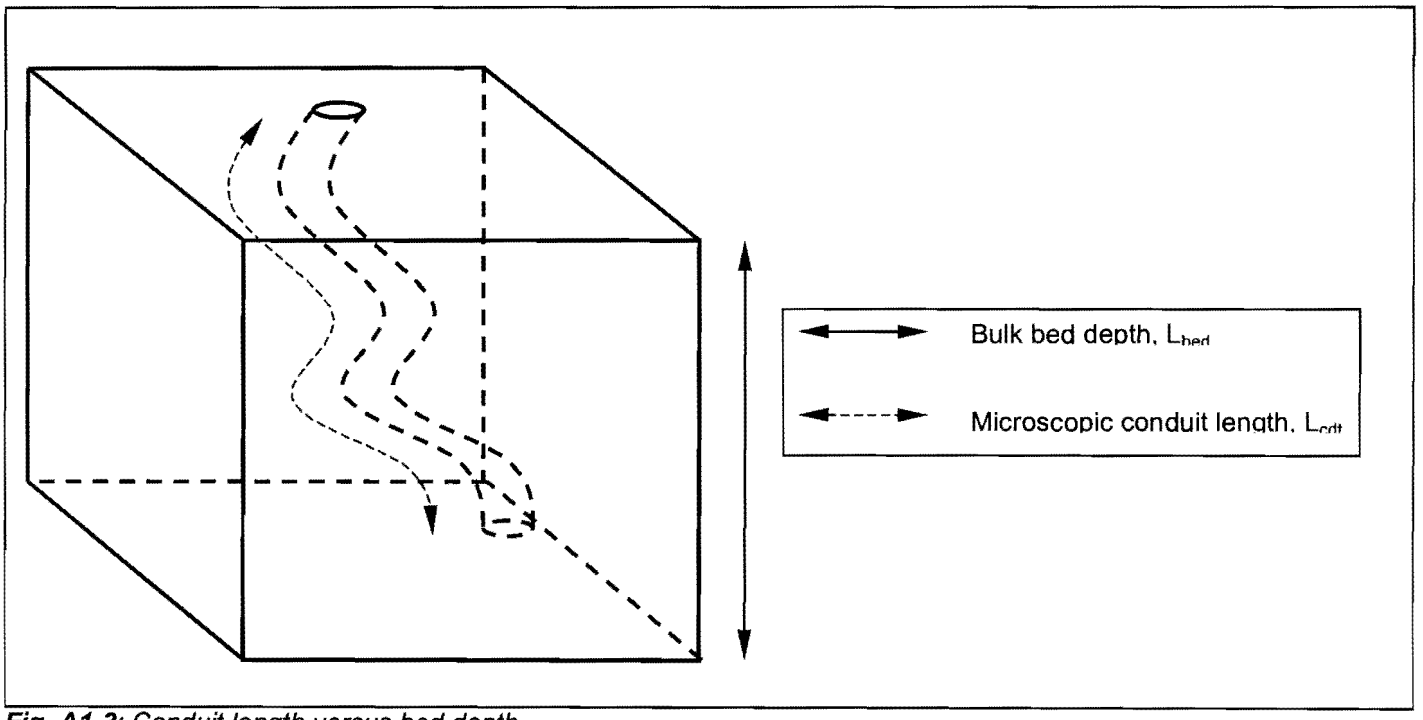

***Fig. A1-3**: Conduit length versus bed depth*

A consolidated layer of particles can be considered as a bed of material permeated by a set of uneven conduits. For a consolidated layer of particles of volume specific surface area S_v the m ratio (equation A1-23) would be

$$m = \frac{[\text{Volume of pores}]}{S \times [\text{Volume of particles}]} = \frac{\varepsilon_{cl} Q_{cl}}{S(1-\varepsilon_{cl}) Q_{cl}} = \frac{\varepsilon_{cl}}{S(1-\varepsilon_{cl})} \quad \text{(A1-31)}$$

ε_{cl} is equivalent to ε. Substituting (A1-31) in (A1-30)

$$v = \frac{\varepsilon^3}{S^2(1-\varepsilon_{cl})^2 \theta \mu \tau^2 L_{bed}} \Delta P = \underbrace{\frac{\varepsilon^3}{S^2(1-\varepsilon_{cl})^2 \theta \tau^2}}_{k} \frac{\Delta P}{\mu L_{bed}} \quad \text{(A1-32)}$$

This is of the same form as equation A1-1 and the term indicated by '{' gives the Carmen-Kozeny equation for permeability:

$$k = \frac{\varepsilon_{cl}^3}{S^2(1-\varepsilon_{cl})^2 \theta \tau^2} \quad \text{(A1-33)}$$

Normally the following approximation is used

$$\theta \tau^2 = 2.5 \times \left(\sqrt{2}\right)^2 = 5 \quad \text{(A1-34)}$$

For a consolidated layer consisting of monosized spherical particles of size d_{part} volume specific surface area is given by

$$S = \frac{[\text{Surface area}]}{[\text{Volume}]} = \pi d_{part}^2 \Big/ \frac{\pi d_{part}^3}{6} = \frac{6}{d_{part}} \quad \text{(A1-35)}$$

Or in general

$$S \approx \frac{6}{d_{part}} \quad \text{(A1-36)}$$

Substitution of equation A1-34 and A1-36 in A1-33 gives

$$k \approx \frac{\bar{d}_{part}^2 \varepsilon_{cl}^3}{180(1-\varepsilon_{cl})^2} \quad \text{(A1-37)}$$

If ε_{cl} is approximated as 40 %, as is generally true for filtered casted green bodies, then

$$k \approx \frac{\bar{d}_{part}^2 0.4}{180 \times 0.6^2} \approx 1 \times 10^{-3} \bar{d}_{part}^2 \quad \text{(A1-38)}$$

Substitution of equation A1-38 in A1-33 gives

$$t_{fin} \approx \frac{z \mu_{sl} L_{susp,0}^2}{2 \times 10^{-3} \bar{d}_{part}^2 (1+z)^2 \Delta P} \quad \text{(A1-39)}$$

With other variables constant, equation (A1-39) simplifies to

$$t_{fin} \propto \frac{1}{\bar{d}_{part}^2} \quad \text{(A1-40)}$$

Appendix A2: Compilation and limitations of fig. 4-2.

Fig. 4-2 was compiled by assembling data from several authors (Howes, 1962; Seal, 1958; Evans and Phaal, 1962; and Liu and Ownby, 1991). Its aim is to get an impression of temperature-oxygen activity combinations that are hazardous in terms of graphitisation.

Classification was done by means of the authors' descriptions and classified as 'significant', 'none', or 'intermediate'. Unfortunately this is somewhat subjective. Experimental conditions vary greatly, and Evans and Phaal (1962) do not give duration of exposure. Table A2-1 lists details of data.

Although it was compiled for oxygen activity, data for vacuum are also included. The oxygen activity can be expected to be smaller than the value indicated by the data in these cases. Accordingly, arrows are used to indicate an oxygen potential of less than that shown by the data in these cases. However, bear in mind that any aggressive species can induce graphitisation, and it possible that a non-oxygen species' effect on graphitisation can be greater or smaller than that of oxygen. Thus, pointing the arrows downward may not give the true picture.

The alumina matrix or reactions between the matrix and diamond or graphite can be sources of oxygen pressure or potentially aggressive gaseous species. Several reactions are possible:

$$Al_2O_3 \leftrightarrow 2\ Al(g) + 1\frac{1}{2}\ O_2 \qquad (A2\text{-}1)$$

$$Al_2O_3 \leftrightarrow 2\ Al(l) + 1\frac{1}{2}\ O_2 \qquad (A2\text{-}2)$$

$$Al_2O_3 \leftrightarrow 2\ Al(s) + 1\frac{1}{2}\ O_2 \qquad (A2\text{-}3)$$

$$Al_2O_3 \leftrightarrow Al_2O(g) + O_2 \qquad (A2\text{-}4)$$

$$Al_2O_3 \leftrightarrow 2\ AlO(g) + \frac{1}{2}\ O_2 \qquad (A2\text{-}5)$$

$$Al_2O_3 + 4\frac{1}{2}\ C \leftrightarrow \frac{1}{2}\ Al_4C_3 + 3\ CO \qquad (A2\text{-}6)$$

$$Al_2O_3 + 3\ C \leftrightarrow \frac{1}{2}\ Al_4C_3 + 1\frac{1}{2}\ CO_2 \qquad (A2\text{-}7)$$

$$Al_2O_3 + 1\frac{1}{2}\ C \leftrightarrow \frac{1}{2}\ Al_4C_3 + 1\frac{1}{2}\ O2 \qquad (A2\text{-}8)$$

Table A2-1 *Details of graphitisation data used in fig. 4-2.*

#	Reference	Temperature (°C)	Pressure (mm Hg)	O_2 pressure/ Vacuum.	Time	Face	Description	Remarks	Graphitisation classification
H1	Howes (1962)	1 400	5×10^{-6}	Vacuum	20 h	All over	'no nuclei detected [optically]'	The vacuum of '5x10-6 or better has usually been maintained'.	None
H2	Howes (1962)	1 600	5×10^{-6}	Vacuum	5 h	All over	'no nuclei detected [optically]'	The vacuum of '5x10-6 or better has usually been maintained'.	None
H3	Howes (1962)	1 700	5×10^{-6}	Vacuum	<15 min	All over	'nuclei...not...detectable'	The vacuum of '5x10-6 or better has usually been maintained'.	None
H4	Howes (1962)	1 700	5×10^{-6}	Vacuum	>15 min	All over	'nuclei...detectable'	The vacuum of '5x10-6 or better has usually been maintained'.	Intermediate
H5	Howes (1962)	1 700	5×10^{-6}	Vacuum	30 min	All over	'nuclei... seen as isolated propeller shapes'	The vacuum of '5x10-6 or better has usually been maintained'.	Intermediate
H6	Howes (1962)	1 700	5×10^{-6}	Vacuum	15 min	All over	Micrograph	The vacuum of '5x10-6 or better has usually been maintained'.	Intermediate
H7	Howes (1962)	1 700	5×10^{-6}	Vacuum	45 min	All over	Micrograph	The vacuum of '5x10-6 or better has usually been maintained'.	Intermediate
H8	Howes (1962)	1 700	5×10^{-6}	Vacuum	2 h	All over	Micrograph	The vacuum of '5x10-6 or better has usually been maintained'.	Significant
H9	Howes (1962)	1 800	5×10^{-6}	Vacuum	5 min	All over	Micrograph	The vacuum of '5x10-6 or better has usually been maintained'. Follow on from H7.	Significant
H10	Howes (1962)	1 900	5×10^{-6}	Vacuum	5 min	All over	'surface... completely covered', Micrograph	The vacuum of '5x10-6 or better has usually been maintained'.	Significant
S1	Seal (1958)	1 200	10^{-4}	Vacuum	15-30 min	All over	'Slight dulling of surface'		Intermediate
S2	Seal (1958)	1 400	10^{-4}	Vacuum	15-30 min	All over	'Definite grey colour'		Intermediate
S3	Seal (1958)	1 500	10^{-4}	Vacuum	15-30 min	All over	'Diamond appears dark grey but still translucent'		Intermediate

***Table A2-1** continued.*

#	Reference	Temperature (°C)	Pressure (mm Hg)	O_2 pressure/ Vacuum.	Time	Face	Description	Remarks	Graphitisation classification
S4	Seal (1958)	1 800	10^{-4}	Vacuum	15-30 min	All over	'Diamond black, opaque and starting to break up'		Significant
S5	Seal (1958)	2 000	10^{-4}	Vacuum	15-30 min	All over	'Small black fragments'		Significant
EP1a	Evans and Phaal (1962)	700	0.06	O_2	Not given	{111}	'covered with a grey layer of carbon'		Intermediate
EP1b	Evans and Phaal (1962)	700	0.5	O_2	Not given	{111}	'covered with a grey layer of carbon'		Intermediate
EP2a	Evans and Phaal (1962)	700	0.06	O_2	Not given	{110}	'covered with a grey layer of carbon'		Intermediate
EP2b	Evans and Phaal (1962)	700	0.5	O_2	Not given	{110}	'covered with a grey layer of carbon'		Intermediate
EP3a	Evans and Phaal (1962)	700	0.06	O_2	Not given	{100}	'not covered'		None
EP3b	Evans and Phaal (1962)	700	0.5	O_2	Not given	{100}	'not covered'		None
EP4a	Evans and Phaal (1962)	850	0.06	O_2	Not given	{111}, {110}, {100}	'coated with a carbon layer'		Significant
EP4b	Evans and Phaal (1962)	850	0.5	O_2	Not given	{111}, {110}, {100}	'coated with a carbon layer'		Significant
EP5a	Evans and Phaal (1962)	1 350	0.4	O_2	Not given	{111}, {110}	'thin coating of carbon'		Significant

***Table A2-1** continued.*

#	Reference	Temperature (°C)	Pressure (mm Hg)	O_2 pressure/ Vacuum.	Time	Face	Description	Remarks	Graphitisation classification
EP5b	Evans and Phaal (1962)	1 000	0.4	O_2	Not given	{111}, {110}	Carbon layer 'appreciably thicker'		Significant
EP6a	Evans and Phaal (1962)	650	0.4	O_2	Not given	{100}	'free of a visible carbon layer'		None
EP6b	Evans and Phaal (1962)	850	0.4	O_2	Not given	{100}	'free of a visible carbon layer'		None
EP6c	Evans and Phaal (1962)	850	0.4	O_2	Not given	{100}	'carbon layer'		Intermediate
EP6d	Evans and Phaal (1962)	1000	0.4	O_2	Not given	{100}	Carbon layer of 'appreciably thickness'		Significant
E1a	Evans (1979)	1 500	10^{-4}	Vacuum	1 h		'black surface coating'		Significant
E1b	Evans (1979)	1 500	10^{-6}	Vacuum	1 h		'clear and unchanged'		None
LO1a	Liu and Ownby (1991)	600	760	O_2	Not given		'The normal graphitisation...occurs'	Thumbsuck estimate?	Significant
LO1b	Liu and Ownby (1991)	800	760	O_2	Not given		'The normal graphitisation...occurs'	Thumbsuck estimate?	Significant

(From an equilibrium point of view it is immaterial if the reacting carbon is diamond or graphite, since the change Gibbs free energy change between graphite and diamond is comparatively small, as can be seen in table A2-1.) One or more of the listed reactions may apply. In the absence of more information, the single reaction giving the maximum oxygen potential is conservatively taken in fig. 4-2 to be the only cause of oxygen activity. In appendix A2 it is shown to be reaction A2-4 ($Al_2O_3 \leftrightarrow Al_2O(g) + O_2$).

Equilibrium may take some time to be achieved in large pores. However, in the final stages of HIPping the alumina matrix is in intimate contact with the diamond surfaces, and it is likely that an equilibrium oxygen activity is reached.

The effect of the encapsulating titanium is not taken into account. The titanium can act as an oxygen getter, bringing down the oxygen activity.

Activity and pressure is equated here, but they may not necessarily be interchangeable.

The gaseous products are taken to be present in stoichiometrical quantities.

Appendix A3: Calculation of activities

The equilibrium value of the activity of, for instance, O_2 can be estimated from the basic thermodynamic relation:

$$\Delta G = -RT \ln K \qquad \text{(A3-1)}$$

where, for instance for reaction A3-1,

$$K \approx \left(P_{O_2}^{1½} P_{Al(g)}^{2}\right)_{equilibrium} \qquad \text{(A3-2)}$$

with P in atmosphere, if used in this equation. ΔG can conveniently be estimated with

$$\Delta G = \overline{\Delta H} - T\,\overline{\Delta S} \qquad \text{(A3-3)}$$

Where values for $\overline{\Delta H}$ and $\overline{\Delta S}$ for the actual equations are unavailable, they can be estimated by summing equations, as in table A3-1.

If the Al_2O_3 partially vaporizes in stoichiometrical quantities, the activities of the gaseous species can be related by their coefficients, for instance for reaction A3-1

$$P_{Al(g)} = \frac{2}{1½} P_{O_2} \qquad \text{(A3-4)}$$

Equation A3-2 can then be written as

$$K \approx \left(P_{O_2}^{1½}\left(\frac{2}{1½}P_{O_2}\right)^2\right)_{equilibrium} = \frac{16}{9} P_{O_2}^{3½} \qquad \text{(A3-5)}$$

and then P_{O_2} can be calculated from

$$P_{O_2,\,equilibrium} = \left(\frac{9}{16}\mathcal{K}\right)^{\frac{1}{3½}} \qquad \text{(A3-6)}$$

Similar calculations can be made for the other reactions and their results are listed in table A3-1.

If the Al(g) pressure at a temperature do not exceed the saturation pressure of Al(g), no Al(l) or Al(s) can be present. Then reactions A3-2 and A3-3 are unrealisable. This is in fact the case as illustrated in fig. A3-2.

Gibbs free energy and activities of gases are shown in fig. A3-2 and A3-3. Note that reaction A3-4 ($Al_2O_3 \leftrightarrow Al_2O(g) + O_2$) gives the maximum oxygen potential.

***Table A3-1**: Enthalpies and entropies.*

Reaction	Index/ Operation	$\overline{\Delta\mathcal{H}}$ (J/mol)	$\overline{\Delta\mathcal{S}}$ (J/K.mol)	Valid range (°C)	Gas activity (atm)	Reference
$Al_2O_3 \leftrightarrow 2\,Al(l) + 1½\,O_2$	A	1 685 627	327	660 - 2050		McColm
$2\,Al(l) + ½\,O2 \leftrightarrow Al_2O(g)$	B	-170 544	49	660-2000		McColm
$Al(l) + ½\,O_2 \leftrightarrow AlO(g)$	C	14 655	56	1227-1728		Garbers-Craig (1996)
$4\,Al(l) + 3\,C(graphite) \leftrightarrow Al_4C_3$	D	-173 761	-21	1227-1729		Garbers-Craig (1996)
$C(graphite) + O2 \leftrightarrow CO_2$	E	-394 968	1	500-2000		McColm
$C(graphite) + ½\,O_2$ « CO	F	-114 281	86	200-2000		McColm
$C(graphite) \leftrightarrow C(◊)$	G	1 442	-4	25-900		McColm
$Al(l) \leftrightarrow Al(g)$	H	304 346	109	660-2520		McColm
$Al(l) \leftrightarrow Al(s)$	I	-10 784	-12	25-660		McColm
$Al_2O_3 \leftrightarrow 2\,Al(g) + 1½\,O_2$	A + 2H	2 294 319	545		$P_{O_2,\,equilibrium} = \left(\frac{9}{16}K_{equilibrium}\right)^{\frac{1}{3½}}$	
$Al_2O_3 \leftrightarrow 2\,Al(l) + 1½\,O_2$	A	1 685 627	327		$P_{O_2,\,equilibrium} = K_{equilibrium}^{\frac{1}{1½}}$	
$Al_2O_3 \leftrightarrow 2\,Al(s) + 1½\,O_2$	A + 2I	1 664 059	303		$P_{O_2,\,equilibrium} = K_{equilibrium}^{\frac{1}{1½}}$	
$Al_2O_3 \leftrightarrow Al_2O(g) + O_2$	A + B	1 515 083	376		$P_{O_2,\,equilibrium} = K_{equilibrium}^{\frac{1}{2}}$	
$Al_2O_3 \leftrightarrow 2\,AlO(g) + ½\,O_2$	1 + 2C	1 714 936	438		$P_{O_2,\,equilibrium} = \frac{1}{16}K_{equilibrium}^{\frac{1}{2½}}$	
$Al_2O_3 + 4½\,C(graphite) \leftrightarrow ½\,Al_4C_3(s) + 3\,CO$	A + ½D + 3F	1 255 904	573		$P_{CO,\,equilibrium} = K_{equilibrium}^{\frac{1}{3}}$	
$Al_2O_3 + 3\,C(graphite) \leftrightarrow ½\,Al_4C_3(s) + 1½\,CO_2$	A + ½D + 1½E	1 006 295	317		$P_{CO_2,\,equilibrium} = K_{equilibrium}^{\frac{1}{1½}}$	
$Al_2O_3 + 1½\,C(graphite) \leftrightarrow ½\,Al_4C_3 + 1½\,O_2$	A + ½D	1 598 747	316		$P_{O_2,\,equilibrium} = K_{equilibrium}^{\frac{1}{1½}}$	

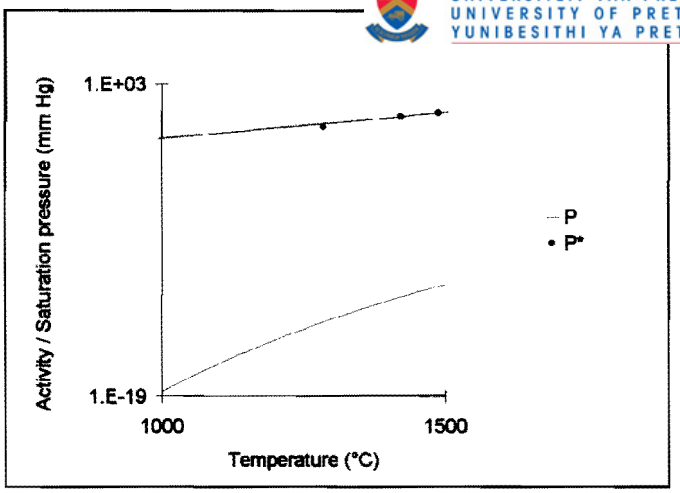

***Fig. A3-1**: Al(g) activity from reaction A3-4 compared with the activity needed for the precipitation of alumina. Aluminium saturation pressure from Perry and Green(1984).*

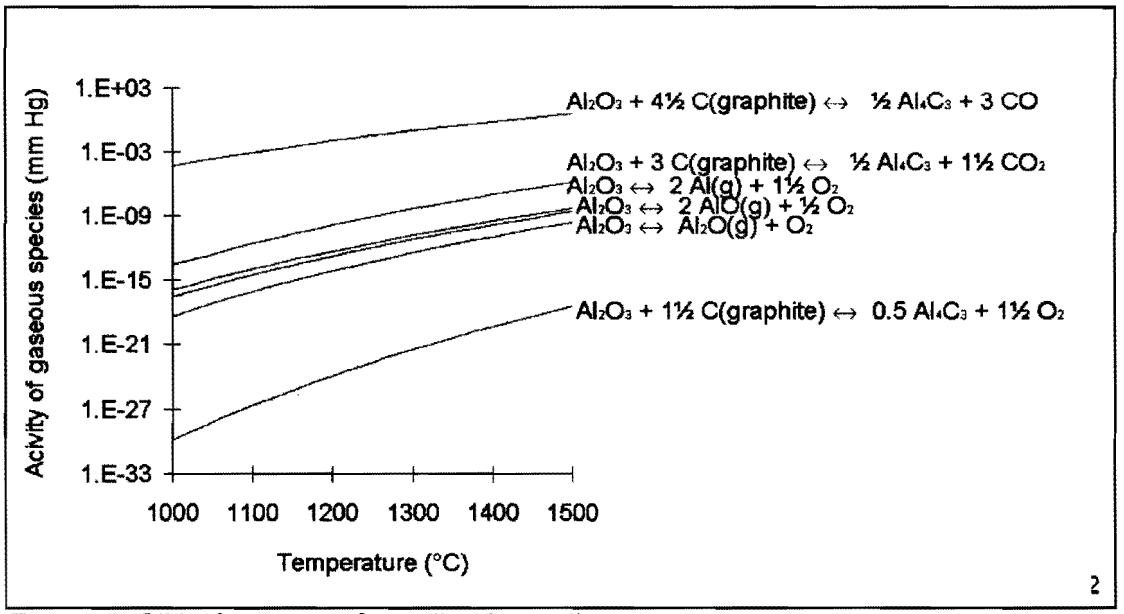

***Fig. A3-2**: Gibbs free energy for realisable reactions.*

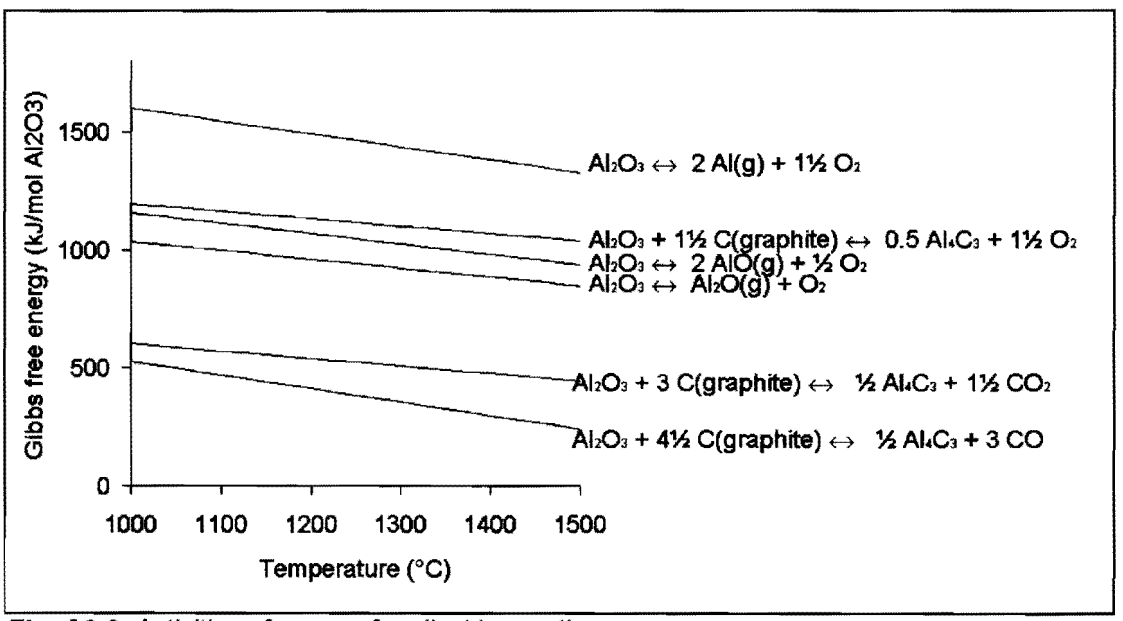

***Fig. A3-3**: Activities of gases of realisable reactions.*

Appendix A4: Estimation of composite Young's modulus

Young's modulus (E) is needed for the calculation of K_c by equation 5-9

Paul (1960) gives three equations for E of a composite material: Two equations respectively giving the upper and lower limits for E and an equation giving a good general approximation.

The lower limit of composite E is given by

$$E_{lower\ limit} = \frac{1}{\frac{f_1}{E_1} + \frac{f_2}{E_2}} \tag{A4-1}$$

The upper limit is given by

$$E_{upper\ limit} = \frac{1 - \upsilon_1 + 2k_p(k_p - 2\upsilon_1)}{1 - \upsilon_1 - 2\upsilon_1^2} f_1E_1 + \frac{1 - \upsilon_2 + 2k_p(k_p - 2\upsilon_2)}{1 - \upsilon_2 - 2\upsilon_2^2} f_2E_2 \tag{A4-2}$$

where k_p is given by

$$k_p = \frac{\upsilon_1(1+\upsilon_2)(1-2\upsilon_2)f_1E_1 + \upsilon_2(1+\upsilon_1)(1-2\upsilon_1)f_2E_2}{(1+\upsilon_2)(1-2\upsilon_2)f_1E_1 + (1+\upsilon_1)(1-2\upsilon_1)f_2E_2} \tag{A4-3}$$

The general approximation given is:

$$E_{approximate} = E_1\left(\frac{E_1 + (E_2 - E_1)f_2^{2/3}}{E_1 + (E_2 - E_1)f_2^{2/3}(1 - f_2^{1/3})}\right) \tag{A4-4}$$

The properties of alumina and diamond necessary to use the above equations are listed in table A4-1

***Table A4-1**: Elastic properties of diamond and alumina.*

Material	Young's modulus, E (GPa)	Poisson's ratio, υ
Alumina	380-400 (Pierson, 1993)	0.22 (Pierson, 1993)
Diamond (natural)	700-1 200 (Ownby, 1990)	0.10-0.29 (Ownby, 1990)

Taking into account the extent of Young's modulus for diamond and alumina, the absolute lower limit for a diamond-alumina composite is set by equation A4-2 with the lower values of E, i.e. $E_{diamond}$ = 700 GPa and $E_{alumina}$ = 380 GPa.

It would have been a simple matter to set the upper limit for Young's modulus if a single value for Poisson's ratio for the diamond used was known. Having a possible range of 0.10 to 0.29 for $\upsilon_{Diamond}$ complicates matters.

It is not noted by Paul, but it can be shown that for with all other variables, including υ_2 constant, and if

$$\upsilon_{1,\,minimum} \leq \upsilon_2 \leq \upsilon_{1,maximum} \qquad \text{(A4-5)}$$

then the global maximum for $E_{Upper\ limit}$ occurs when $\upsilon_1 = \upsilon_2$ The absolute upper limit for a diamond-alumina composite's Young's modulus is therefore set by equation 9-3 with the higher values of E, i.e. $E_{diamond}$ = 1 200 GPa and $E_{alumina}$ = 400 and with $\upsilon_{diamond} = \upsilon_{alumina}$ = 0.22.

The general approximation also gives 'inner' upper and lower bounds due to the possible variation in component E.

The possible variations in composite E is shown in fig. A4-1. From fig. A4-1 the value taken for composite E for the calculation of toughness in equation 9-1 is taken as 460 GPa.

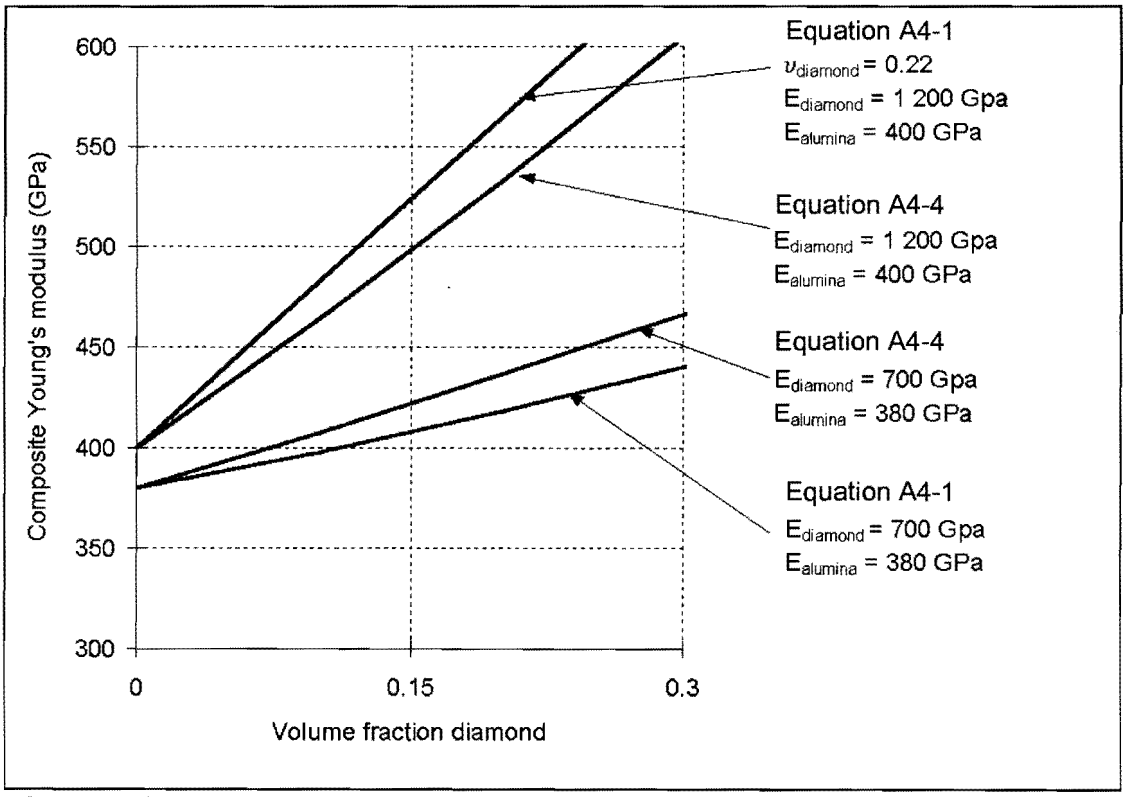

Fig. A4-1 *Limits and approximations to E.*

Appendix A5: Complete wear testing data

***Table A4-1**: Wear testing data. 'Wear rate' and 'apparent starting wear' as defined in fig. 5-5.*

Time (s)	LX 11	15◊-α-pH-H1250	0◊-α-Pα-H1200	15◊-α-CP-H1200	15◊-α-HP-H1250	15◊-α-CP-H1250	0◊-α-HP-H1300	15◊-α-HP-H1300	0◊-α-HP-H1300	0◊-α-Pα-H1350	15◊-α-CP-H1350	0◊-α-Pα-H1400	15◊-α-CP-H1400
10		218	111	180		210	92			170	263	275	494
26									239				
30		388	195	392		461	134	320		336	520	375	880
40					413								
60		604	283	628	673	595	203	454		523		572	
90									304				
120			399				310						
150									425				
100	136												
200	196												
300	235												
Wear rate (µm/s)	0.50	7.68	2.53	8.87	13.00	7.44	1.98	4.47	1.49	6.99	12.85	5.99	19.30
Apparent starting wear (µm)	90	147	108	104	-107	174	76	186	190	110	135	208	301
r^2	0.985	0.998	0.971	0.993	1	0.919	0.996	1	0.964	0.994	1	0.995	1

References

Adams, D. (1980). *The restaurant at the end of the universe.*

Adcock, D. S. and Mcdowall, I. C. (1957). The mechanism of filter pressing and slip casting. *Journal of the American Ceramic Society*, **40** (10), 355-362.

Aksay, I. A. and Schilling, C. H. (1984). Mechanics of colloidal filtration. In *Advances in ceramics*, (ed. J. A. Mangels and G. L. Messing), Volume 9, *Forming of ceramics*, pp. 85-93. American Ceramic Society, Westerville.

Aksay, I. A., Lange, F. F., and Davis, B. I. Uniformity of Al_2O_3-ZrO_2 composites by colloidal filtration. *Communications of the American Ceramic Society*.

Atkins, P. W. (1990). *Physical chemistry*, (4th edn). Oxford University Press, Oxford.

Axén, N. and Jacobson, J. (1994). A model for the wear resistance of multiphase materials. *Wear*, **174**, 187-199.

Baldoni, B. G., Wayne, S. F., and Buljan, S. T. (1986). *ASLETrans*. **29**, 347-352.

Besson, J. and Abouaf, M. (1991). Grain growth enhancement in alumina during hot isostatic pressing. *Acta Metall. Mater.* , **39** (10), 2225-2234.

Blau, P. J. (1989). *Friction and wear transitions of materials*. Noyes, Park Ridge.

Cameron, C. P. and Raj, R. (1990). Better sintering through green-state deformation processing. *Journal of the American Ceramic Society*, **73** (7), 2032-2037.

Chou, C. and Senna, M. (1987). Correlation between rheological behavior of aqueous suspensions of Al_2O_3 and properties of cast bodies: effect of dispersant and ultrafine powders. *American Ceramic Society Bulletin*.

Chu, M., Bhushan, B., and De Jonghe, L. C. (1992). Processing of diamond/alumina composites for low wear applications. *Journal of Materials Research*, **7** (11), 3010-3018.

Chuanzhen, H. and Xing, A. (1996). Development of advanced composite tool material. *Materials Research Bulletin*, **31** (8), 951-956.

Coble, R. L. (1961). Sintering crystalline solids. I. Intermediate and final stage diffusion models. *Journal of Applied Physics*, **32** (5), 787-792.

Davies, G. J. (1972). Graphitization of diamond at zero pressure and at a high temperature. Ph. D. Thesis. University of Reading.

Davies, G. J. and Evans, T. (1972). Graphitization of diamond at zero pressure and at a high temperature. *Proceedings of the Royal Society of London*, **A328**, 413-427.

Deeg, E. (1953). Die Scherbenbildung beim Schlicker-Giessprozess als Diffusionsproblem. *Ber. DKG*, **30**, 129-138.

Dietzel, A. and Mostetzky, H. (1956). Vorgänge beim Wasserentzug aus einem keramischen Schlicker durch die Gipsform. *Ber. DKG*, **33**, 7-18.

Dörre, E. and Hübner, H. (1984). *Alumina*. Springer-Verlag, Berlin.

Einstürzende Neubauten (1992). *Interim*. Mute. New York.

Evans, S. (1994a). Reactivity of diamond surfaces. In *Properties and growth of diamond*, (ed. G. Davies), pp. 64-67. INSPEC, London.

Evans, S. (1994b). Graphitisation of diamond surfaces. In *Properties and growth of diamond*, (ed. G. Davies), pp. 68-69. INSPEC, London.

Evans, T. (1979). Changes produced by high temperature treatment of diamond. In *The properties of diamond*, (ed. J. E. Field), pp. 403-24. Academic, New York.

Evans, T. and Phaal, C. (1962). *Proc. Fifth Biennial Conf. on Carbon*, pp. 147-153. Pennsylvania State University.

Fries, R. and Rand, B. Slip casting and filter pressing. In *Materials science and technology*, (ed. R. W. Cahn, P. Haasen, and E. J. Kramer), Volume 17A, *Processing of ceramics*, (volume ed. R. J. Brook), pp. , VCH.

Garbers-Craig, A. (1996). Notes accompanying a course on refractories at the University of Pretoria.

Gubarevich, T. M. and Tyshetskaya, A. V (1992). Synthesis and study of oxide-ultradispersed diamond systems. *Zhurnal Prikladnoi Khimii*, **65**, (1), 34-37. (Translation. Plenum Publishing.)

Hampton, J. H. D., Savage, S. B., and Drew, R. A. L. (1988). Experimental analysis and modelling of slip casting. *Journal of the American Ceramic Society*, **71** (12), 1040-1045.

Hampton, J. H. D., Savage, S. B., and Drew, R. A. L. (1992). Experimental analysis of fine particle migration during ceramic filtration processes. *Journal of the American Ceramic Society*, **75** (10), 2726-2732.

Heertjes, P. M. (1964). Filtration. *Transactions of the Institution of Chemical Engineers*, **42** (12), T266-T274.

Howes, V. R. (1962). The graphitization of diamond. *Proceedings of the Physical Society*, **80**, 648-662.

Hutchings, I. M. (1992). *Tribology: Friction and wear of engineering materials*. Edward Arnold, London.

Ikegami, T., Kotani, K., and Eguchi, K. (1987). Some roles of MgO and TiO_2 in densification of a sinterable alumina. *Journal of the American Ceramic Society*, **70** (12), 885-890.

ISO 3685: Tool-life testing with single point turning tools, (1993, 2nd edn). International Organization for Standardization, Geneva.

Katz, A. J. and Thompson, A. H. (1986). Quantitive prediction of permeability in rock. *Physical Review B*, **34** (11), 8179-8181.

Katz, A. J. and Thompson, A. H. (1987a). Prediction of rock electrical conductivity from mercury injection measurements. *Journal of Geophysical Research*, **92** (B1), 599-607.

Katz, A. J. and Thompson, A. H. (1987b). Mercury injection in porous media: A resistance Devil's staircase with percolation geometry. *Phys. Lett.*, **58** (1), 29-32.

Knight, D. S. and White, W. B. (1989). Characterization of diamond films by Raman spectroscopy. *J. Mater. Res.*, 4, (2), 385-393.

Krell, A. and Blank, P. (1995). Grain size dependence of hardness in dense submicrometer alumina. *Journal of the American Ceramic Society*, **78** (4), 1118-1120.

Kume, S., Suzuki, K., and Yoshida, H. (1992). Preparation of diamond-alumina composite by hot isostatic pressing. *Reports of the Government Industrial Research Institute, Nagoya*, **41**, (3), 99-105. (In Japanese. The information quoted is from a literature search abstract.)

Lancaster, J. K. (1990). Material-specific wear mechanisms: relevance to wear modeling. *Wear*, **141**, 159-183.

Lange, F. F. and Miller, K. T. (1987). Pressure filtration: consolidation kinetics and mechanics. *American Ceramic Society Bulletin*, **66** (10), 1498-1504.

Lawn, B. R., Evans, A. G., and Marshall, D. B. (1980). Elastic/plastic indentation damage in ceramics: The median/radial crack system. *Journal of the American Ceramic Society*, **63**, 574-581.

Letoit, A (a.k.a. Kombuis, K.) (1994). *Niemandsland & beyond!*. Shifty and Tic...Tic...Bang.

Li, X. S. and Low, I. M. (1994). Evaluation of advanced alumina-based ceramic tool inserts when machining high tensile steel. *Journal of Materials Science*, **29**, 3121-3127.

Li, X. S., Low, I. M., Wager, J. G., and Perera, D. S. (1993). Cutting performance of ceramic coated tools in machining high tensile steel. *MD*, **44**, 101-110.

Liu, J. and Ownby, P. D. (1991). Normal-pressure hot-pressing of α-alumina-diamond composites. *Journal of the American Ceramic Society*, **74**, (10), 2667-68.

Lukasiewicz, S. J. and Reed, J. S. (1988). Specific permeability of porous compacts as described by a capillary model. *Journal of the American Ceramic Society*, **71** (11), 1008-1014.

McColm, I. J. (1990). *Ceramic hardness*. Plenum. New York.

McColm, I. J. *Ceramic science for materials technologists*. Leonard Hill.

Msibi, C (1997). *Green body formation of a ceramic composite materiak by colloidal processing routes*. M Sc Thesis, University of the Witwatersrand.

Noma, T. and Sawaoka, A. (1984). Toughening in very high pressure sintered diamond-alumina composite. *Journal of Materials Science*, **19**, 2319-22.

Noma, T. and Sawaoka, A. (1985). Effect of heat treatment on fracture toughness of alumina-diamond composites sintered at high pressures. *Journal of the American Ceramic Society*, **68**, (2), C36-C37.

Ownby, P. D. Engineering properties of diamond and graphite. *Journal of the American Ceramic Society*.

Paul, P. (1960). Prediction of elastic constants of multiphase materials. *Transactions of the Metallurgical Society of AIME*, **218**, 36-41.

Perry, R. H. and Green, D. (ed.) (1984). *Perry's Chemical Engineers' Handbook*, (6th edn). McGraw-Hill, New York.

Petzow, G. (1976). *Metallographic etching*. American Society for Metals, Metals Park.

Pierson, H. O. (1993). *Handbook of carbon, graphite, diamond and fullernes*. Noyes, Park Ridge.

Roosen, A. and Bowen, H. K. (1988). Influence of various consolidation techniques on the green microstructure and sintering behavior of alumina powders. *Journal of the American Ceramic Society*, **71** (11), 970-977.

Schwelm, M. (1992). Untersuchungen zur Dispergierbarkeit und zum Druckschlickerguss von Si_3N_4 mit Y_2O_3-Al_2O_3 Sinteradditiven. Ph. D. thesis. University of Stuttgart.

Shin, D., Orr, K. K., and Schubert, H. (1990). Microstructure-mechanical property relationships in hot isostatically pressed alumina and zirconia toughened alumina. *Journal of the American Ceramic Society*, **73** (5), 1181-1188.

Singh, C. K. and Vajpayee, S. (1980). Evaluation of flank wear on cutting tools. *Wear*, **62**, 247-254.

Smith, J. M. (1981). *Chemical Engineering Kinetics*, (3rd edn). McGraw-Hill, Auckland.

Smith, P. A. and Haber, R. A. (1995). Effect of particle packing on the filtration and rheology behavior of extended size distribution alumina suspensions. *Journal of the American Ceramic Society*, **78** (7), 1737-1744.

Smith, P. A. and Haerle, A. G. (1995). Particle crowding analysis of slip casting, *Journal of the American Ceramic Society*, **78** (3), 809-812.

Smith, P. A., Kerch, H., Krueger, S., Long, G. G., Keller, J., and Haber, R. A., (1994). Pore sizes and filtration rates from two alumina slips. *Journal of the American Ceramic Society*, **77** (7), 1777-1782.

Sozin, Y. I., Simkin, E. S., and Ositinskaya, T.D. (1992). On the Graphitization of diamond. *Sverkhtverdye Materialy*, **14**, (4), 62-64.

Stachowiak, G. W. and Stachowiak, G. B. (1994). Wear behaviour of ceramic cutting tools. *Key Engineering Materials*, **96**, 137-164.

Tiller, F. M. and Tsai, C. (1986). Theory of filtration of ceramics: I, Slip casting. *Journal of the American Ceramic Society*, **69** (12), 882-887.

Turning and boring tools, pp. 16-17. Toshiba. (Marketing pamphlet).

Uematsu, K., Itakura, K., Uchida, N., Saito, K., Miyamoto, A., and Miyashita, T. (1990). Hot isostatic pressing of alumina and examination of the hot isostatic pressing map. *Journal of the American Ceramic Society*, **73** (1), 74-78.

Velamakanni, B. V. and Lange, F. F. (1991). Effect of interparticle potentials and sedimentation on particle packing density of bimodal distributions during pressure filtration. *Journal of the American Ceramic Society*, **74** (1), 166-172.

Watson, J. D. and Crick F. H. C. (1953). Molecular structures of nucleic acids. *Nature*.

Yeh, T. and Sacks, M. D. (1988a). Low-temperature sintering of aluminum oxide. *Journal of the American Ceramic Society*, **71** (10), 841-844.

Yeh, T. and Sacks, M. D. (1988b). Effect of particle size distribution on the sintering of alumina. *Journal of the American Ceramic Society*, **71** (12), c484-c487.